

4

Josef Eberhardsteiner - Manfred Gingerl - Lubomír Ondříš - Rudolf Beer
EXPERIMENTÁLNY VÝSKUM PEVNOSTI ANIZOTROPNÝCH TELIES PRI DVOJOSOVOVOM NAMÁHANÍ
ŠIKMO K HLAVNÝM SMEROM MATERIÁLU
EXPERIMENTAL INVESTIGATION OF THE STRENGTH OF ANISOTROPIC SOLIDS UNDER BIAXIAL LOADING
OBLIQUE TO THE PRINCIPAL MATERIAL DIRECTIONS

8

Stanisław Borkowski
METALOTERMICKÝ PROCES V LIATINE - „MIMOPECNÉ SPRACOVANIE“
METALLOTHERMY IN THE CAST IRON “OUT OF THE FURNACE TREATMENT” PROCESS

15

Dušan Štekláč - Miroslav Neslušan
PREROZDELOVANIE TEPLA PRI BRÚSENÍ TITÁNOVEJ ZLIATINY VT9
HEAT DISTRIBUTION WHEN TITANIUM ALLOY VT9 GRINDING

20

Karol Vasilko
NOVÁ METODIKA NA ZOSTROJENIE ZÁVISLOSTI TRVANLIVOSTI NÁSTROJA NA REZNEJ RÝCHLOSTI
A NEW METHOD FOR DURABILITY DEPENDENCE OF A CUTTING TOOL ON A CUTTING SPEED

30

Jaroslav Koutský
PRÍSPEVOK K MODELOVANIU OPTIMALIZÁCIE FORMOVANIA A TEPELNÉHO SPRACOVANIA KONŠTRUKČNÝCH OCELI
CONTRIBUTION TO MODELLING OF THE OPTIMIZATION OF FORMING AND HEAT TREATMENT OF STRUCTURAL STEELS

36

Werner Mombrei - Peter Ottlinger
PRÍSPEVOK K OPTIMALIZÁCI VLASTNOSTÍ OCELE POUŽÍVANEJ PRE ŽELEZNIČNÉ KOLESÁ Z HLADISKA ICH OPOTREBENIA
A CONTRIBUTION TO THE OPTIMIZATION OF WEAR BEHAVIOUR OF STEEL USED FOR RAILWAY WHEELS

39

János Takács - Péter Gál, MSc - Antal Lovas - Joachim Belt
FLUX POKOVANIE ZOSILNENÉ ABSORPCIU AI POVRCHOV PRI CHARAKTERISTICKEJ VLNovej DÍŽKE CO₂
LASEROVÉHO ŽIARENIA
FLUX COATING ENHANCED ABSORPTION OF AI SURFACES AT THE CHARACTERISTIC WAVELENGTH OF CO₂
LASER IRRADIATION

44

Stefania Greszczyk - Grzegorz Lipowski
REOLOGICKÉ VLASTNOSTI CEMENTOVÝCH ZMESÍ OBSAHUJÚCICH POPOLČEK S RÔZNOU VEĽKOSŤOU ZŔN
THE RHEOLOGICAL PROPERTIES OF CEMENT PASTES CONTAINING FLY ASH WITH DIFFERENT PARTICLE SIZE
DISTRIBUTION

48

Andrzej Surowiecki - Zenon Zamiar
MODEL ZEMNÉHO ZÁKLADU S VYSTUŽENÍM V HLBOKOM VÝKOPE
MODEL OF EARTHEN FOUNDATION WITH REINFORCEMENT IN A DEEP EXCAVATION

52

Sylwester Kobiela - Grzegorz Troszczyński
ZISŤOVANIE POZDÍŽNYCH SÍL NA OHÝBANOM NOSNÍKU
INDEPENDENT FORMATION OF LONGITUDINAL FORCES IN BENT BEAMS

EXPERIMENTÁLNY VÝSKUM PEVNOSTI ANIZOTROPNÝCH TELIES PRI DVOJOSOVOVOM NAMÁHANÍ ŠIKMO K HLAVNÝM SMEROM MATERIÁLU

EXPERIMENTAL INVESTIGATION OF THE STRENGTH OF ANISOTROPIC SOLIDS UNDER BIAXIAL LOADING OBLIQUE TO THE PRINCIPAL MATERIAL DIRECTIONS

Realistická konečno-prvková analýza medzného zaťaženia konštrukčných častí ako aj škrupinových konštrukcií vyrobených z anizotropných materiálov vyžaduje vhodné konštitutívne rovnice na predpoveď chovania sa deformácie a medznej pevnosti dvojosofo zaťažených telies. Avšak je nedostatok vhodných biaxiálnych experimentálnych údajov, zvlášť v situáciách, keď sa uvažuje, že hlavné smery zataženia nie sú totožné s hlavnými smermi materiálových vlastností.

Z teoretického hľadiska musí byť splnený vzťah napätie-deformácia. Nie je zásadný rozdiel v zohľadňovaní rôznych druhov anizotropných materiálov, ako sú biologické tkanivá (ľudská koža), tkanivá (textil), vystužené polyméry a iné druhy plasticke deformovaných membrán. Avšak návrh experimentu, konštrukcia zaťažovacieho zariadenia a postup zaťažovania sú silno závislé od tvaru a veľkosti danej vzorky (alebo vzhľadom na potreby výskumu) a od mechanických vlastností uvažovaného materiálu.

V tomto článku je ukázaný vývoj vhodného skúšobného zariadenia ako aj skúšobných vzoriek pre prípad ortotropického dreva. Cieľom výskumu je určenie pevnosti materiálu a dvojsového vzťahu napätie-deformácia dreva, keď je zaťažované šikmo k štruktúre materiálu.

Realistic finite element ultimate load analyses of structural details as well as of shell structures made of anisotropic materials require suitable constitutive equations for the prediction of the deformational behavior and ultimate strength of biaxially loaded solids. However, there is a lack of adequate biaxial experimental data, particularly if loading situations are considered where the principal loading directions do not coincide with the principal material directions.

From the theoretical point of view one has to obey the stress-strain relationship. There is no principal difference in dealing with different kinds of anisotropic materials, such as biological tissues (human skin), anisotropic rubbers, woven fabrics (textures), reinforced polymers and any kind of plastic deformed membranes. However, the design of the experiment, the construction of the loading device and the loading procedure are strongly influenced by the shape and size of the test specimen available (or in view to the goal of the investigation necessary) and by the mechanical properties of the material under consideration.

In this paper the development of an adequate testing device as well as a testing specimen is shown for the case of orthotropic wood. The goals of this investigation are the determination of the material strength and the biaxial stress-strain relationship of wood when loaded oblique to the grain direction.

1. Mechanical Fundamentals

For the description of the mechanical properties of an anisotropic material it is suitable to use the generalized Hooke's Law. However, in all cases with large deformations we have to be aware that the stress-strain relationship up to failure could be non-linear. In such cases the linearized descriptions are usually restricted to small deformation steps (see Fig. 1).

Therefore in such an investigation a stepwise loading procedure is used as illustrated in Fig. 2 [1]. In case of wood it has been shown in an experimental study that the rheological effects may be neglected if the holding time does not exceed a period of about 15 seconds.

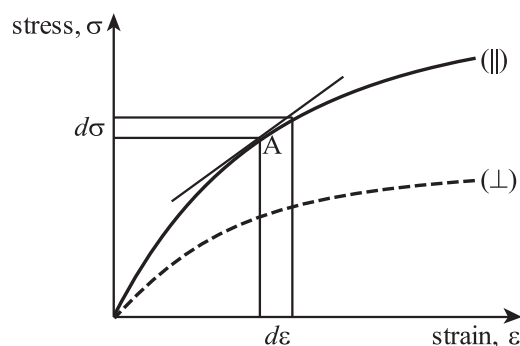


Fig. 1 Stress-strain relation for an anisotropic material with large deformations

* Ass. Prof. Dr. Josef Eberhardsteiner, Dr. Manfred Gingerl, Dr. Lubomír Ondris, Prof. Dr. Rudolf Beer
Institute for Strength of Materials, Vienna University of Technology, Adolf Blamauer-Gasse 1-3, A-1030 Vienna, Austria

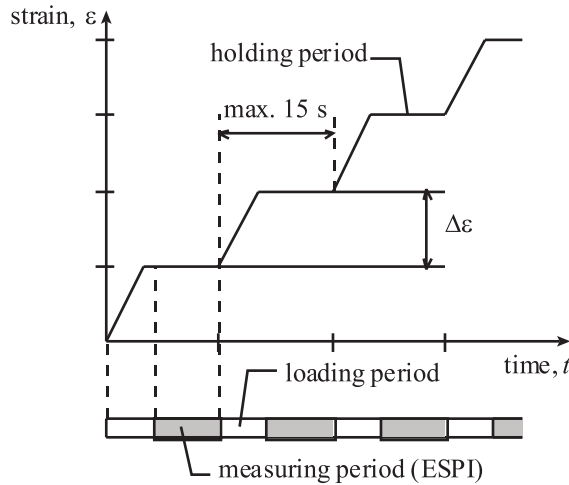


Fig. 2 Stepwise loading procedure

The final deformation is the result of the sum of the small loading steps and the experimental procedure meets the conditions of additivity according to Hencky's strain definition [2]:

$$d\varepsilon_H = \frac{dl}{l}; \quad \varepsilon_H = \int_{l_0}^l d\varepsilon_H \quad (1.1)$$

$$\begin{aligned} \varepsilon_H &= \varepsilon_{H1} + \varepsilon_{H2} = \ln \frac{l_0 + \Delta l_1}{l_0} + \ln \frac{l_0 + \Delta l_1 + \Delta l_2}{l_0 + \Delta l_1} = \\ &= \ln \frac{l_0 + \Delta l_1 + \Delta l_2}{l_0} = \varepsilon_{H, 1+2} \end{aligned} \quad (1.2)$$

With the restriction to plane stress loading of thin test specimens the remaining generalized Hooke's Law is given by equations (2.1) - (2.4)

$$d\varepsilon_x = a_{11}d\sigma_x + a_{12}d\sigma_y + a_{16}d\tau_{xy} \quad (2.1)$$

$$d\varepsilon_y = a_{21}d\sigma_x + a_{22}d\sigma_y + a_{26}d\tau_{xy} \quad (2.2)$$

$$d\varepsilon_z = a_{31}d\sigma_x + a_{32}d\sigma_y + a_{36}d\tau_{xy} \quad (2.3)$$

$$d\gamma_{xy} = a_{61}d\sigma_x + a_{62}d\sigma_y + a_{66}d\tau_{xy} \quad (2.4)$$

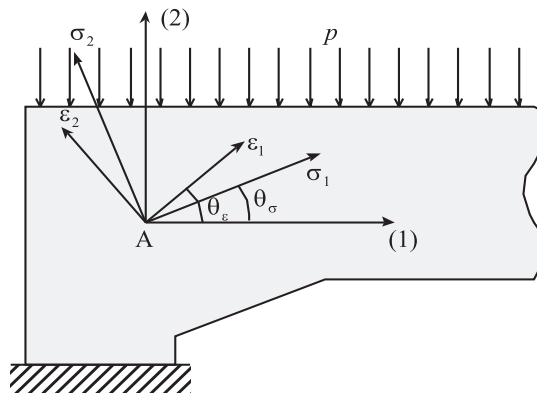


Fig. 3 Example for an investigation of a wooden console

In cases where a numerical investigation of a flat anisotropic structure shows a state of biaxial stress and strain (x-y plane) with non-coincident principal directions (Fig. 3) usually no information about failure can be found in the literature. In order to eliminate this deficiency, a comprehensive experimental investigation of the stiffness and strength behavior of the material under arbitrary two-dimensional loading conditions was carried out in advance for which an adequate method had to be developed.

The experimental parameters of such biaxial investigations are the ratio between the applied principal stress components and the angle between principal loading direction and principal material direction θ_σ (Fig. 4). The design of an adequate testing procedure (loading device as well as test specimen) is strongly influenced by the material under investigation, by shape and size of the test specimen available and of course by the goal of investigation.

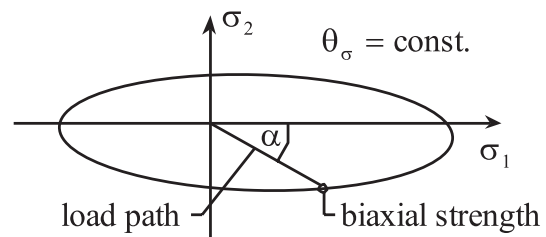


Fig. 4 Failure envelope

The aim of this experimental study is to provide information about the ultimate strength behavior under biaxial loading oblique to the grain direction of wood. Due to the fact that the specimen's surfaces ($z = \pm t / 2$) are stress-free the strains in z-direction, concerning Eqn. (2.3), will be neglected in the following considerations. From this it follows that only 6 coefficients of the generalized Hooke's Law (2.1) - (2.4) are essential.

2. Experimental Setup

With the viewpoint of the special task of this investigation the test specimen of finite size has to simulate an infinite element of the material assumed in a numerical calculation. That leads to some essential requirements [3]: first, a homogeneous testing field (humidity, density, grain direction and grain density) and, second, failure due to the applied homogeneous stress and strain distributions should occur within the region of the testing field. Beside a very careful selection and storage of the material it is necessary to optimize the loading procedure, which is most important for the construction for both, the loading device as well as the test specimen developed by the authors. The final shape of the test specimen is shown in Fig. 5 and the loading device is shown in Fig. 6.

In order to achieve homogeneous states of stress and strain with this equipment a certain strategy of loading was necessary, which is described by Eqns. (3.1) - (3.3):

$$d\varepsilon_x = a_{11}d\sigma_x + a_{12}d\sigma_y \quad (3.1)$$

$$d\varepsilon_y = a_{21}d\sigma_x + a_{22}d\sigma_y, \quad (3.2)$$

$$d\gamma_{xy} = a_{61}d\sigma_x + a_{62}d\sigma_y, \quad (3.3)$$

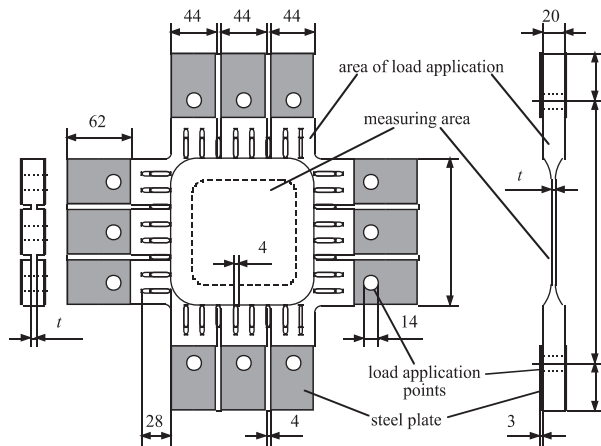


Fig. 5 Test specimen

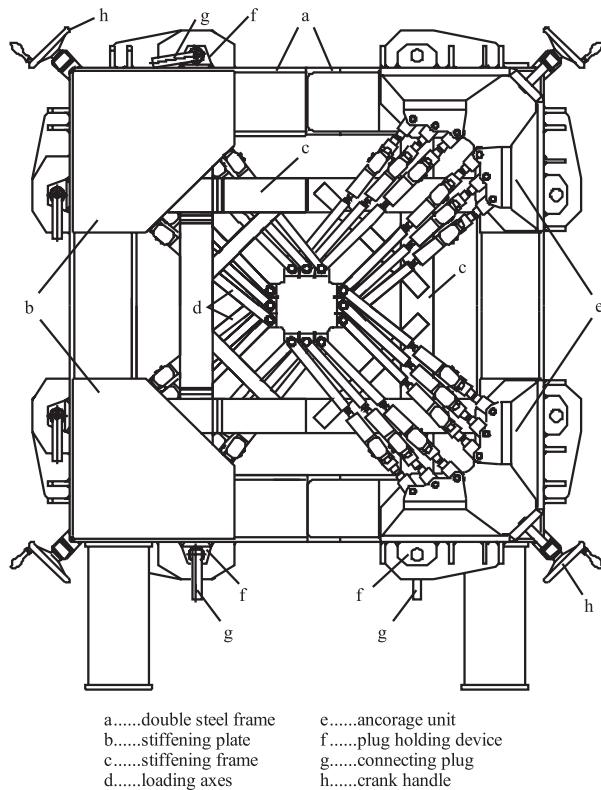


Fig. 6 Hydraulic loading device

That means that the test specimen was loaded in such a way that shear stresses are vanishing in the principal directions of the testing device. A FE study showed the necessary movement of the loading points in order to obtain this specific state of stress for any angle between the principal directions of the stresses and the

grain direction of wood within the testing field. In this way it was also possible to avoid unwanted stress and strain concentrations at the corners of the test specimen.

The very specific properties of wood require a contactless measuring method for the deformation analysis of the specimen [4]. Beyond that the chosen method must be at least two-dimensional, full-field accurate and in real-time. Therefore, from the viewpoint of the enormous amount of necessary experiments from all available optical methods the Electronic Speckle-Pattern Interferometry (ESPI) is the only practicable one.

The developed ESPI system, described in detail in [1], is mounted at the hydraulic loading device through two independent frame sets in order to avoid vibrations to the optical set-up. The measuring system allows a full-field analysis of two in-plane components and one out-of-plane component of the state of deformation in the measuring region (140 x 140 mm) of a biaxial specimen (Fig. 5).

3. Experimental Results

The displacement-controlled experiments were characterized by a proportional stepwise loading until fracture was reached. The applied displacement steps varied from 4 to 10 μm . The experimentally obtained failure envelopes for the investigated grain directions $\varphi = 0^\circ, 7.5^\circ, 15^\circ, 30^\circ$ and 45° reflect the strong influence of grain direction on the biaxial strength behavior of solid wood as it is known from uniaxial strength tests. The obtained experimental results form an essential basis for further developments in material modelling. In Figs. 7 to 10 representative experimental results are shown.

Fig. 7 contains the stepwise progression of load application forces for an experimental configuration characterized by a grain angle of $\varphi = 15^\circ$ and a displacement ratio of $\kappa = +1 : -2$. The latter results in a tensile loading in horizontal direction and in a compressive loading in vertical direction. The shown results

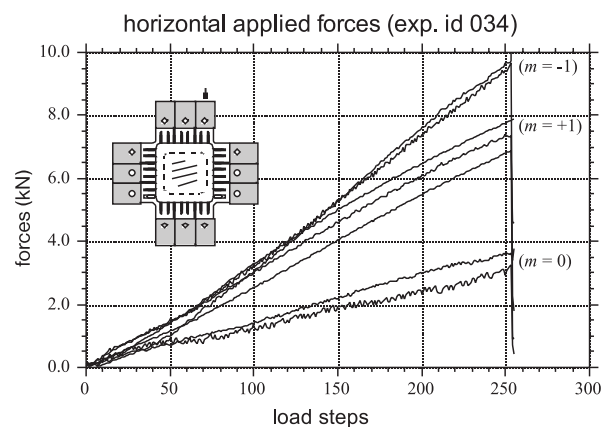


Fig. 7 Load application forces resulting from displacement ratio $\kappa = +1 : -2$

indicate that the forces at the middle load application point ($m = 0$) are much lower than the ones at the outer load application points ($m = \pm 1$).

The biaxial strength values for a representative number of displacement ratios and a grain direction of $\varphi = 30^\circ$ are shown in Fig. 8. For each displacement ratio six experiments were carried out. The obtained fracture points in the biaxial stress space are in good correlation with an ellipse resulting (e.g. from a quadratic failure criterion).

In Fig. 9 analogous results for a grain direction of $\varphi = 0^\circ$ are presented. However, in addition to Fig. 8, the ratio of the principal stress components, σ_2/σ_1 , and its propagation until fracture is illustrated. Considering this stress ratio, an almost proportional behavior was observed for tensile loading normal to the grain direction ($\sigma_2 > 0$). For compressive loading normal to the grain direction ($\sigma_2 < 0$), however, significant nonlinearities were detected. In order to eliminate stability problems as a reason of this phenomenon, experiments with a load history consisting of loading, unloading and reloading were carried out. Fig. 10 contains the stress-strain relationship for such a non-proportional experiment with uniaxial compression normal to the grain direction ($\varphi = 0^\circ$, $\kappa = 0: -1$). The results in this Figure are characterized by a deformation behavior which is well-known from the classical plasticity theory. Therefore, this theory can be used for the mathematical description of the stiffness degradation of wood under compressive loading.

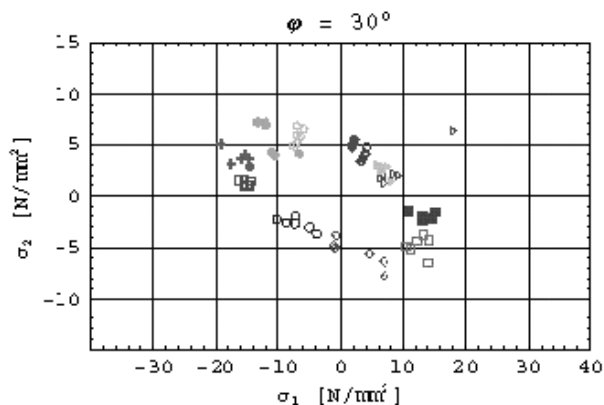


Fig. 8 Biaxial strength envelope for grain direction $\varphi = 30^\circ$

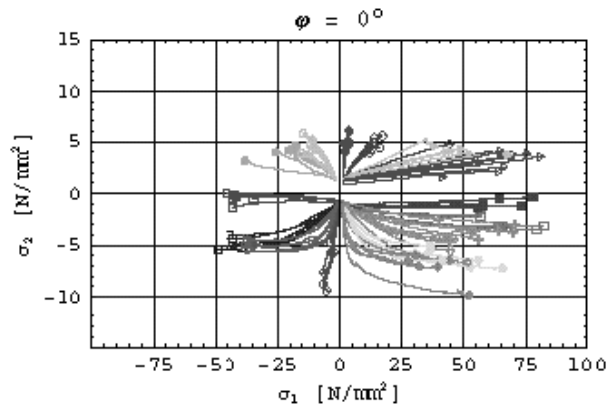


Fig. 9 Biaxial strength envelope for grain direction $\varphi = 0^\circ$

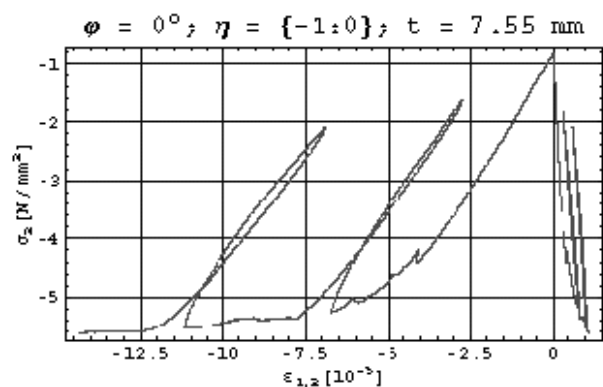


Fig. 10 Stress-strain relationship for non-proportional loading

Acknowledgement

The authors gratefully acknowledge the support of the Austrian Fund for Scientific Research, the Austrian Ministry of Science and Transport, and the "Hochschuljubiläumsstiftung der Stadt Wien" allowing the presented work.

Reviewed by: P. Košťal, V. Kompš

Literatúra - References

- [1] GINGERL, M.: *Realisierung eines optischen Deformationsmeßsystems zur experimentellen Untersuchung des orthotropen Materialverhaltens von Holz bei biaxialer Beanspruchung*, Ph. D. Thesis, Vienna University of Technology, 1998.
- [2] MALVERN, L. E.: *Introduction to the Mechanics of a Continuous Medium*, Series in Engineering of the Physical Sciences, Prentice-Hall, 1969.
- [3] EBERHARDSTEINER, J.: *Experimentelle Untersuchung mechanischer Eigenschaften von Fichtenholz bei biaxialer Beanspruchung schräg zur Faserrichtung*, Habilitation, Vienna University of Technology, 2000, in print.
- [4] EBERHARDSTEINER, J.: *Biaxial testing of orthotropic materials using electronic speckle pattern interferometry*, Measurement 16, p. 139-148, 1995.

Stanislaw Borkowski *

METALOTERMICKÝ PROCES V LIATINE – „MIMOPECNÉ SPRACOVANIE“

METALLOTHERMY IN THE CAST IRON “OUT OF THE FURNACE TREATMENT” PROCESS

Výroba vysokoakostných liatin v malých množstvách sa stáva v súčasnosti aktuálnym problémom. Existujúce technológie tavenia liatiny sú málo progresívne. V práci sú prezentované teoretické základy získania legovanej liatiny (Cr, Ti) pri použití metalotermie. Zdrojom týchto prvkov sú ich oxidy. Proces metalotermického spracovania prebieha bez zníženia teploty tekutého kovu, dochádza k zvýšeniu obsahu prídavných prvkov a zníženiu obsahu uhlíka a síry.

Production of high-quality cast irons in a batch production is topical current problem. Existing technologies of melting cast iron are not very progressive. The basic theoretical knowledges of obtaining of alloyed cast iron (Cr, Ti) by using metalothermy are presented in this work. The oxides are sources of this elements. The metalothermy treatment process is running without decrease of liquid metal temperature, comes to increase of quantity addition elements and reduction of quantity of carbon and sulphur.

1. A theoretical basis of acquiring metals from their oxygen compounds

A process of acquiring metals or their alloys is connected with a course of chemical reactions. The course interlocks many internal factors (e.g. quantity of reacting factors), concentration of reacting substances, an aggregation state of reacting substances and reaction products, thermal effect as well as external factors, (e.g. pressure and reaction rates).

Metals, as acquired results of metallurgical processes, according to a purity grade, may be monophase, while alloys are usually multiphase and determine a part of a structural constituents mixture. An occurrence range of individual phases or their mixtures is shown on adequate equilibrium system diagrams (*heterogeneous systems*).

In metallurgical processes, according to the mutual interaction of the system and its environment, which is a conversion of mass and energy between them, there are two *types of the system*[1]:

- “an open system” – a conversion of both mass and energy between the system and its environment is possible;
- “a closed system” – only a conversion of energy between the system and its environment is possible. There is no conversion of mass between them.

A state of the examined chemical reaction may be defined, with the aid of a collection of thermodynamic variables that can be divided into two main groups:

- *thermodynamic variables*;
- *a state quantity*.

To the *first* group belong: temperature T , pressure P , volume V and concentration c . To the *second* group belong: internal energy U , entropy S , enthalpy H , chemical potential μ and free energy F .

A connection between enthalpy, entropy and temperature may be described as a formula below:

$$G = H - TS \quad (1)$$

where: G - Gibbs free enthalpy or thermodynamic potential or Gibbs free energy.

A thermodynamic potential, during a spontaneous process proceeded in a permanent temperature and under a permanent pressure, tends to approach its minimum value. Reaching this minimum value determines achieving the equilibrium state.

In practice, knowledge of S , H , G value changes (not their absolute values) is sufficient. Then the formula (1) is as follows:

$$\Delta G = \Delta H_{298}^0 - T\Delta S_{298}^0 \quad (2)$$

where: ΔH - the enthalpy change of the reaction while = const. and $T = 298$ K;

ΔS - the entropy change of the reaction while $T = 298$ K, T - temp. in Kelvin.

It is more convenient to use this quotation because ΔH_{298}^0 and ΔS_{298}^0 can be found in tables.

* Prof. dr. hab. Ing. Stanislaw Borkowski

Technical University of Czestochowa, Department of Management, Division of Production Engineering

Acquiring metals or their alloys as results of exothermic reactions between metal (a reducer) and metal compounds (mainly oxygen compounds) is a process called *metallothermy* [2]. If we use aluminium as a reducer - then the process is called *aluminothermy*, silicon - *silicothermy*, calcium - *calciothermy*. Except for pure metals, alloys can be used for reduction, eg. $Ca-Si$, $Al-Ca-Si$, $Al-Fe-Si$. The metal oxide reduction process is presented as an underneath formula:



The reaction proceeds in an easier way when a difference in a propinquity to them between a metal Me'' reached from reduced oxide and metal - the reducer is more significant. The thermodynamic potential, also called the oxygen potential, terms the estimation of oxides durability. The estimation is presented as follows:

$$\Delta G_T^0 = -RT \ln p_{O_2} \quad (4)$$

where: R - universal gas constant,

p_{O_2} - oxygen pressure in equilibrium with metal oxide at a particular temperature.

A thermodynamic potential change that occurs during the formation of a few oxides from their chemical elements, (depending on the temperature values) is shown on Fig. 1.

Reduction conditions may be defined as a temperature dependence on the thermodynamic potential ΔG_T^0 . The reaction can be

initiated at $\Delta G_T^0 < 0$. The superior the depreciating (detrimental) ΔG_T^0 values, the easier the reaction runs. A reciprocal course of thermodynamic potential changes determines that the magnesium reduction of aluminium oxides as well as silicon, chromium and iron oxides is possible. The aluminium reduction is suitable for silicon oxides as well as for chromium and iron oxides. Silicon, however, reduces chromium oxides and iron oxides only. Under the pressure of 98,07 kPa it is not possible to apply the aluminium reduction for magnesium oxides, because ΔG_T^0 for this reaction is > 0 . A metalthermic reaction initiates if in any place of the mixture the ignition temperature is achieved. Heat emission creates a reaction around the ignition place. Exothermic mixtures lighting up is caused by dint of *initiators* (igniting mixtures), e.g. magnesium with sodium nitrate or aluminium with barium peroxide. The reaction initiators, in the metal or alloy production process from metalthermic methods, are situated in the proper place of charge and lighten up with a glowing bar. The igniting mixtures satisfy requirements by dint of a low ignition temperature as well as a great thermal effect.

Using the enthalpy values ΔH_{298}^0 it is possible to determine which metalthermic reactions will spontaneously proceed (without the heat from the outside).

German research [2] angles that the quantity of emitted heat for 1g of the charge shouldn't be lower than 2300 J. A unitary thermal effect can be counted as follows:

$$H_{298}^0 = \frac{\Delta H_{298}^0}{molMe'O + molMe''} \quad (5)$$

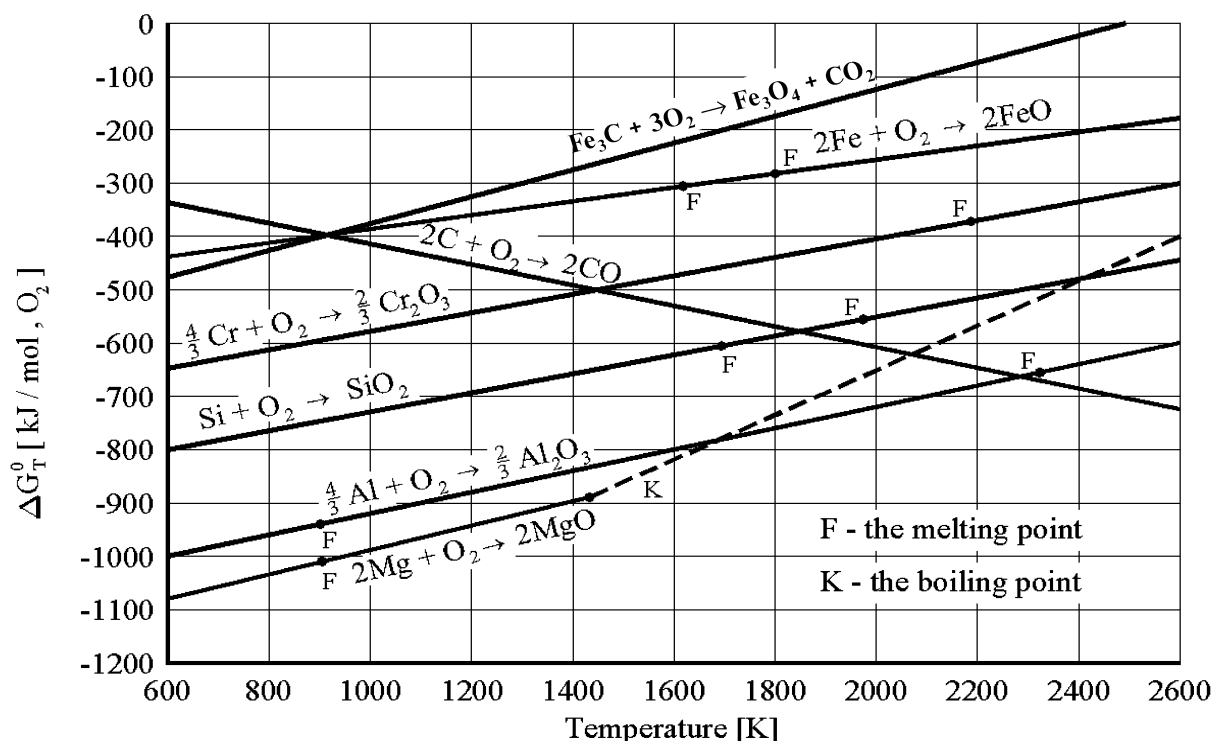
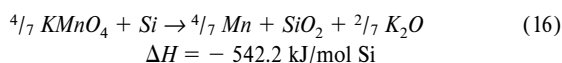
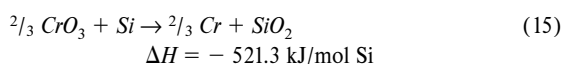
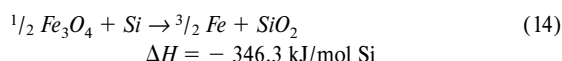
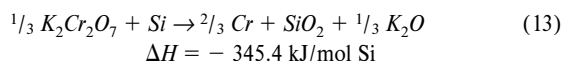
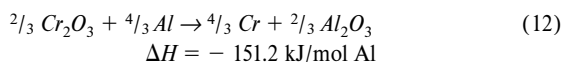
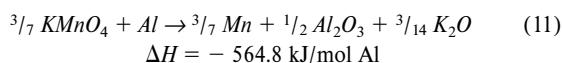
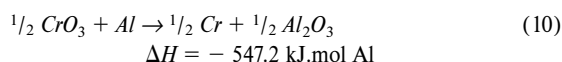
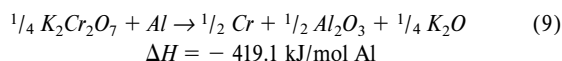
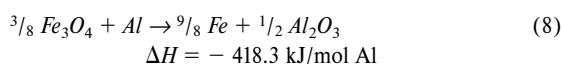
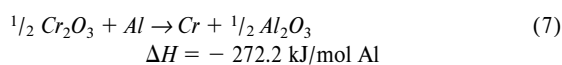
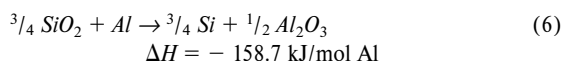


Fig. 1 The temperature values of the thermodynamic potential change of the creating oxides Mg, Al, Si, Cr, Fe [2]

Russian research [3] angles that for a proper metalthermic reaction course a unitary thermal effect, not lower than 2700 J is required. Metalthermic processes run spontaneously if $-\Delta H_{298}^0 > > 300 \text{ kJ/g}$ - atom of the reductor. A great output and purity of the diminished element can be obtained. As an example the *enthalpy value* for a mole of the reaction reducer - aluminium or silicon has been posed.



Recent research indicated that the reactions marked as (6), (7) and (12) do not run spontaneously.

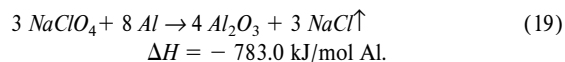
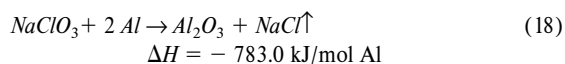
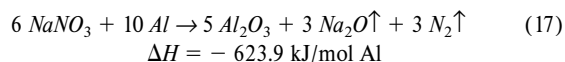
A question if these reactions courses can be accomplished appears.

Training indicates some ways of the *heat effect extention*.

The most important ways are presented below:

1. *An electric energy lead*. The process may also be called *electro-silicothermy* in case of silicon oxides reduction. This alternate design cannot be used in the "out-of-klin" treatment.
2. *An addition of iron oxide and aluminium oxide mixture to the charge - ferromit mixtures* (reaction 8). A heat excess helps the right reaction. The method is suitable for iron alloy productions because, in case pure metals are obtained, iron pollutes them.

3. *Using an oxide of a higher oxidation number as a part of the charge*, e.g. in the chromium production a portion of Cr_2O_3 should be replaced by CrO_3 (reactions 10 and 15).
4. *Using oxy-salts of the reducing element instead of the oxides*. For example one can use $\text{K}_2\text{Cr}_2\text{O}_7$ instead of Cr_2O_3 (reactions 9 and 13). If manganum presence in a product is acceptable then KMnO_4 can be a part of the charge (reactions 11 and 16).
5. *An addition of peroxides to the charge*. You can use barium or calcium that in connection with aluminium, silicon or magnesium emit a great heat quantity. The reaction products (barium oxide or calcium oxide) and a reductor run to the metallurgical slag and do not pollute metals.
6. *Making addition of a great oxygen amount salt to the charge*. These salts, in addition with aluminium, set a prominent heat value (e.g. chromates, dichromates, permanganates, nitrates, chlorates, perchlorates). Nitrates, chlorates and perchlorates, in connection with aluminium, set products as well as heat effect as follows:



Reaction products run to the slug (Al_2O_3) or they leave the reaction environment, being in a gaseous state.

7. *The charge heating*. During this reaction, for every 100 K the heat effect grows for 125,6 J/g of the charge. This procedure is not suitable for the low ignition temperature mixtures, because during the heat process self-ignition can happen.

Temperature of metalthermic processes. It's quite difficult to measure metalthermic processes' temperatures. The most often an optical pyrometer is used during the measurements. A basic difficulty arises from the fact, that a temperature of a system surface in a short time equals the reaction temperature. The surface is covered with the oxygen of the reductor [3].

The burning temperature of the thermite mixture was measured pyrometrically at the temp. of 2200 – 2400 °C. The measurements pose that this temperature should reach 3200 ± 200 °C. Photometric measurements however pose that it reaches the temperature of 3200 ± 50 °C. The temperatures achieved during the metalthermic reactions exceed the melting temperatures of the reduced metals. So one can put forward a proposal that there will be no heat losses during the "out of the furnace treatment" reaction.

2. A chromium oxides reduction with aluminium - chromium output

There is another parameter describing metalthermic processes (except for the heat effect). It's their *efficiency* measured by an

output of the reduced metal in the aluminothermic process. The output is connected with the equilibrium constant, which, for the reaction (7), is shown as follows:

$$K_p = \frac{a_{Cr}^2 \cdot a_{Al_2O_3}}{a_{Al}^2 \cdot a_{Cr_2O_3}} \quad (20)$$

where: a - activity of chemical elements and molecules of the system.

For the system, created by chromium aluminium trioxides as well as the products of their reactions, for the measurements mole fractions of the slag products as well as reacting substances instead of the activity can be used. After their replacement to the formula (20) the equation will be given as follows:

$$K_p = \frac{n_{Cr}^2 \cdot n_{Al_2O_3}}{n_{Al}^2 \cdot n_{Cr_2O_3}} \quad (21)$$

where: n - an amount of substantial moles for the reaction (7) in the state of equilibrium related to 1 mole of Cr_2O_3 .

The system created by the reaction (7) consists of two phases: a metal phase (Cr) and the slag (Al_2O_3). At the stable pressure the state of quotation can be determined by the metal bath temperature as well as by one of the factors concentration. The concentrations of the other system factors are presented as follows:

$$n_{Cr} = 2(1 - n_{Cr_2O_3})^2 \quad (22)$$

$$n_{Al_2O_3} = 1 - n_{Cr_2O_3} \quad (23)$$

$$n_{Al} = 2n_{Cr_2O_3} \quad (24)$$

so:

$$K_p = \frac{(1 - n_{Cr_2O_3})^3}{n_{Cr_2O_3}^3} \quad (25)$$

Making an assumption that the reaction (7) runs almost to the end (when $n_{Cr_2O_3} \ll 1$ and $n_{Cr_2O_3} \approx 1$) we get:

$$K_p = 1/n_{Cr_2O_3}^2 \quad (26)$$

Resisting on the temperature and a state of chemical equilibrium, a Cr_2O_3 mole account can be calculated:

$$n_{Cr_2O_3} = \sqrt[3]{\frac{1}{K_p}} \quad (27)$$

$$\lg K_p = \Delta G_T^0 / 19,55T \quad (28)$$

The formulas (22 - 28) allow to calculate K_p , n_{CrO} , n_{Al} , as well as the chromium output in the equilibrium state of the reaction (7) at the temperatures of 2000, 2250 and 2500 K.

A chromium output was calculated from the formula as follows:

$$U_{Cr} = \frac{100n_{Cr}}{n_{Cr} + n_{Cr_2O_3}} \quad (29)$$

Findings were compiled in the chart below:

Temperature [K]	2000	2250	2500
K_p	$1.4 \cdot 10^{11}$	$3.7 \cdot 10^9$	$2.1 \cdot 10^8$
$n_{Cr_2O_3}$	$1.9 \cdot 10^{-4}$	$6.5 \cdot 10^{-4}$	$1.7 \cdot 10^{-3}$
n_{Al}	$3.8 \cdot 10^{-4}$	$1.3 \cdot 10^{-3}$	$3.4 \cdot 10^{-3}$
A chromium output [%]	99.98	99.93	99.83

The received results indicate two facts: first - a theoretical chromium output in its aluminium trioxide reduction process is very high and in the temperatures of industrial conditions equals over 99 %. Second a chromium output decreases as the temperature increases.

Under the industrial conditions a chromium output from the aluminothermic process equals 88 %. A question "where is the source of the considerable divergence in the chromium output" appears.

The above problem can be considered resisting on the thermodynamic potential change during the process of chromium receiving, using the aluminothermic method (Fig. 2).

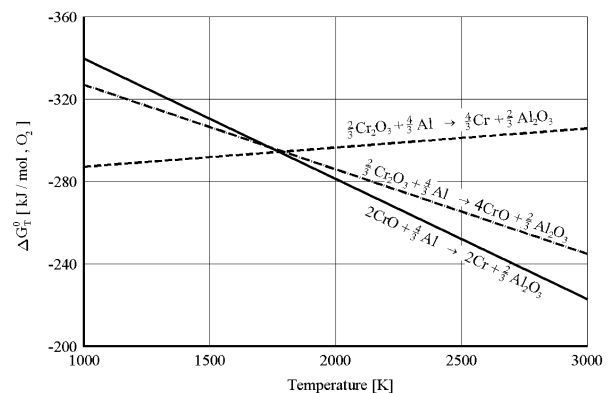
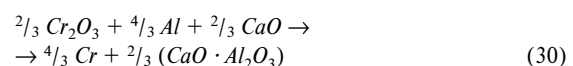


Fig. 2 Thermodynamic potential change for aluminium reduction process of chromium oxides depending on the temperature [3].

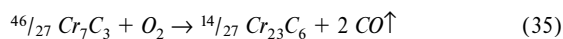
At the temperature of over 1835 K the reduction process should run as follows: $Cr_2O_3 \rightarrow CrO \rightarrow Cr$. Probability of this course rises with the temperature growth. A forming chromium oxide CrO passes into the slag, giving a durable complex $Cr^{2+} - AlO^{2-}$. A slag search shows that chromium presented in the complex is not only in the combined state, but pure metal drops, bounded by the slag, determine its great majority. The chromium losses are the main cause of its low output in industrial conditions.

As a counteraction of chromium oxide CrO forming which, at the temperature of 1800 K, is more durable than Cr_2O_3 , calcium oxide is added to the charge. Presence of this compound boosts the system reactivity, chromium trioxide becomes more active and the reaction (7) shifts to the right.

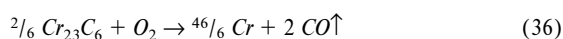
The reaction course (7) is presented as follows:



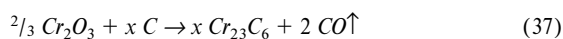
imperceptible. The other carbide $Cr_{23}C_6$ determines a result of the reaction as follows:



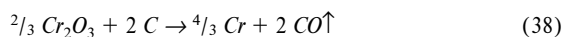
Cr_7C_3 is a substrate of the reaction whose amount is regulated by the (33) and (34) reactions. Forming the $Cr_{23}C_6$ carbide doesn't decrease a chromium output, because free chromium determines the result of its reaction with oxygen, according to the reaction (36) as follows:



$Cr_{23}C_6$ carbide also becomes the result of the reaction below:



Reaching the temperature over 2200 K determines the reaction course condition. From Fig. 3 one can specify a direct chromium trioxide reduction reaction with carbid, according to the reaction as follows:



Thermodynamic conditions of the reaction are more beneficial than the (7) reaction only at over 2300 K. The possibilities of Cr_3C_2 , $Cr_{23}C_6$ and Cr formation shouldn't be excluded from the thermodynamic analysis of $Cr-C-O$ system. A probability of their formation decreases as they are listed.

Carbide oxide is one of the (33) ÷ (38) reactions product which as gas simply leaves the reaction environment. Forming the carbid oxide involves a carbid contents decrease in the system.

Silicon, following carbid, and oxygen, is another chemical element to analyse. The thermodynamic potential change during a silicon reduction of chromium trioxide is shown as below:

$$\Delta G^0_T = - 49200 + 7,5 T \quad (39)$$

Comparing both formulas: (33) and (40) an inference that, for every temperature value the (7) reaction is more justifiable than reaction (15) appears.

During the Cr-C-O system and the (15) reaction analysis, carbid and silicon were considered in a solid state, while oxygen was considered in a gaseous state. In the slag carbid and silicon are in a dissolved state, while oxygen is in an ionized state. It causes an increase in activity of these elements, activity of oxygen in particular. There is a lack of data for the liquid iron - exothermic mixtures system analysis.

Some other reactions may run between carbid and chromium trioxide. Reaching the temperature of 2100 K determines a condition of their course. A high temperature is reached by the system as a result of reaction (7) course mainly.

Nascent metallic chromium may react with slag oxygen and mixture oxygen. Chromium trioxide determines the product of the reaction. The course of the reaction is objectionable because there

is a lack of aluminium and a forming product (Cr_2O_3) may pass the slag, decreasing a chromium output. That's why free oxygen in the slag or mixture is harmful. Free oxygen in the mixture estimates liquid oxygen in a binding material, which is used for integrating mixture elements.

Burning exothermic chromium mixture in contact with a liquid slag creates an open system, because it gives the heat and chromium away to the slag and absorbs mainly carbon from it.

4. Exothermic mixture elements for the "out of the furnace" treatment

Making full use of the professional literature [2, 3], small publications [4, 5] as well as personal experiments [6, 7] in the above field, exothermic alloy mixtures contain:

- a source of an alloy element;
- an oxidizer - nitrates, chromates, dichromates, chlorates, perchlorates, sodium, silicon or calcium permanganates;
- a reducer - aluminium, calcium, silicon, manganate or their alloys;
- a binder - water-glass, cement, an organic binder;
- a reaction initiator - a burning up mixture - magnesium dust and sodium nitrate or barium peroxide with aluminium;
- a flux - calcium oxide or calcium fluoride.

Pure metals, ferroalloys or chemical compounds are sources of alloying elements. In case of exothermic chromium mixtures-chromium sources may be: ferrochromium, chromium concentrate (60 % Cr_2O_3 , 14% FeO), chromium trioxide, chromates, dichromates.

As a reducer an aluminium powder is used. It should fulfill two conditions:

- its grains' dimension should not transgress 0.3 mm;
- its' oxygen contents is max. 0.05 %.

A process of alloying elements conversion from the exothermic mixture to the liquid slag is connected with a chemical reaction course. The right effect requires a great surface of mixture factors, an uniform composition.

To get a mixture factors contact, its composition contains a binder which is the main source of smoke and dross coming to the slag.

Because of these reasons some other ways of factors connection are used where possible. In this work [2] agglomeration was applied. A salt recrystallization process can be used as well. In each method of exothermic mixture factors connection water is added as well as drying at the temperature range of 383 - 413 K is used.

A point lay-out initiator is also used. That procedure doesn't bring positive results to the reaction initiation. A volume lay-out initiator is used to reduce the mixture burning time [4]. Magnesium alloys can also be applied as factors of burning mixture. The burning of the exothermic mixture during the "out of the furnace" treatment succeeds as a result of its contact with liquid metal.

Not every mixture contains flux. In this work [8] the flux (fluorite) was added to accelerate a modifier assimilation grade of the liquid metal. Fluorite is also a factor of the self-fusible ferrochromium [9]. However, no flux is added to the mixture that consists of chromite.

Making full use of the above facts we can ascertain that the flux presence in the exothermic mixtures proclaims an open problem.

The exothermic mixtures composition should be assorted to have the exothermic reactions' thermal effect between the alloying

element's oxygen compounds and the reducer, the oxidizer and the initiating factor greater enough to cover the heat losses for the mixture heating up as well as for some of its factors fusion. The too great heat effect causes an impetuous reaction course which aggravates the industrial safety. However, the insufficient amount of emitted heat causes the temperature decrease of the melt as well as the decrease of the inserted elements' output [10].

Reviewed by: T. Liptáková, A. Sládek

Literatúra - References

- [1] BENESCH, R., JANOWSKI, J., MAMRO, K.: *Metallurgia želaza*, Podstawy fizyko chemiczne procesów. Wyd. Śląsk, Katowice 1979.
- [2] DURRER, R., FOLKERT, G.: *Metallurgia ferrosplavov*, tłum. z j. niemieckiego. Metallurgia, Moskva 1976.
- [3] LIKISEV N.P. i inni: *Aluminotermia*. Metallurgia Moskva 1978.
- [4] BORKOWSKI St.: *Obróbka żeliwa w kadzi tytano-chromo-aluminowymi egzotermicznymi mieszaninami*, Autoreferat pracy kandydackiej. Wyd. K P, Kijów 1978.
- [5] GIEREK, A., ZWOLIŃSKI, T., KATRA, J.: *Próby pozapiecowego wprowadzenia dodatków stopowych do ciekłych żeliw przy pomocy brykietów egzotermicznych*. Hutnik 2/1972.
- [6] WARCHALA, T., BORKOWSKI, St.: *Żeliwo niskochromowe uzyskiwane na drodze redukcji tlenków*. Sprawozdanie 1/1983 K. O. Politechniki Częstochowskiej.
- [7] WARCHALA, T., BORKOWSKI St.: *Aluminotermia w procesie otrzymywania żeliwa niskochromowego*. Archiwum Nauki o Materiałach, tom 9, zeszyt 2, 1988
- [8] ADAMCZYK, R. i inni: *Modyfikator złożony stosowany w procesie modyfikacji stopów żelaza*. Patent PRL nr 113556.
- [9] GIEREK, A. i inni: *Samotopliwy żelazochrom i sposób jego stosowania*. Patent PRL nr 67357.
- [10] BORKOWSKI St.: *Sterowanie jakością tworzyw odlewniczych na przykładzie żeliwa*. Wyd. Wydawnictwo Naukowo-Techniczne, Warszawa 1999.

Dušan Štekláč - Miroslav Neslušán *

PREROZDEĽOVANIE TEPLA PRI BRÚSENÍ TITÁNOVEJ ZLIATINY VT9

HEAT DISTRIBUTION WHEN TITANIUM ALLOY VT9 GRINDING

Prerozdeľovanie tepla pri obrábaní patrí medzi fenomenologické charakteristiky tohto procesu, pretože významne ovplyvňuje funkčné vlastnosti obrobených povrchov. Článok sa zaoberá prerozdeľovaním tepla v zóne rezania pri brúsení titánovej zliatiny VT9. Analýza prerozdeľovania tepla je tu založená na experimentálnom meraní teploty na brúsenom povrchu (teplota styku brúsneho kotúča a obrobnku) a tangenciálnej zložky reznej sily. Prerozdeľovanie tepla pri brúsení titánovej zliatiny je odlišné od prerozdeľovania tepla pri brúsení kalenej ložiskovej ocele 14 209.4 ako jedného z klasických predstaviteľov brúsených kalených ocelí predovšetkým pre veľmi nízku tepelnú vodivosť titánových zliatin.

Úvod

Titán a jeho zliatiny sú atraktívne materiály vzhľadom na jedinečný pomer medzi hmotnosťou a pevnosťou, ktorú si udržiavajú aj za zvýšených teplôt a ich výnimočnú odolnosť voči korózii. Titánové zliatiny sa zaraďujú medzi ťažkoobrábateľné materiály. Súčiastky vyrobené z titánových zliatin sú obyčajne vystavované únavovému zaťaženiu. Titán a jeho zliatiny sa najviac používajú v leteckom priemysle, kde sa používajú na rámy lietadiel a súčiastky motorov. Obrábanie s nízkymi hodnotami rezných parametrov obyčajne vedie k vysokým hodnotám únavovej pevnosti, ktorá je oveľa vyššia (takmer 5x) ako únavová pevnosť zodpovedajúca drastickým podmienkam obrábania [1]. Kahles a ost. [2] konštatovali, že povrch titánových zliatin sa ľahko poškodí počas operácií obrábania, predovšetkým počas brúsenia. Aj napriek tomu, že brúsenie je vykonávané správne v bežných rezných podmienkach, vedie k značnému zníženiu únavovej pevnosti vplyvom poškodenia povrchu.

Poškodzovanie povrchu pri brúsení je zväčša tepelne indukované a dane nielen teplotou, ktoré sa v zóne rezania vytvorí, ale aj teplotou povrchových vrstiev brúsených častí, jej gradientom a pomerom tepla vstupujúceho do obrobnku k celkovému vytvorenému teplu. Pri brúsení klasických ložiskových ocelí a aplikácii Al_2O_3 brúsneho kotúča väčšina tepla vstupuje do obrobnku (90 %) [3,4]. Je to dané kinematikou procesu a skutočnosťou, že tepelná vodivosť klasických ložiskových ocelí (46 W/m.K) je vyššia ako Al_2O_3 brúsneho kotúča ($6 \div 30$ W/m.K, široký rozsah prezentovaného).

Heat distribution in machining is one of phenomenological characteristics of this process because it significantly influences functional properties of machined surfaces. The paper deals with heat distribution in the cutting zone when grinding titanium alloy VT9 based on experimental measurement of surface temperature and tangential component of cutting force. Heat distribution when grinding titanium alloy VT9 differs from heat distribution when grinding conventional roll bearing steel 14 209.4 as a typical representative of ground hardened steels first of all because of low heat conductivity of titanium alloys.

Introduction

Titanium and its alloys are attractive materials due to their unique high strength-weight ratio that is maintained at elevated temperatures and their exceptional corrosion resistance. Titanium alloys are classified as difficult-to-machine materials. Machined parts made of titanium alloys are usually exposed to fatigue load because the major application of titanium has been in the aerospace industry, where it is used in airframes and engine components. Gentle machining operations usually result in a high cyclic fatigue strength that is much higher (up to nearly 5 times) than that of the corresponding abusive cutting conditions [1]. Kahles et al. [2] claim that the surface of titanium alloys is easily damaged during machining operations, especially during grinding. Even properly processed grinding practice using conventional parameters result in appreciably lower fatigue strength due to surface damage.

The damage of a workpiece when grinding is usually thermally induced and given not only by the heat generated in the cutting zone, but also by the temperature on the surface of a ground part, its gradient and the ratio of the heat entering the workpiece to the total heat. Most of energy enters the workpiece (90 %) when grinding conventional roll bearing steels and application alumina grinding wheel [3,4]. This is given by kinematical conditions and the fact that the heat conductivity of conventional roll bearing steels (46 W/m.K) is higher than alumina grinding wheel ($6 \div 30$ W/m.K, wide range of the presented values). Heat

* Doc. Ing. Dušan Štekláč, CSc., Dr. Ing. Miroslav Neslušán

Department of Technological Engineering, University of Žilina, Veľký diel, SK-010 26 Žilina, Slovak Republic,
Tel.: +421-89-513 2786, +421-89-513 2785, e-mail: neslusan@fstroj.uz.sk

vaných hodnôt). Prerodžovanie tepla pri brúsení titárovej zliatiny VT9 sa odlišuje od prerodžovania tepla pri brúsení klasických ložiskových ocelí vzhľadom na zlé tepelné vlastnosti titánových zliatin (tepelná vodivosť titánových zliatin je 7,5 W/m.K).

Metodika experimentov

Experimentálna analýza prerodžovania tepla je založená na „Teórii pohybujúcich sa tepelných zdrojov“ (Jaeger [5]). Tepelný zdroj konštantného tepelného toku na jednotku plochy q , dĺžky $2l$, sa pohybuje po povrchu polonekonečného nehybného telesa konštantnou rýchlosťou v_w . Tepelný zdroj je umiestnený do priesečníku osí x, z . Dvozmerný ustálený stav rozvrhnutia teploty pre takýto model je opísaný rovnicou (1)

$$\Theta \frac{\pi k v_w}{2q\alpha} = \int_{X-L}^{X+L} e^{-u} K_0 \{(Z^2 + u^2)^{0.5}\} du, \quad (1)$$

kde Θ - nárast teploty nad teplotu okolia ($^{\circ}\text{C}$),
 α - tepelná difuzivita (m^2/s),
 k - tepelná vodivosť ($\text{W}/\text{m.K}$),
 q - tepelný tok ($\text{m}^2.\text{kg}/\text{s}$),
 l - polovica dĺžky zdroja (m),
 K_0 - modifikovaná Besselová funkcia,
 u - merná energia brúsenia (J/m^3),
 X, Z, L - bezrozmerné veličiny ($X = v_w * x/2\alpha, Z = v_w * z/2\alpha, L = v_w * l/2\alpha$).

Takazawa numericky integroval rovnicu (1). Jej zjednodušený tvar je rovnica (2)

$$\Theta \frac{\pi k v_w}{2Rq\alpha} = 3.1L^{0.53} \exp(-0.69L^{-0.37} Z) \quad (2)$$

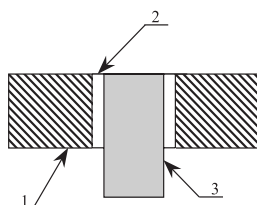
a rovnica pre teplotu na povrchu Θ_s ($z = 0$) je

$$\Theta_s = 0.947\alpha^{0.47} k^{-1} F_c R v_c v_w^{-0.47} l_c^{-0.47}, \quad (3)$$

kde R - koeficient prerodžovania tepla,
 F_c - tangenciálna zložka reznej sily (N),
 v_c - rezná rýchlosť (m/s),
 l_c - dĺžka kontaktu (m).

$F_c * v_c$ je celková energia, ktorá sa v zóne rezania vytvorí Q_c . Koeficient prerodžovania tepla R môže byť vypočítaný z rovnice (3), ak sa do nej dosadia namerané hodnoty Θ_s a F_c .

Meranie F_c bolo vykonané na piezoelektrickom dynamometri KISTLER súčasne s meraním teploty. Meranie teploty bolo vykonané prostredníctvom poloumelého termočlánku (obrázok 1) navrhnutého Peklenikom [6] a zdokonaleného Guom a Wagerom [7] (obe veličiny merané cez A/D kartu do PC).



Obr. 1 Termočlánok podľa Peklenika na meranie teploty,
 1 - obrobok, 2 - izolácia, 3 - vodič, 4 - spoj termočlánku, rozotrený kov
 Fig. 1 Peklenik method for measurement of temperature (1 - workpiece,
 2 - insulation, 3 - wire conductor, 4 - hot junction, smeared metal)

distribution when grinding titanium alloy VT9 differs from heat distribution when grinding conventional roll bearing steels because of poor thermal properties of titanium alloys (heat conductivity of titanium alloys is 7.5 W/m.K).

Experimental method

Experimental analysis of heat distribution is based on “Moving Heat Source Theory” (Jaeger [5]). The heat source of constant heat flux per unit area q , length $2l$, moves along the surface of a semi-infinite stationary body at a constant velocity v_w . The origin of coordinate axes x, z is at the center of the heat source. A two-dimensional, steady-state temperature distribution for this model is obtained as

$$\Theta \frac{\pi k v_w}{2q\alpha} = \int_{X-L}^{X+L} e^{-u} K_0 \{(Z^2 + u^2)^{0.5}\} du \quad (1)$$

where Θ - temperature rise above ambient ($^{\circ}\text{C}$),
 α - thermal diffusivity (m^2/s),
 k - thermal conductivity ($\text{W}/\text{m.K}$),
 q - heat flux ($\text{m}^2.\text{kg}/\text{s}$),
 l - half length of band source (m),
 K_0 - the modified Bessel function,
 u - specific grinding energy (J/m^3),
 X, Z, L - dimensionless quantities ($X = v_w * x/2\alpha, Z = v_w * z/2\alpha, L = v_w * l/2\alpha$).

Takazawa obtained a solution for the equation (1) by numerical integration. Its simplified form is

$$\Theta \frac{\pi k v_w}{2Rq\alpha} = 3.1L^{0.53} \exp(-0.69L^{-0.37} Z) \quad (2)$$

and the equation for a maximum temperature rise Θ_s ($z = 0$) is

$$\Theta_s = 0.947\alpha^{0.47} k^{-1} F_c R v_c v_w^{-0.47} l_c^{-0.47} \quad (3)$$

where R - energy partition,
 F_c - tangential force component (N),
 v_c - wheel speed (m/s),
 l_c - contact length (m).

$F_c * v_c$ is the total energy created in the cutting zone Q_c . The energy partition R can be calculated by substituting the maximum temperature rise Θ_s and the tangential grinding force F_c into equation (3).

The measurement of F_c was done by a piezoelectric KISTLER dynamometer together with the measurement of temperature. The temperature was measured by thermocouple technique (Fig. 1) introduced by Peklenik [6] and improved by Gu and Wager [7] (both quantities measured through A/D card to PC).

Podmienky experimentov: $v_c = 25$ m/s, $v_w = 4$ m/min, brúsny kotúč A99 60LVS, obrábané materiály boli titánová zliatina VT 9 (tepelná difuzivita $2,87 \cdot 10^{-6}$ m²/s, medza pevnosti $R_m = 900$ MPa, žihaná) a kalená ložisková oceľ 14 209.4 (tepelná difuzivita $12,4 \cdot 10^{-6}$ m²/s). Štruktúra zliatiny VT9 je tvorená α a β fázou. Jej chemické zloženie je uvedené v tabuľke 1.

The experimental conditions: $v_c = 25$ m/s, $v_w = 4$ m/min, grinding wheel A99 60LVS, machined materials titanium alloy VT 9 (thermal diffusivity $2.87 \cdot 10^{-6}$ m²/s, yield strength $R_m = 900$ MPa, after annealing) and hardened roll bearing steel 14 209.4 (thermal diffusivity $12.4 \cdot 10^{-6}$ m²/s). The structure of VT9 consists of α and β phase. Its chemical composition is in Table 1.

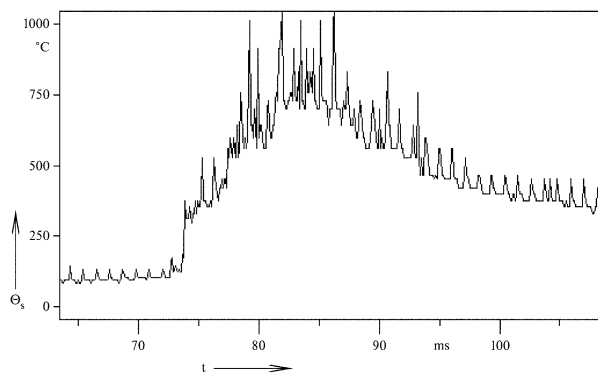
Chemické zloženie titánovej zliatiny VT9
Chemical composition of titanium alloy VT9

Tab. 1
Table 1

Element	Al	Mn	Si	Zr	O ₂	N ₂	H ₂	C	Fe
%	5.8 - 7	2.8 - 3.8	0.2 - 0.3	0.8 - 2.5	≤ 0.15	≤ 0.05	≤ 0.015	≤ 0.1	≤ 0.25

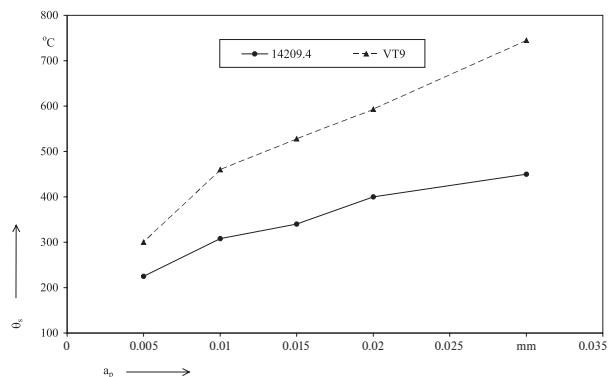
Výsledky experimentov

Experimental results



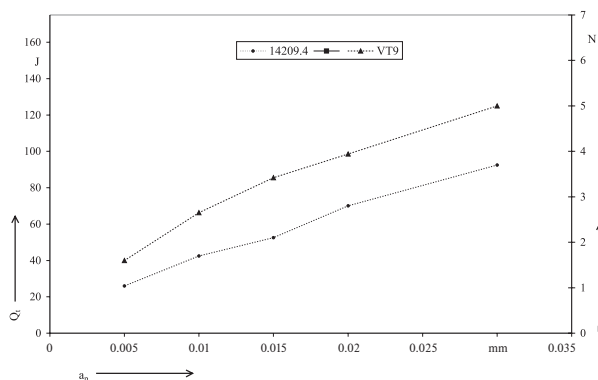
Obr. 2 Záznam teploty pri brúsení titánovej zliatiny VT9
($a_p = 0,03$ mm)

Fig. 2 Typical measured temperature rise when grinding titanium alloy VT9 ($a_p = 0.03$ mm)



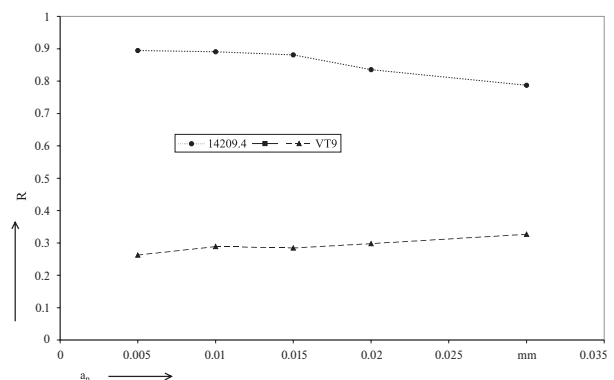
Obr. 3 Teplota na povrchu pre kalenú ložiskovú oceľ a titánovú zliatinu VT9

Fig. 3 Surface temperature for hardened roll bearing steel and titanium alloy VT9



Obr. 4 Celkové množstvo vyvinutého tepla Q_t a tangenciálna zložka reznej sily F_c pripadajúce na 1 mm šírky brúsenia

Fig. 4 Total heat Q_t and tangential component of grinding force F_c per 1 mm of grinding width



Obr. 5 Koeficient prerozdelenia tepla R

Fig. 5 Partition Ratio R

Teplota na povrchu Θ_s je maximum hladkej krivky preloženej cez nameraný záznam. Vplyv hĺbky rezu na túto teplotu je zobra-

The temperature on the surface Θ_s was obtained by putting a smooth curve through the measured trace. Figure 3 presents

zený na obrázku 3. Celkové množstvo vyvinutého tepla je dané meraním tangenciálnej zložky reznej sily a reznej rýchlosti, obrázok 4.

Koeficient prerozdeľovania tepla R (obrázok 5) je pomer množstva tepla vstupujúceho do obrobku k celkovému teplu, ktorý je možné vypočítať z rovnice (3) na základe nameraných Θ_s (obrázok 3) a tangenciálnej zložky reznej sily F_c (obrázok 4).

Diskusia a záver

Pri operáciách brúsenia sa takmer všetka energia brúsenia premieňa na teplo v zóne rezania. Pri brúsení bez aplikácie reznej kvapaliny je teplo zo zóny rezania odvádzané: obrobkom, brúsnym kotúčom a trieskou. Maximálne možné množstvo tepla odvádzané trieskou môže byť vyjadrené na základe objemu odobratého kovu, jeho hustoty, merného tepla a rozdielu medzi teplotou tavenia materiálu a teplotou okolia [8]. Na základe tejto úvahy maximálne množstvo tepla vstupujúceho do triesky je pre 14 209.4 približne 8 % a 4,5 % pre titánovú zliatinu. Veľké množstvo vyvinutého tepla vstupuje do obrobku, čo má za následok extrémne vysoké teploty v mieste styku brúsneho kotúča a obrobku.

Ako preukázali výsledky experimentov, malé množstvo tepla vstupuje do brúsneho kotúča pri brúsení kalených ocelí. Na druhej strane približne 65 % tepla je odvádzané brúsnym kotúčom pri brúsení titánovej zliatiny. Veľké mechanické a tepelné zaťaženie brúsných zŕn pri brúsení titánových zliatin má za následok zvýšenie intenzity opotrebovania brúsneho zrna a silnej adhézie obrábaného materiálu a brúsných zŕn. [9]. Maximálny nárast teploty pre titánovú zliatinu je oveľa vyšší ako pre kalenú oceľ, hoci množstvo energie vstupujúcej do titánovej zliatiny je menšie, vzhľadom na to, že tepelná vodivosť titánovej zliatiny je oveľa menšia (v porovnaní s kalenou oceľou).

Vysoká teplota a jej veľký gradient často vedie k tepelnému poškodeniu dokončovaných povrchov. Toto poškodenie môže byť indikované štrukturálnymi zmenami v povrchových vrstvách, zmenou mikrotvrdoosti, viditeľným opalom povrchu, vznikom trhlin alebo ťahovými zvyškovými napätiami. Tlakové napätie je žiaduce, pokiaľ ide o únavovú pevnosť, kým vzniku ťahových napätí je žiaduce sa vyhnúť. Ťahové zvyškové napätia pod brúsnym povrchom sú dané tepelnou expozíciou podpovrchových vrstiev, predovšetkým rozdielnym ohrievaním a ochladzovaním vrstiev rôzne vzdialených od povrchu. Rovnica (2) umožňuje vypočítať teplotu vo vrstvách pod povrchom (obrázok 6).

Gradient teploty je väčší pre titánovú zliatinu ako pre kalenú ložiskovú oceľ. Hoci teplo vstupujúce do titánovej zliatiny je nižšie ako teplo vstupujúce do kalenej ocele, teplota na povrchu a gradient teploty je vyšší. Povrch titánových zliatin je preto možné ľahko poškodiť počas operácií brúsenia, predovšetkým pri drastických podmienkach obrábania (vyššie hodnoty a_p), ktoré sa používajú v záujme zvýšenia produktivity výroby. Teplota na povrchu a energia vstupujúca do obrobku rastú s rastúcou hĺbkou rezu.

Aj napriek tomu, že teplota, ktorej je povrch súčiastok z titánových zliatin vystavený takmer neprekračuje prevádzkovú

a relation of surface temperature to a cutting depth. The total heat was determined by measuring a tangential force and wheel speed (Figure 4).

The partitioning ratio R (Figure 5) is the portion of the heat entering the workpiece to the total heat calculated by substituting the maximum temperature rise Θ_s from Figure 3 and the tangential grinding force F_c from Figure 4 into equation (3).

Discussion and conclusion

In grinding operation almost all the grinding energy is converted into heat within a small grinding zone. There are three significant heat sinks in dry grinding: workpiece, grinding wheel and grinding chips. The maximum possible heat entering grinding chips may be expressed in terms of the specific metal removal, the density, the specific heat capacity and the difference between the melting temperature and the ambient temperature [8]. On the basis of this assumption the maximum heat entering the grinding chips is about 8 % for 14 209.4 and about 4.5 % for titanium alloy. A large part of the generated heat flows into the workpiece, which results in extremely high temperatures at the interface between the wheel and the workpiece.

On the base of the experimental results it is possible to say that a small portion of energy enters the grinding wheel when grinding hardened steel. On the other hand about 65 % of heat is entering the grinding wheel when grinding titanium alloy. The high mechanical and thermal load of grains when grinding titanium alloy leads to a high grain wear rate and strong adhesion between a machined material and cutting grain [9]. The maximum temperature rise for titanium alloy is much higher than that of roll bearing steel, although the net energy input for titanium alloy is smaller than for hardened steel. This is because the thermal conductivity of titanium alloy is much smaller than that of the hardened steel.

The high temperature and its high gradient often lead to a thermal damage on finished surfaces. The damage can be indicated by structural changes in the surface layers, change of microhardness, visible surface burn, creation of cracks or tensile residual stresses. The compressive residual stress is beneficial when fatigue strength is being considered, while the tensile residual stresses should be avoided. Tensile residual stresses under the ground surface are given by a thermal exposition of layers under the surface, first of all different heating and cooling layers of different distance from the surface. Equation (2) enables to calculate temperatures in different layers under the surface (Figure 6).

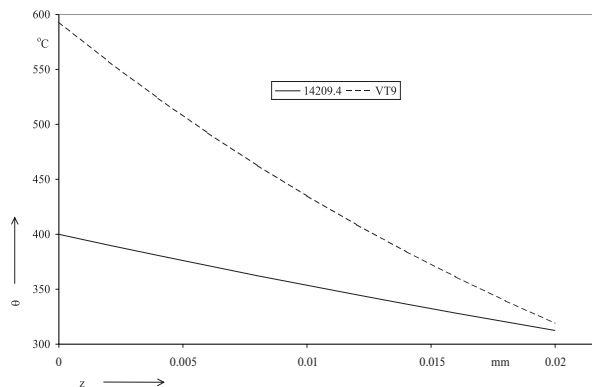
The temperature gradient for titanium alloy is much higher than that for hardened roll bearing. Although the heat entering the titanium alloy is lower than the one entering the hardened steel, surface temperature and temperature gradient are higher and so the surface of titanium alloys is easily damaged during grinding operations, especially during abusive cutting conditions (higher a_p) that are used to increase productivity. The surface temperature and energy entering the workpiece increase with the increase of a cutting depth.

Even though the surface temperature must not overcome the working temperature for the parts made of titanium alloys, the

teplotu, zvyškové napätia touto teplotou indukované môžu viesť k značnému zníženiu únavovej pevnosti vplyvom poškodenia povrchu.

Tepelnému poškodeniu brúsených povrchov súčiastok z titánových zliatin bez zníženia produktivity sa možno vyhnúť použitím brúsnych kotúčov na báze diamantu, alebo KNB, pri aplikácii ktorých rovnakou metódikou merania ako pri kotúči na báze Al_2O_3 sú teploty namerané na povrchu obrobku nižšie. Na druhej strane vysoká cena KNB a diamantových kotúčov limituje ich aplikáciu.

Recenzenti: K. Vasilko, S. Novák



Obr. 6 Teplota pod brúseným povrchom ($a_p = 0,02$ mm)
Fig.6 Temperature under the ground surface ($a_p = 0.02$ mm)

tensile residual stresses induced this temperature can result in appreciably lower fatigue strength due to a surface damage.

The use of diamond and CBN grinding wheels enables to reduce tendency for thermal damage of ground surfaces of parts made of titanium alloys without productivity decreasing. Surface temperatures for CBN and diamond grinding wheels measured by the same technique are significantly lower than those measured for Al_2O_3 . On the other hand, high costs of CBN and

diamond grinding wheels limit their application.

Reviewed by: K. Vasilko, S. Novák

Literatúra - References:

- [1] ZLATIN, N. - FIELD, M.: *Procedures and Precautions in Machining Titanium Alloys*, Titanium Science and Technology, 1 1973, p. 489-504.
- [2] KAHLES, J. F. - FIELD, M. - EYLON, D.- FROES, F. H.: *Machining of Titanium Alloys*, Journal of Metals, IV 1985, p. 27 - 35.
- [3] ROWE, W. B. - BLACK, S. C. - MILLS, B. - QI, H. S. - MORGAN, M. N.: *Experimental Investigation of Heat Transfer in Grinding*, CIRP 44/1/1995, p. 329-332.
- [4] KATO, T. - FUJII, H.: *Energy Partition in Conventional Surface Grinding*, Journal of Manufacturing Science and Engineering, 121/1999, p. 393-398.
- [5] JEAGER, J. C.: *Moving Source of Heat and the Temperature at Sliding Contact*, Proc. of the Royal Society of New South Wales, 76/1942, p. 203-224.
- [6] PEKLENIK, J.: *Ermittlung von geometrischen and physicalischen Kenngrößen für die Grundlagenforschung des schleifens*, PhD. Thesis, 1957, Aachen.
- [7] GU, D. Y. - WAGER, J. G.: *New Evidence on the Contact Zone in Grinding*, CIRP 37/1/1988, p. 335-338.
- [8] ROWE, W. B. - PETTIT, J. A. - BOYLE, A. - MORUZZI, J. L.: *Avoidance of Thermal Damage in Grinding and Prediction of the Damage Threshold*, CIRP 37/1/1988, p. 327-330.
- [9] VASILKO, K. - BOKUČAVA, G.: *Brúsenie kovových materiálov*, ALFA Bratislava 1988.

Karol Vasilko *

NOVÁ METODIKA NA ZOSTROJENIE ZÁVISLOSTI TRVANLIVOSTI NÁSTROJA NA REZNEJ RÝCHLOSTI

A NEW METHOD FOR DURABILITY DEPENDENCE OF A CUTTING TOOL ON A CUTTING SPEED

V celej histórii rozvoja teórie obrábania sa na opis závislosti medzi trvanlivosťou rezného nástroja a reznou rýchlosťou používa Taylorov vzťah, ktorý vznikol r. 1905. Predložená práca analyzuje doterajšie pokusy o vylepšenie tohto vzťahu. Návrh vyúsťuje do metódy zostrojenia $T-v$ závislosti, ktorá zabezpečuje výrazne lepšiu zhodu s experimentom. V druhej časti práce je metodika verifikovaná experimentálne na významnom počte typických príkladov.

1. Súčasný stav poznania a použitia $T-v$ závislosti

Najdôležitejšia zákonitosť obrábania-vzťah medzi trvanlivosťou rezného nástroja a reznou rýchlosťou je predmetom záujmu výskumných pracovníkov v celej histórii procesu poznávania obrábania ako technologickej metódy.

Už v r. 1905 Američan TAYLOR definoval priebeh tejto závislosti a zostrojil ju v dvojitej logaritmickú sústavu, pričom jej matematické vyjadrenie malo tvar:

$$T = \frac{C_T}{v^m} \quad (1)$$

kde C_T je trvanlivosť nástroja pri reznej rýchlosti $v = 1$ a m je tangens závislosti

V tomto tvare sa traktuje doteraz [2, 3, 5].

Od uvedenej doby bolo zaznamenaných oveľa viac úspešných alebo menej úspešných pokusov o presnejšiu definíciu a matematický opis tejto funkcie. V r. 1933 SAFONOV [4] definoval vzťah:

$$T = \frac{C_T}{v^{bv}} \quad (2)$$

kde b je konštanta.

Vzťah opisuje $T-v$ závislosť o niečo presnejšie, je však komplikovanejšia pre praktické použitie a nezahrňuje klesajúcu vetvu krivky.

Za úspešný pokus možno označiť prístup TEMČINA, ktorý v r. 1957 vylepšil Taylorov vzťah tým, že mu v menovateli pridal člen:

$$\frac{C_T}{v^m} \quad (3)$$

In the entire history of the development of the metal cutting theory Taylor's which appeared in 1905, has been used to describe the relation between a cutting tool durability and a cutting speed. This relation was established in 1905. This work presents the analysis of the up to now attempts carried out to improve the mentioned relation. The submitted proposal results in the method of creation of the $T-v$ relation, which provides a much better identity with the experiment. In the second part of the work the method is verified experimentally on a series of experimental results.

1. The current state of the $T-v$ relation and its use

The most important principle of cutting – a relation between the durability of a cutting tool and a cutting speed has been the subject of interest of research workers in the whole history of the process of a cutting acquisition as a technological method.

As early as in 1905, the American scientist TAYLOR defined the course of this relation and created it as a double logarithmic set; its mathematical formula was as follows:

$$T = \frac{C_T}{v^m} \quad (1)$$

The formula has been used up to now [2,3,5].

Since that time, there were many, more or less successful, attempts to provide a more precise definition and mathematical description of this function. In 1933 SAFONOV [4] defined the relation:

$$T = \frac{C_T}{v^{bv}} \quad (2)$$

The relation describes $T-v$ relation more precisely, however, it is more complicated for practical use and it does not comprise a declining curve.

In 1957 TEMČIN successfully improved the TAYLOR's relation by adding a term to a denominator:

$$\frac{C_T}{v^m} \quad (3)$$

* Prof. Ing. Karol Vasilko, DrSc.

Faculty of Production Technologies, Technical University of Košice, with the seat in Prešov, Plzenská 10, SK-080 01 Prešov
E-mail: vasilko@fvt.sk

kde T_m je maximálna hodnota trvanlivosti v celom rozsahu sledovaných rezných rýchlostí.

Celý vzťah potom nadobudne tvar:

$$T = \frac{C_T}{v^m + \frac{C_T}{T_m}} \quad (4)$$

Rozdiel oproti klasickému Taylorovmu vzťahu je ten, že pri malých hodnotách rezných rýchlostí veľkosťou prevažuje druhý člen v menovateli a vzťah konverguje k priamke, rovnobežnej s osou rezných rýchlostí. Naopak, pri dostatočne veľkej reznej rýchlosti je prvý člen v menovateli výrazne väčší ako druhý a vzťah sa transformuje na Taylorov.

Ďalší pokus sa vzťahuje k japonskému autorovi VU [8], ktorý v r. 1963 definoval vzťah:

$$T = \frac{C_T}{v^{b_0 + b_1 v}} \quad (5)$$

kde b_0 a b_1 sú konštanty.

V rovnakom roku GRANOVSKIJ [8] definoval vzťah:

$$T = a_0 + a_1 \cos y + a_2 \cos 2y + \dots + a_n \cos ny + b_1 \sin y + b_2 \sin 2y + \dots + b_n \sin ny \quad (6)$$

kde: $y = \frac{2\pi(v - v_o)}{v_n - v_o}$; pričom: $v_o \leq v \leq v_n$

KONEVŠOV a KSJUNINA [5] definovali v r. 1964 nasledovný vzťah:

$$T = 100e^{\sqrt{1 - b(\ln v - \ln v_{100})}} \quad (7)$$

Z ďalších pokusov si pozornosť zaslúži MATCHISEN, ktorý v r. 1965 odvodil vzťah:

$$T = \frac{C_T - av + bv^2}{v} \quad (8)$$

Tým sa však reťaz neuzatvára. Spomedzi novších riešení treba uviesť autorov KÖNIG a DEPEREUX [1] s modifikovaným vzťahom:

$$T = \frac{k}{(v + v_o)^z} \quad (9)$$

a poľského autora FTOREKA s tromi vzťahmi [1]:

$$\begin{aligned} T e^{av} &= D \\ T a^{av} &= E \\ T e^{(v + v_o)} &= H_o \end{aligned} \quad (10)$$

V r. 1981 BÉKÉS [1] publikoval vzťah:

$$T^{\frac{1}{p}} = C_o + C_1 v^{\frac{1}{q}} + C_2 f^{\frac{1}{r}} \quad (11)$$

where T_m is maximal value of durability in the whole range of cutting speeds.

The whole relation is then as follows:

$$T = \frac{C_T}{v^m + \frac{C_T}{T_m}} \quad (4)$$

Compared to the classical Taylor's relation, the difference lies in the fact that with small values of cutting speeds, the second in the denominator prevails and the relation converts to a straight line which is parallel to the axis of the cutting speeds. On the contrary, if the cutting speed is sufficient, the first term in the denominator is considerably bigger than the second term and the relation converts to the Taylor's one.

The next is connected with the name VU [8] who in 1963 defined the following relation:

$$T = \frac{C_T}{v^{b_0 + b_1 v}} \quad (5)$$

In the same year GRANOVSKIJ [8] defined the relation:

$$T = a_0 + a_1 \cos y + a_2 \cos 2y + \dots + a_n \cos ny + b_1 \sin y + b_2 \sin 2y + \dots + b_n \sin ny \quad (6)$$

where: $y = \frac{2\pi(v - v_o)}{v_n - v_o}$, while: $v_o \leq v \leq v_n$.

NONEVŠOV and KSJUNINA [5] defined the following relation in 1964:

$$T = 100e^{\sqrt{1 - b(\ln v - \ln v_{100})}} \quad (7)$$

MATCHISEN also deserves attention as in 1965 he defined the following relation:

$$T = \frac{C_T - av + bv^2}{v} \quad (8)$$

The chain, however, had not been closed by this. Newer solutions are connected with the following authors: KONIG-DEPEREUX [1] with a modified relation

$$T = \frac{k}{(v + v_o)^z} \quad (9)$$

and Polish author FTOREK with three relations [1]:

$$\begin{aligned} T e^{av} &= D \\ T a^{av} &= E \\ T e^{(v + v_o)} &= H_o \end{aligned} \quad (10)$$

In 1981 BÉKÉS [1] published the relation:

$$T^{\frac{1}{p}} = C_o + C_1 v^{\frac{1}{q}} + C_2 f^{\frac{1}{r}} \quad (11)$$

Do komplexu treba uviesť GRANOVSKÉHO [1], ktorý v r. 1985 uviedol nasledovný vzťah:

$$T = C_T v^h e^{-cv} \quad (12)$$

Zo súčasných pozícií predstavujú záujem najmä polynómy, s ktorými sa pomerne ľahko realizujú výpočty. Bez problémov sa diferencujú a sú známe aparáty na výpočet ich koeficientov a viac sú vhodné na použitie výpočtovej techniky.

Napriek uvedeným riešeniam možno pretrvávanie Taylorovho vzťahu zdôvodniť tým, že je jednoduchý pri praktických aplikáciách a to napriek argumentu, že súčasná výpočtová technika dokáže pracovať so vzťahmi ľubovoľnej zložitosti. Základným postulátom pri definícii klasického Taylorovho vzťahu je správna voľba kritéria otupenia, pri ktorom ho definujeme. Toto kritérium vychádza z použitia nástroja, ktorý pracuje pri reznej rýchlosti blízkej optimálnej, pre použitý rezný materiál. Je zrejme, že pri takejto voľbe nebudú ostatné rezné nástroje využité až do otupenia, teda nebudú využité ich rezné vlastnosti. Aplikácia NC obrábacích strojov, ktorá vedie k používaniu intenzívnych rezných podmienok a definovanej frekvencii výmeny nástrojov si žiada uplatniť nový pohľad na kritérium otupenia. V ideálnom prípade treba využiť každý nástroj do otupenia. V realizácii tohto cieľa postupujeme v ďalšom.

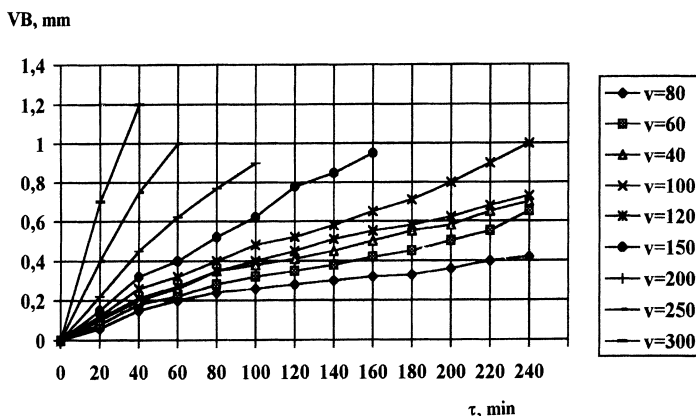
2. $T-v$ závislosť s konštantným kritériom otupenia

Ako je známe, klasický prístup k zostrojeniu $T-v$ závislosti spočíva v získaní experimentálnej krivky $VB = f(\tau)$ pri rozličných rezných rýchlostiach.

Zo sústavy kriviek sa odčítajú trvanlivosti nástrojov pri konštantnom kritériu otupenia. Na obr. 1 je sústava takýchto experimentálnych kriviek, získaná za podmienok:

- rezný materiál: SK P 20
- obrábaný materiál: oceľ 12 060.1
- nástrojový ortogonálny uhol čela: $\gamma_o = 0^\circ$
- nástrojový ortogonálny uhol chrbrta: $\alpha_o = 8^\circ$
- nástrojový uhol nastavenia: $\kappa_r = 60^\circ$
- uhol sklonu reznej hrany: $\lambda_o = 0^\circ$
- polomer zaoblenia hrotu noža: $r_\epsilon = 1$ mm
- $a_p \times f = 1 \times 0,31$ mm

Na obr. 2 je zodpovedajúca $T-v$ závislosť. Krivka je nahradená Taylorovým vzťahom tak, že tento platí v rozsahu rezných rýchlostí nad $200 \text{ m} \cdot \text{min}^{-1}$.



Obr. 1 Experimentálne krivky $VB = f(\tau_s)$

Fig. 1 Experimental curves $VB = f(\tau_s)$

To name all, in 1985 GRANOVSKIJ introduced the following relation [1]:

$$T = C_T v^h e^{-cv} \quad (12)$$

At present attention is especially drawn by polynomials, by the help of which calculations can be done easily. They are differentiated without any problems and there are apparatuses to calculate their coefficients. Moreover, they are suitable for the use of computer technique.

Leaving out of the account the mentioned solutions, the topicality of the Taylor' relation can be explained by the fact that it is simple for practical applications in spite of fact that the latest computing technique is able to work with relation of any difficulty.

The basis postulate of the definition of the classical Taylor's relation is correct choice of the blunting through which it is defined. This criterion is based on the use of a tool working at a cutting speed, which is close to an optimal one for a used cutting material. It is obvious that which such a choice the other cutting tools will not be utilized until blunting appears, i.e. their cutting properties will not be utilized. The application of NC cutting tools, which leads to the applications of intensive cutting conditions as well as a defined frequency of tool change, requires a new approach to blunt criterion of blunting. Each cutting tool should be utilized until it is blunt. The realization of this aim is shown in the following.

2. $T-v$ relation with constant blunt criterion

As it is known, the classical approach to a creation of the $T-v$ relation is based on obtaining an experimental curve $VB = f(\tau)$ with various cutting speeds.

From the set of curves the tools durability with a constant criterion of blunting is subtracted. In Fig. 1 there is a set of such experimental curves obtained under the following conditions:

- cutting material: P 20
- worked material: steel 12 060.1
- tool orthogonal race angle: $\gamma_o = 0^\circ$

- tool orthogonal back angle: $\alpha_o = 8^\circ$
- tool approach angle: $\kappa_r = 60^\circ$
- back slope angle: $\lambda_o = 0^\circ$
- point radius: $r_\epsilon = 1$ mm
- $a_p \times f = 1 \times 0.31$ mm

In Fig. 2 shows a corresponding $T-v$ relation. The curve is substituted by Taylor's relation so that it is valid within in the range of cutting speeds over $200 \text{ m} \cdot \text{min}^{-1}$.

Ako vidno, exponent $m = 5,7$, $C_v = 250$.

Odtiaľ: $C_T = C_v^m = 4,6 \cdot 10^{13}$.

Experiment ukazuje skutočnosť, že mimo oblasti, kde je krivka nahradená priamkou, sa pri aplikácii Taylorovho vzťahu dopúšťame rádovej chyby. To je vlastne dôvod záujmu autorov o túto problematiku.

As it can be seen, the exponent $m = 5,7$, $C_v = 250$.

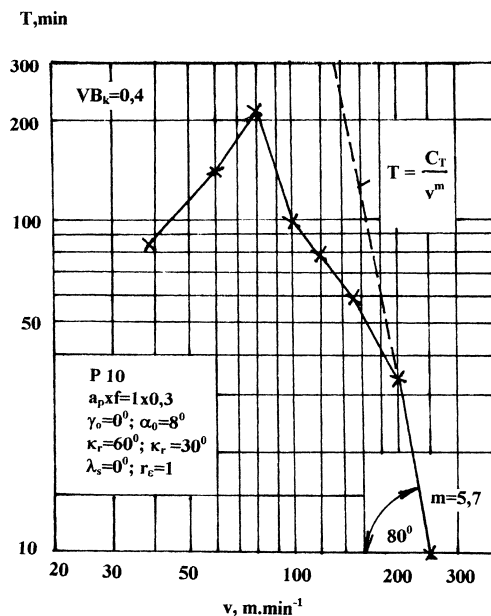
Hence: $C_T = C_v^m = 4,6 \cdot 10^{13}$.

The experiment shows that outside the areas where the curve is substituted by a straight line, we make a serious mistake in the applications of the Taylor's relation. This is in fact the reason why many authors are interested in this problem.

3. $T-v$ závislosť pri variabilnom kritériu otupenia

O možnosti, zostrojiť $T-v$ závislosť s variabilnými kritériami otupenia sa objavuje zmienka v monografii GRANOVSICH z r. 1985 [3]. Nebola však definovaná metóda, ako jednotlivé kritériá stanoviť. Bližšie štúdium veľkého množstva kriviek závislosti $VB = f(\tau)$ vedie k záveru, že existuje pomerne presne definované kritérium otupenia, ktoré sa aplikuje pri „optimálnej“ reznej rýchlosti podľa metód ZOREVA a LARINA. Možno reálne očakávať, že tieto metódy sa dajú uplatniť aj pri neúplných krivkách opotrebenia. Z toho vychádzajú aj ďalšie úvahy.

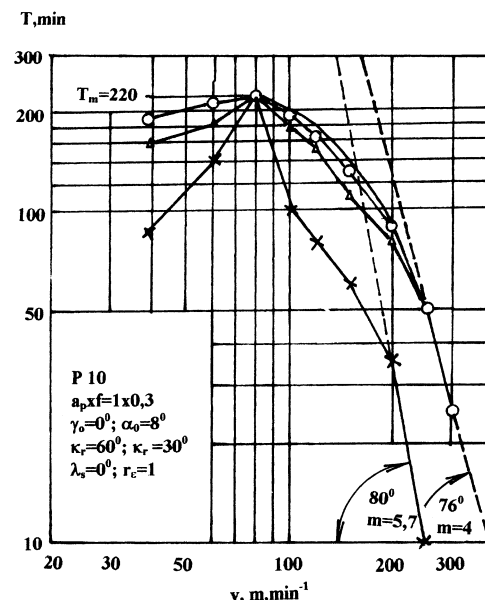
Zvoľme si pre pokus súbor kriviek z obr. 1. Pri reznej rýchlosti $80 \text{ m} \cdot \text{min}^{-1}$ je kritérium otupenia vizuálne zrejme a je v tom prípade $VB_k = 0,4 \text{ mm}$. Ak od tohto bodu preložíme priamku smerom k podobnému bodu na krivke pre rýchlosť $60 \text{ m} \cdot \text{min}^{-1}$ a ďalej, ohraničili sme „intuitívne“ kritérium otupenia aj pre ostatné rezné rýchlosti. Ak podľa nich zostrojíme krivku $T-v$, bude sa výrazne odlišovať od obr. 2. Jej priebeh je na obr. 3 (trojuholníky). Pri identifikácii uhla sklonu $T-v$ závislosti a exponentu m zistujeme, že je menší. Ďalší rozdiel spočíva v tom, že pri menších rezných rýchlostiach ($40 - 60 \text{ m} \cdot \text{min}^{-1}$) sú zaznamenané vyššie hodnoty trvanlivosti, ako pri klasickom postupe. Maximum trvanlivosti je menej výrazné. Všetky tieto odlišnosti sú sprievodným znakom vyššieho kritéria otupenia, prakticky v celom rozsahu rezných rýchlostí.



Obr. 2 $T-v$ závislosť, získaná z obr. 1
Fig. 2 $T-v$ relation, obtained from Fig. 1

3. $T-v$ relation with a variable criterion of blunting

The possibility of creation of the $T-v$ relation with a variable criteria of blunting appears in the monograph by GRANOVSICH, 1985 [3]. However the method how to determine different criteria was not defined. Closer studies of a large number of the relation curves $VB = f(\tau)$ lead to the conclusion that there is a relatively precise definition of the criterion of blunting which is applied with the “optimal” cutting speed according to the methods of ZOREV and LARIN. It can be actually expected that those methods can also be used also for incomplete wear curves. The following approaches are based on the above mentioned conclusions.

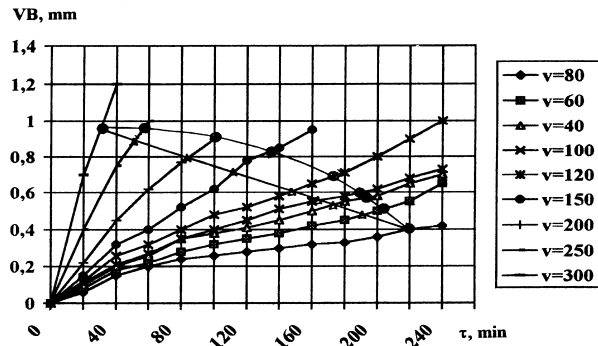


Obr. 3 $T-v$ závislosti pri konštantných a variabilných kritériách otupenia
Fig. 3 $T-v$ relation during constant and variable wear criteria

For the experiment, let us choose the set of curves from Fig.1. With the cutting speed $80 \text{ m} \cdot \text{min}^{-1}$ the criterion the blunting is visually evident, and in this case it is $VB_k = 0.4 \text{ mm}$. If we draw a straight line from this point towards a similar point on the curve for speed $60 \text{ m} \cdot \text{min}^{-1}$ and further on, we also bordered “intuitive” criterion of blunting for other cutting speeds. If we draw a $T-v$ curve according to this, it will be very different from Fig. 2. Its course is in Fig. 3 (triangles). At the identification of the slope angle of the $T-v$ relation and the exponent m , we find out that it is smaller.

The next difference is that with smaller cutting speeds (40 to $60 \text{ m} \cdot \text{min}^{-1}$), higher durability than during a classical process are recorded. Durability maximum is less significant. All the differences is an

Pokúsme sa zvoliť kritériá otupenia odlišne. Na obr. 4 je hranicou kritérií kružnica. Zodpovedajúca $T-v$ závislosť je na obr. 3. Vznikla plynulejšia krivka, pričom exponent m má rovnakú hodnotu. Tento postup napovedá, že sa bližšie ku správemu kritériu otupenia.



Obr. 4 Lineárne a kruhové kritérium otupenia
Fig. 4 Linear and arched weak criterion

accompanying feature of a higher criterion of blunting practically in the whole range of cutting speeds.

Let us try to choose the criteria of blunting differently. In Fig. 4 the border of criteria is a circle. The corresponding $T-v$ relation can be seen in Fig. 3. A more fluent curve was created, while the exponent m has the same value. This approach indicates that we are approaching the correct criterion of blunting.

3.1. Zovšeobecnený opis $T-v$ závislosti

Z obr. 3 vidno, že aplikácia klasického Taylorovho vzťahu by neprinesla pokrok oproti doterajším postupom. Preto na opis $T-v$ závislosti sa použil TEMČINOV vzťah (4), ktorý bol úspešne aplikovaný aj v ďalších doterajších prácach [6, 8, 9, 10]. Jeho prednosťou je skutočnosť, že je postavený na Taylorovom vzťahu, čím je jeho užívateľom blízky.

Dôležité je stanoviť hodnotu T_m , ako maximálnu trvanlivosť, ktorá sa dosiahne v celom rozsahu rezných rýchlostí. Jej stanovenie súvisí s tým, ako presne sa odhadne rezná rýchlosť, ktorej zodpovedá maximálna trvanlivosť a pri nej sa vykoná experiment.

V predchádzajúcom experimente bola táto hodnota reznej rýchlosti pre rezný materiál P 10 zhodou okolností odhadnutá presne (80 m.min^{-1}).

Druhým dôležitým parametrom je konštanta C_T . Treba upozorniť, že v tomto prípade má iný význam, ako u klasickej Taylorovej závislosti, teda nie je to už úsek na osi trvanlivosti. Táto skutočnosť žiada stanoviť C_T analyticky. Po úprave Temčinovho vzťahu dostávame:

$$C_T = \frac{T_v^m T_m}{T_m - T} \quad (13)$$

T a v sú konkrétne hodnoty trvanlivosti a reznej rýchlosti, odčítané z klesajúcej vetvy krivky a to z jej úseku, kde už predpokladáme platnosť Taylorovho vzťahu. V sledovanom prípade boli dosadené hodnoty: $v = 300$, $T = 25$, $T_m = 220$, $m = 4$, čo po dosadení dáva: $C_T = 2,3 \cdot 10^{11}$.

Po dosadení do vzťahu (4) možno pre ľubovoľné zvolené v vypočítať T . Výsledok je nasledovný:

$v, \text{m.min}^{-1}$	39	60	80	100	120	150	200	250	300
T, min	220	219	214	203	185	149	87	40	25

Na obr. 3 je takto vypočítaná krivka znázornená plnou čiarou. Vidno veľmi dobrú zhodu tejto krivky s experimentom, neporovnateľne väčšiu, ako pri aplikácii Taylorovho vzťahu. Analýza via-

3.1 Generalized description of $T-v$ relation

From Fig. 3 it can be seen that the application of the classical Taylor's relation would not lead to any progress when compared to the up to now approaches. Therefore, to describe $T-v$ relation the Temčín's relation was used (4). It was successfully applied also in other up to the present works [6, 8, 9, 10]. The advantage of this relations the fact that it is based on the Taylor's relation and therefore it is well known to the users.

It is important to determine T_m value as maximum durability which can be obtained within the entire range of cutting speeds. Its determination depends on the accuracy of the cutting speed estimate which corresponds with the maximum durability. The experiment is carried out under the mentioned conditions.

In previous experiment the value of the cutting speed for the cutting material P 10 was by a coincidence precisely estimated (80 m.min^{-1}).

Another important parameters is the constant C_T . It should be noted that in this case it has different meaning when compared to the classical Taylor's relation, i.e., this is not a section on durability axis. This fact requires that C_T is determined analytically. After the Temčín's relation is modified we obtain:

$$C_T = \frac{T_v^m T_m}{T_m - T} \quad (13)$$

T and v are particular values of both a durability and a cutting speed which are subtracted from a declining branch range of the curve in the section where the validity of the Taylor's relation is expected. In the observed case, there were the following values used: $v = 300$, $T = 25$, $T_m = 220$, $m = 4$, which after the substitution is $C_T = 2,3 \cdot 10^{11}$.

After substitution to the relation (4), it is possible to calculate T for any optional v . The result is as follows:

In Fig. 3, the curve calculated this way is represented by a bold line. A very good coincidence of this curve with the experiment is evident, it is incomparably higher than with the applica-

cerých prípadov ukázala, že maximálna chyba je len 8 %. Táto skutočnosť dáva reálnu nádej na aplikáciu použitého vzťahu v praxi.

3.2 Exaktné kritériá otupenia

Voľba kritérií otupenia podľa predchádzajúceho postupu sa vyznačuje nepresnosťou a subjektivitou. Preto cieľom ďalších aktivít bolo nájsť exaktnejší postup. Návodom sa stal LARINOV postup stanovenia optimálneho otupenia [7]. Ako je známe, tento postup spočíva v nasledovnom:

Je potrebné definovať hrúbku reznej platničky „ b “, ktorú možno odstrániť pri preostrovaní. Pre tento účel môže byť volená ľubovoľne, pretože nám nejde o konkrétnu hodnotu počtu preostrení, ale hľadané lokálne maximum.

Pre zvolené hodnoty kritéria otupenia (napr. 0,1; 0,2; 0,3 ... mm) sa určí teoretický počet preostrení nástroja „ n “, podľa vzťahu:

$$n = \frac{b}{VB_k} \quad (14)$$

Napr.: Ak hodnota, ktorú možno z platničky odbrúsiť je 3 mm, bude počet preostrení pre jednotlivé VB_k nasledovný:

VB_k	0,1	0,2	0,3	0,4	0,5	0,6	0,7	0,8	0,9	1
n	30	15	10	7,5	6	5	4,3	3,8	3,3	3

Pochopiteľne, n nemusí byť celé číslo.

V ďalšom sa zostrojí závislosť: $nT=f(VB_k)$ pre každú reznú rýchlosť, pričom T je vždy zodpovedajúca trvanlivosť pri konkrétnom VB_k a v .

Tento postup bol uplatnený pre niektoré krivky z obr. 1. Výsledok je na obr. 5. Ide v podstate o závislosť životnosti nástroja na zvolenom kritériu VB_k . Z každej krivky je vyhodnotené maximum a jemu zodpovedajúce optimálne VB_k . Hodnoty konkrétnych VB_k sú spätne vynesené na krivky opotrebenia a dostávame situáciu podľa obr. 6.

Je vidieť, že predchádzajúce pokusy sa len približili k tejto situácii. Zatiaľ nie je cieľom určiť rovnicu tejto čiary. Dôležité je, že tento postup možno považovať za exaktný, pretože berie do úvahy reálne zákonitosti procesu obrábania.

Komplexný výsledok je na obr. 7, kde je krivka závislosti $T-v$ vytvorená na základe obr. 6 a jej vyhodnotenie podľa uvede-

tion of the Taylor's relation. The analysis of several cases showed that the maximum error was only 8 percent. This fact leads to the conclusion that there is much hope of the application of used relation in the practice.

3.2 Exact criteria of blunting

The choice of the criteria of blunting according to the previous method is accompanied by inaccuracy and subjectivity. Therefore, the aim of further activities was to find more exact approach. It appeared that the forgotten Larin's approach could be the method of determination of the optimal blunting [7]. As we know, this approach is based on the following.

It is necessary to define thickness of the cutting plate „ b “ which can be removed during the re-sharpening. For this purpose it can be chosen freely because we do not consider a concrete value of the re-shapening number, but the we searched local maximum.

For the chosen values of the criterion of blunting (e.g. 0.1; 0.2; 0.3 ... mm) a theoretical number of re-sharpenings of a tool „ n “ is determined according to the relation:

$$n = \frac{b}{VB_k} \quad (14)$$

For example: If the value which can be removed from the plate by grinding is 3 mm, the number of the re-sharpening for the individual VB_k is as follows:

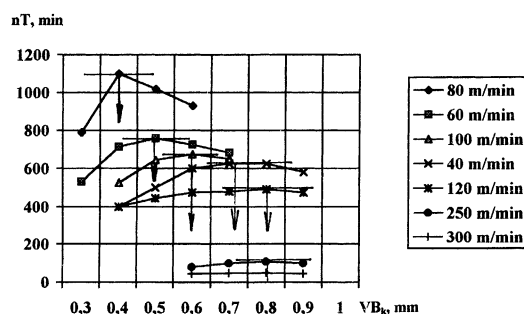
Of course, n does not have to be a whole number.

In the following the relation is determined for each cutting speed: $nT = f(VB_k)$ whereas T is always a corresponding durability of a concrete VB_k and v .

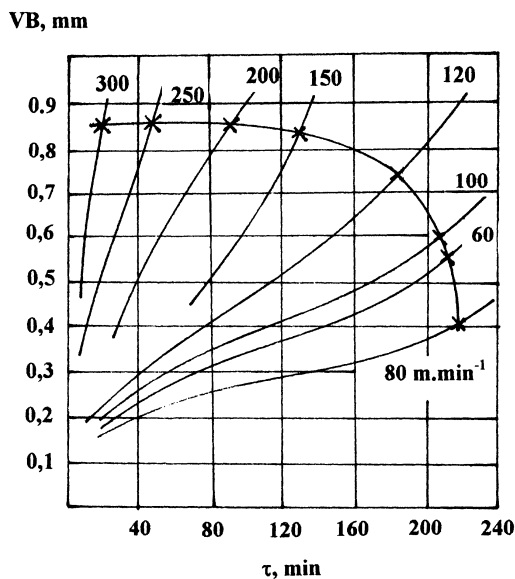
This approach was applied to some curves from Fig. 1. The result is shown in Fig. 5. Basically, it refers to the dependence of the tool durability upon the chosen VB_k criterion. Of each curve, the maximum and a corresponding optimal VB_k is evaluated. The values of concrete VB_k are given back on the curves of wear and we obtain a situation according to Fig. 6.

It can be seen that previous tests were only approaching this situation. So far the aim is not to create the equation of this line. It is important that this approach can be considered as an exact one because into account the realistic principles of the cutting process.

A complex result can be found in Fig. 7, where the curve of $T-v$ is created on the base of Fig. 6 and its evaluation is done according to the



Obr. 5 Krivky závislosti životnosti nástroja od kritéria otupenia
Fig. 5 Relation curves of tool durability on wear criterion



Obr. 6 Závislosť $VB = f(\tau)$ s kritériami otupenia z obr. 5
Fig. 6 Relation $VB = f(\tau)$ with wear criteria from Fig. 5

ného postupu. Chyba nie je väčšia, ako je rozptyl nameraných hodnôt trvanlivosti.

V súvislosti s týmto výsledkom sa natiska možnosť aplikovať túto novú $T-v$ závislosť na bežné výpočty v technológii obrábania. Takto by bolo možné spresniť pojem obrábatelnosť materiálu a reznosť nástroja.

V ďalšej sérii skúšok sa budeme venovať verifikácii naznačeného postupu v rozličných prípadoch obrábania a stanovenia metodiky zostrojenia exaktnej $T-v$ závislosti.

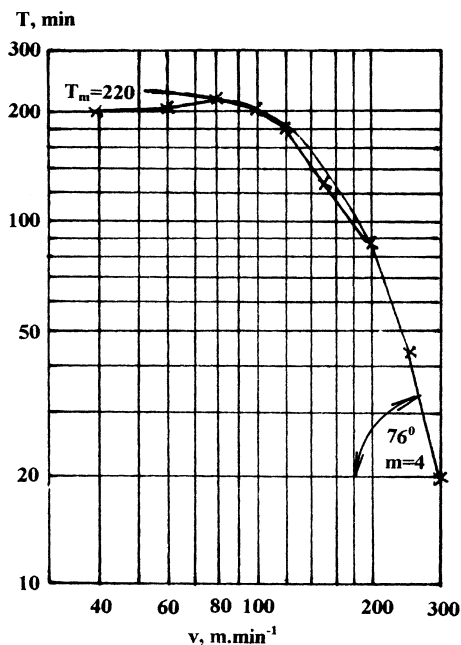
3.3 Verifikácia postupu zostrojenia $T-v$ závislosti a návrh metodiky

Na obr. 8 je priebeh piatich kriviek opotrebenia, ktoré boli získané v uvedených podmienkach. V spodnej časti je diagram závislosti: $nT = f(VB)$, s vyhodnotením jednotlivých VB_k .

Na obr. 9 je výsledná $T-v$ závislosť, pričom krúžkami sú znázornené experimentálne hodnoty. Výsledok je v podstate zhodný s predchádzajúcim. Napriek menšiemu počtu rezných rýchlostí je $T-v$ závislosť dostatočne presná. Naznačuje to možnosť zmenšit rozsah experimentálnych skúšok.

Na obr. 10 je súbor štyroch kriviek opotrebenia, získaných podrobným meraním (po 10 minútach obrábania).

V dolnej časti je diagram $nT = f(VB)$ pri troch rezných rýchlostiach. Zhoda je podobná ako v predchádzajúcich prípadoch.



Obr. 7 $T-v$ závislosť, získaná z obr. 6
Fig. 7 $T-v$ relation obtained from Fig. 6

given method. The error is not more important than the dispersion of the measured durability values.

Referring to this results, the possibility of the application of this new $T-v$ relation with the common calculations of the cutting technology appears. Thus, it would be possible to specify the term "cutting" of the material as well as a "cutting tool efficiency".

The following series of tests deals with the verification of the outlined procedure with the various cases of cutting and the determination of the methodology of the creation of the exact $T-v$ relation.

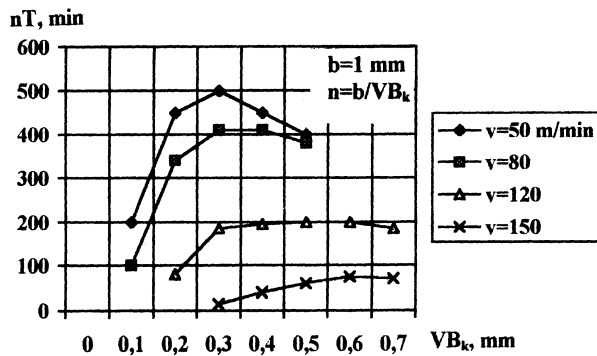
3.3 Verification of the creation procedure of the $T-v$ relation and the methodology proposal

Fig. 8 shows the course of the five wear curves which were obtained under the given conditions. In the lower part, there is a diagram of the relation $nT = f(VB)$ with the individual VB_k evaluation.

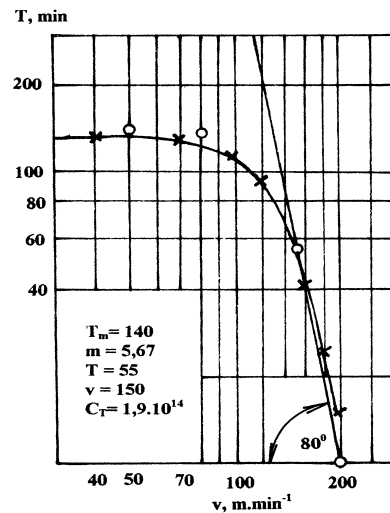
In Fig. 9 there is a final $T-v$ relation while the circles mark the experimental values. The result is, in fact, identical with the previous one. In spite of a lower number of cutting speeds, the $T-v$ relation is sufficiently precise. It shows the possibility of decreasing range of experimental tests.

In Fig. 10 there is a set of four wear curves obtained by a detailed measuring (after 10 minutes of cutting).

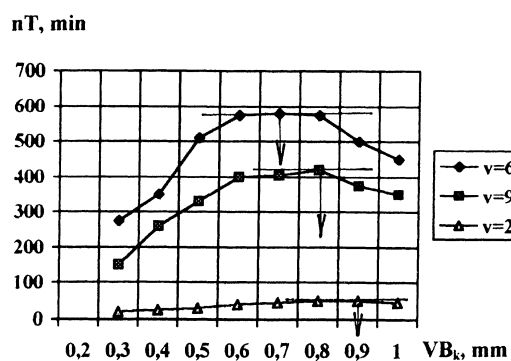
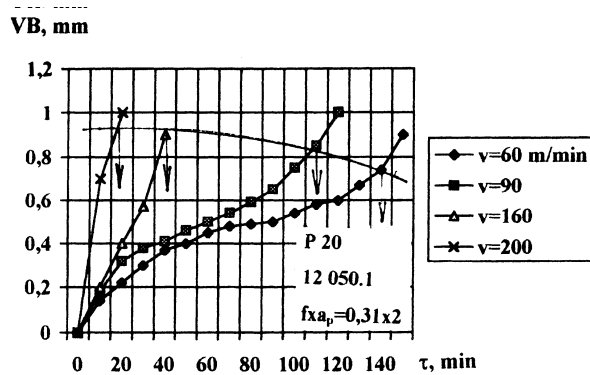
In the lower part, there is a diagram $nT = f(VB)$ with 3 cutting speeds.



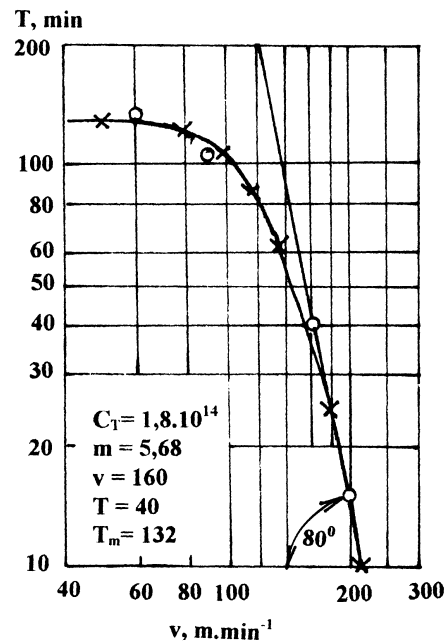
Obr. 8 Experimentálne krivky $VB = f(\tau)$ a $nT = f(\tau)$
Fig. 8 Experimental curve $VB = f(\tau)$ and $nT = f(\tau)$



Obr. 9 Závislosť $T = f(v)$
Fig. 9 Relation $T = f(v)$



Obr. 10 Iný príklad experimentálnej závislosti
Fig. 10 Other case of experimental relation



Obr. 11 Ďalší príklad experimentálnych výsledkov
Fig. 11 Next case of experimental results

Ďalší príklad experimentu je na obr. 11. Ukazuje na ďalšiu možnosť skrátenia skúšok, ktorá spočíva v nasledovnom:

- zostrojiť krivku opotrebenia pri reznej rýchlosti, ktorú pre daný rezný materiál podľa skúseností a údajov výrobcu možno považovať za optimálnu, dávajúcu maximálnu trvanlivosť. Z tejto krivky možno stanoviť T_m a VB_k ,

Another example of the experiment is in Fig. 11. It shows another possibility of the tests shortening which lies in the following:

- to set a wear curve at a cutting speed which for a given cutting material, according to the experience as well as the information from the producer, can be considered as optimal and, at the same time, providing a maximum durability. This curve is used to derive T_m and VB_k ,

- zostrojíť dve krivky opotrebenia pri rezných rýchlostiach, výrazne vyšších od v_1 . Z kriviek možno určiť VB_k (pre obe rezné rýchlosti) a m .

Na obr. 12 je $T-v$ závislosť.

V ďalšom príklade je pokus o overenie metodiky s použitím troch kriviek opotrebenia. Na obr. 13 sú krivky opotrebenia pri rôznych rezných rýchlostiach: 70, 100 a 130 $\text{m}\cdot\text{min}^{-1}$. Ako obrábaný materiál bola použitá vývojová oceľ pre valivé ložiská (NLO), ktorá má vyššiu pevnosť a asi o triedu horšiu obráбатeľnosť sústružením ako klasická (14 109.3) - obr. 9. Z hľadiska metodiky skúšok vidno, že nebolo potrebné sledovať krivku opotrebenia nad $VB = 0,4$ mm. Skúšky pri vyšších rezných rýchlostiach vyžadovali pomerne krátky čas.

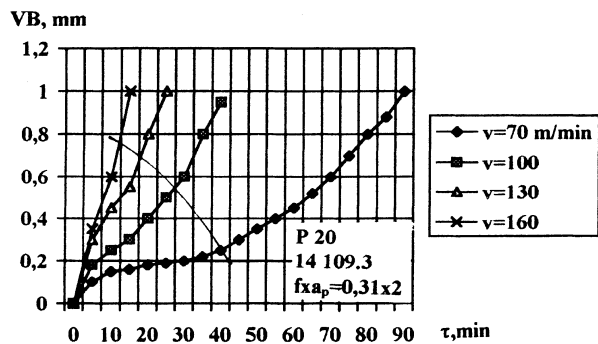
Krivky pre $z = nT = f(VB)$ boli zostrojené len prvé dve rezné rýchlosti, čo na základe skúseností postačuje na zostrojenie $T-v$ závislosti, ktorá je na obr. 14.

- to set two wear curves with cutting speeds which are much higher than v_1 . The curves are used to determine VB_k (for both cutting speeds) and m .

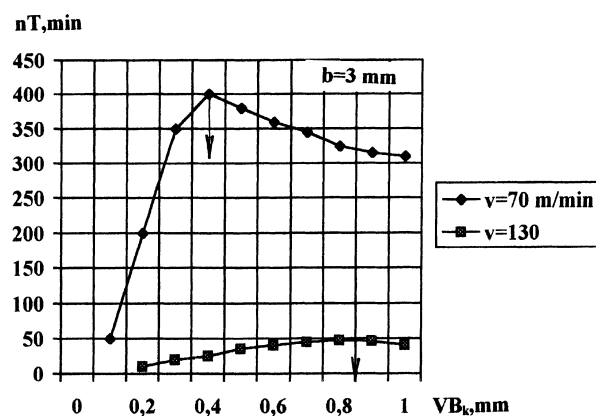
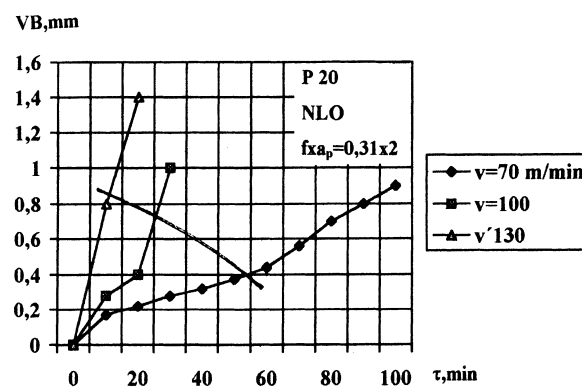
In Fig. 12 there is the $T-v$ relation.

The following example presents a test which was carried out to verify the methodology with the use of three wear curves. In Fig. 13 there are wear curves at different cutting speeds 70, 100 and 130 $\text{m}\cdot\text{min}^{-1}$. As a cutting material, research steel for bearing parts (NLO) was used. This steel has a higher strength and is approximately one class worse as regards workability by turning than the classical one (14209.3) - Fig. 9. From the point of view of the methodology of tests it follows that it was not necessary to observe the wear line over $VB = 0.4$ mm. The tests with higher cutting speeds required relatively short time.

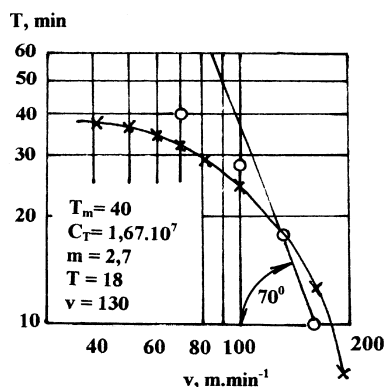
Curves for $z = f(VB)$ were created only for two cutting speeds which is sufficient for creation of the $T-v$ relation which is in Fig. 14.



Obr. 12 $T-v$ závislosť
Fig. 12 $T-v$ relation



Obr. 14 $T-v$ závislosť
Fig. 14 $T-v$ relation



Obr. 13 Experimentálna závislosť $VB = f(\tau)$ a $nT = f(VB)$
Fig. 13 Experimental relation $VB = f(\tau)$ and $nT = f(VB)$

4. Záver

Naznačený postup na získanie $T-v$ závislosti možno úspešne použiť miesto klasickej skúšky pri konštantnom kritérii otupenia. Pritom časové a materiálové nároky na jeho realizáciu zodpove-

4. Conclusion

The outlined procedure of obtaining the $T-v$ relation can be successfully used instead of a classical test with a constant criterion of blunting. At the same time, the material and the time require-

daju napr. známej skúške BEZPROZVANNÉHO, alebo skúške pri zmenšenom kritérii otupenia. Oproti nim sa však navrhnutý postup vyznačuje výrazne väčšou presnosťou.

Recenzenti: J. Zongor, J. Salaj

ments for its realization correspond with, for example, a well known test of BEZPROZVANNYJ, or a test with a lower criterion of blunting. Comparing to them, the suggested approach shows a considerably higher accuracy.

Reviewed by: J. Zongor, J. Salaj

5. Literatúra - References

- [1] BÉKÉS, J.: *Inžinierska technológia obrábania kovov*. Bratislava Alfa, 1981, 398 s.
- [2] BUDA, J., SOUČEK, J., VASILKO, K.: *Teória obrábania*. Bratislava Alfa, 1988, 391 s.
- [3] DMOCHVSKI, J.: *Podstawy obróbki skawaniem*. Warszawa. Państwowe wydawnictwo naukowe, 1987, 586 s.
- [4] GILMAN, A. M. et al.: *Optimizacija režimov obrabotki na metallořežuščich stankach*. Moskva: Mašinstrojenije, 1975, 304 s.
- [5] GRANOVSKIJ, G. I., GRANOVSKIJ, V. G.: *Rezanije metallov*. Moskva: Mašinstrojenije, 1975, 304 s.
- [6] KLUŠIN, M. I.: *Obobščennyje zavisimosti dlja razčeta režima rezanija*. In: *Fizika rezanija metallov*. AN Armenskoj SSR, Jerevan, 1971
- [7] LARIN, M. N.: *Osnovy frezerovanija*. Moskva. Mašgiz, 1947
- [8] PODURAJEV, V. N.: *Avtomatičeskije regulirujemyje i kombinirovannyje processy rezanija*. Moskva: Mašinstrojenije, 1977, 302 s.
- [9] VASILKO, K., HRUBÝ, J., LIPTÁK, J.: *Technológia obrábania a montáže*. Bratislava: Alfa, 1991, 494 s.
- [10] VASILKO, K., BOKUČAVA, G.: *Presnejšie vyjadrenie T-v závislosti*. *Náradie* 19, 1989, č. 4
- [11] ZOREV, N. N.: *Metod opredelenija optimal'nogo iznosa i optimal'noj stojkosti po krivym iznosa*. *Stanki i instrument*, 1949, č. 8.

Jaroslav Koutský *

PRÍSPEVOK K MODELOVANIU OPTIMALIZÁCIE FORMOVANIA A TEPELNÉHO SPRACOVANIA KONŠTRUKČNÝCH OCELÍ

CONTRIBUTION TO MODELLING OF THE OPTIMIZATION OF FORMING AND HEAT TREATMENT OF STRUCTURAL STEELS

Na Katedre materiálov a strojárenskej metalurgie Západočeskej univerzity v Plzni bolo vytvorené nové laboratórium technologických procesov modelovania, vybavené dvoma stanicami Silicon Graphic Indigo R 5000, jednou stanicou 500AU DEC OSF/1 so systémami Forge 2D a 3D, Hypermesh a Systus & Sysweld. V rámci vedeckovýskumných projektov boli vykonané práce z oblasti modelovania optimalizácie technologických procesov, napr. simulácia vplyvu studeného tvarovania na štruktúru ocele P9000 alebo simulácie voľného kovania pri výrobe hriadelov z CrMo ocele. Čiastočné výsledky preukazujú dobrú zhodu medzi experimentálnymi výsledkami a simuláciou.

New laboratory of technological processes modelling, equipped with two Silicon Graphic Indigo R 5000 stations, one 500au DEC OSF/1 station with software systems Forge 2D and 3D, Hypermesh, Systus and Sysweld, was built up at the Department of Material Science and Technology at WBU Plzeň. Some research projects aimed at the modelling and optimization of technological processes, e. g. simulation of cold deformation influence on the structure of P900 steel, or simulation of free forging of shafts manufactured from CrMo steel were carried out. Partial results give a good agreement between experimental results and simulation.

1. Introduction

Recently the influence of external effect of the environment on material properties - influence of thermal exposition, stress, chemical effect, magnetic field, etc. - was solved above all by the manner indicated in Fig. 1.

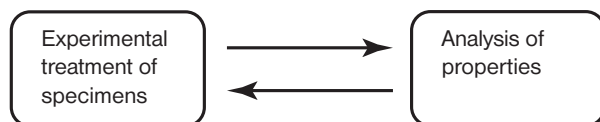


Fig. 1

Without any doubts laboratory experiments save costs of real technological processes but the verification of correct technology by experimental tests and analyses which follow, spends time, money and human capacity. That's a reason why simulation programmes, appearing in the last decades, which allow quantitative and qualitative description and graphical monitoring of processes passing in solid, liquid and gaseous systems, have found a broad application. If a simulation programme reflects the system in which the process occurs with sufficient accuracy, calculated values approach to those determined by experiments. This is the way how to make the optimization of technology more efficient.

The modelling of optimum technology development can be demonstrated as follows. In the case of good agreement between

calculated and tested properties, a great part of experimentally verified technological processes can be modelled and thus the number of real tests rapidly decreased.

Each process in system of solids is influenced by numerous factors and it is not possible to describe it quantitatively from all points of view simultaneously.

The existing programmes usually deal with several selected parameters and only the effect of the most important external factors is considered. If the system is influenced by more independent factors, more programmes must be used for finding out the values. The combination of two, or more programmes gives the possibility to approach to the real changes in material and to the needs of technological practice.

2. Modelling of heterogenous systems

Most of real solid subjects do not consist of homogeneous matter having the same properties and same structure in any place. Materials of objects created by human and natural activity often include many different phases mutually different in chemical composition, crystallic structure and properties. To study heterogeneous systems, it is necessary to know the properties of each present phase as well as the structure and behaviour of their boundaries because such specific places can be limiting localities from the view of point of limited properties. The behaviour of material in these places can be different in comparison with the inside of individual monophase areas.

* Prof. Ing. Jaroslav Koutský, DrSc.

Department of Material Science and Technology, University of West Bohemia, Univerzitní 22, CZ-306 14 Plzeň, Czech Republic

The modelling of heterogeneous systems represents new dimensions and enormous amount of unsolved tasks, and for their solution, a combination of two different approaches is necessary, i. e. modelling of continuum and discrete modelling of atomic structures.

2.1 Discrete and continuous model

The atomic structure of real bodies is respected in a discrete model. Individual atoms are substituted by mass particles, each of them being the carrier of definite attributes. The target of mathematical formulation of a discrete model is to add to the particles their properties values; i. e. to perform the transformation from the set of particles into the set of attributed values. Each transformation is generally a function of time.

Methods of mechanics of the system of mass particles can be applied on a discrete model of a flexible body.

The number of particles in the bodies of usual dimensions is so large that the applications of discrete models are practically limited to the description of processes in very small material volumes. A physically correct description of material degradation at cyclic load (1, 2), a description of phases boundaries, calculations connected with crystal lattice defects (dislocations, stacking faults, cracks), etc. are the targets of those research activities.

The mechanical continuum - is the model of a body that abstracts from individual particles and substitutes them by infinite infinitesimal particles. Such substitution is an adequate step in macrovolumes which significantly exceed the dimensions and distances between particles; but which is unacceptable in microvolumes. Individual processes are described by partial differential equations where constants and boundary conditions are determined by macroscopic observation of the process.

There are two basic types of correspondence between the discrete model and continuum:

- The correspondence of intensive (nonadditive) properties (attributes) - the set of discrete model particles can be transformed into the set of "subareas" of continuous model so that the nearest "subarea" of the continuous model can be arranged to each particle of a discrete model. This arrangement is called K. The position of particles of a discrete and continuous model is expressed in the same vector area. The attribute value in the given particle of continuum corresponds to the attribute value in a discrete particle. The correspondence of intensive properties values in continuum, which have not its pattern in a discrete model is not defined.
- The correspondence of extensive (additive) properties (attributes) - to the value of a given global property (relating to the whole system or to its substantial part) in a discrete model corresponds its value in the continuous model. The requirement must be valid for any part of the body. Let is chosen a part of the body in the continuous model as a subset of the whole

body. This subset corresponds with the subset of all particles in a discrete model to which K arrangement allocates subareas of the continuum in the given area. Additive local properties in the continuum model are designed from global properties as their intensities [3].

3. Programmes for modelling on a continuum base

The number of continuum based programmes offered for the use has significantly increased in the last years. Simulation programme interfere now with many activities of engineering practice. The calculation analysis is solved with the help of FEM programme packages. Special tasks are fulfilled by individual programmes which are mutually connected, using the same equipment (graphic labor stations), using the same language with user (interactive pre/post processors, connection with CAD). The tasks up to 3D are solved by these programme sets. Sysweld, Systus and Forge Programmes packages are especially preferred in our applications.

3.1 Sysweld programme package

The modelling of technological operation of the volume and surface heat treatment, welding, tipping and some further surface treatments is carried out by Sysweld programme package.

Thermal deformation and diffusion fields with the possibility to include phase transformations as well as materials structure can be solved [4, 5].

The simulation programme follows above all from the following parameters of the system:

- Phase composition and phase transformations
- Material structure
- Temperature distribution in system
- Concentration distribution of some elements
- Stress and deformation distribution

3.2 Systus programme package

This software is a general system of finite elements enabling to solve the tasks of continuum mechanics, thermal and electromagnetic field tasks. Its nonlinear modulus includes material models which enable to describe the behaviour of material with porosity (Gursan-Tvergaard model). This programme package was recently elaborated in IRSID laboratories (France).

3.3 Forge 3 programme package

3D tasks dealing with calculations of all thermodynamic parameters for cold and hot forming can be solved by Forge 3 programme. It includes a numerical analysis of cold and hot forming of a flexible body by the method of finite elements, further functions of pre- and post-processing. The programme is autogenerative

and during calculation the net of finite elements can be adapted by the subprogramme Mesh, capable to change interactively the density of knots in localities where it is necessary for simulation.

It is supposed that the material model of an investigated body is homogeneous and incompressible in all places. Its behaviour at deformation is described by Norton-Hoff constitutional law:

$$s_{ij} = 2K(\sqrt{3}\bar{\epsilon})^{m-1}\epsilon_{ij} \quad (1)$$

where s - deviator of stress tensor,
 ϵ - deformation velocity tensor,
 $\bar{\epsilon}$ - equivalent deformation velocity,
 K - material constant,
 m - coefficient depending on deformation velocity.

The friction of tool during forming brings the necessity to include shear stress τ - on the interface tool/formed body. Its value depends on the slip rate of deformed material on the tool:

$$\tau = -\alpha K \Delta v \quad (2)$$

where α - and K - variable coefficients depending on the place of contact of a tool with a semi-finished product.

Deformation process is solved by auxiliary system of equations of equilibrium forces. The forces include the behaviour of material according to equation (1), its incompressibility and friction of a deformed body with a tool.

The thermo-viscoplastic analysis is carried out by simultaneous solution of continuum mechanics and thermal problem.

3.4 Task of experimental activity at modelling

Three basic partial parts must be fulfilled at modelling of any system:

- Pre-processing - getting data dealing with the system to be modelled, data entry into the programme, the entry of the environment influence on the system.
- Processing-treatment of input data and own calculations of the system parametres - changes of material properties, intensity of force fields, energies, etc.
- Post-processing - treatment of calculated values, their comparison with experiments.

4. Application of real modelling systems

Thanks to the project of the Czech Ministry of Education, called "250", at our Department of Materials Science and Technology, a new modern laboratory of processes simulation, equipped with two Silicon Graphic Indigo R5000 stations, one 500au DEC OSF/1 graphic station, and Forge 2D and 3D, Hypermesh, Systus and Sysweld software systems was built up and some research programmes were initiated.

4.1 Simulation of cold deformation effect on the structure of P900 steel

Austenitic CrMn steels with N are characterized by high strength, high R_E/R_M value, high toughness, stability of austenitic structure and by excellent stress-corrosion resistance. They are used for the components with extreme mechanical and corrosion load. At the same time paramagnetic behaviour of material must be guaranteed.

The increase of the strength of this type of steel can be reached by different ways. It is possible either to change chemical composition of the steel (to achieve the maximum N concentration) or to optimize technology of the following treatment (i. e. cold forming and heat treatment) of cast semi-product.

Experimental programmes aimed at the optimization process of cold deformation and subsequent treatment are carried out on P900 - Cr18Mn18N steel. During material treatment, stress and deformation tensors in any place of a forged piece, or of a model specimen, are determined. These parameters have a direct effect on the creation of very fine substructure of slip band dislocations and deformation twins inside austenitic grains.

If more slip systems (with moving dislocations inside) are activated and if deformation twins appear on different planes of the type (111), their mutual crossing occurs. Slip bands intersection and above all the intersections of deformation twins create areas of effective blocking of dislocation movement [7]. With respect to the dimensions and mutual distances of deformation twins, ten thousands of such intersections (in volume of approx. $0,2 \text{ mm}^3$) may appear. This effect and further strengthening mechanisms lead to high strength values of these austenitic types. One of the main targets of this research programme is to reach optimum distribution of deformation twins (uniform with the highest density).

The tool to influence the structure by a controlled deformation combined with heat treatment - it is functionally structuring of treated material.

A partial study from a broad program is presented, where computer simulation with the help of Forge 2 (based on FEM) using tensile and pressure tests was carried out.

For the measuring of P900 steel deformation characteristics, tensile tests and some modifications of pressure and torsion tests were used.

The obtained stress-deformation curves allow to assess material behaviour for a computer simulation.

As the tests were strongly influenced by friction some modifications of pressure tests were carried out in order to evaluate the possibility how to decrease the friction. From comparison of individual modifications of pressure test, it is clear, that the effect of increased friction shifts the curves to higher values of deformation stress (Fig. 2). The evident shift of the curves to lower stresses depends on the method used for the elimination of friction; pressure-specimen No. 4 - flat specimen without lubricant, pressure-

specimen No. 9 - Rastragaev method, pressure - specimen No. 14 - grooved face with lubricant use, Larke method of extrapolation. The curves of grooved face specimens are similar to those of flat face; this way to reduce friction on pressure tests is not suitable for the tests at the given conditions. The curves from Rastragaev specimens give lower values of deformation stresses comparing with the former tests modifications.

Depending on deformation the elimination of friction with the help of Larke method brought a further decrease of deformation stresses.

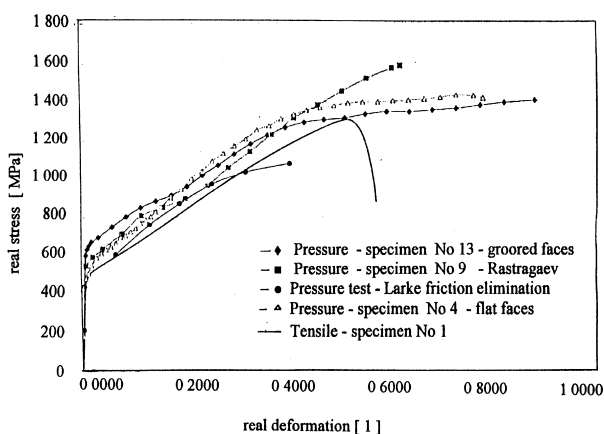


Fig. 2 Comparison of pressure and tensile tests

Comparing individual modifications of pressure tests with tensile ones, it is found that pressure tests curves approach to the tensile one with the decreasing influence of friction (Fig. 2). Based on the analysis of test results describing deformation behaviour, tensile test curve for underformed material was chosen for the evaluation of rheological parameters for computer simulation. In order to obtain relevant coefficients, a part of the curve representing elastic behaviour was removed at first and the part from the beginning of neck formation was removed afterwards. The curve in coordinates real stress - real deformation, describes deformation behaviour of the steel for computer simulation. It approaches to the straight line (by shape) - Fig. 3. In Forge 2 programme some material models are implemented for the description of material behaviour, equation describing material with linear strengthening complies for this case. To get parameters for this equation regressive analysis of cut curve in the Microsoft Excell programme was made. The parameters of regressive straight line are in Fig. 3: $K_0 = 565$ MPa and $a = 3,38$. Friction coefficient value was taken from ring specimen test $\mu = 0,15$. Using these parameters, FEM simulation of pressure and tensile tests was made to compare experimental and calculated values.

4.1.1 Simulation of pressure test

Simulation of pressure test represents the solution of rotationally symmetric task at normal temperature in material with linear strengthening.

At first, the geometric model of testing body (small cylinder) was formed. With respect to the symmetry, one half of the specimen, suffices for simulation. This half was subsequently meshed and calculation net formed by triangles, with nine integral points. Then the geometry of pressing plates was created, modelled as asymmetric and perfectly rigid body. Top plate was firm and bottom mobile as in the case of loading on the MTS 500 kN machine. Deformation velocity was identical with that during pressure tests. After first calculation, stress/deformation relationships obtained by simulation and experiment were compared. Based on this comparison, calculated model of material proved to be "too soft". To achieve maximum agreement between simulation and experiment some calculations with gradually increased parameter a were carried out. Minimum difference between experimental and calculated curves was reached for $a = 3,57$ - Fig. 4.

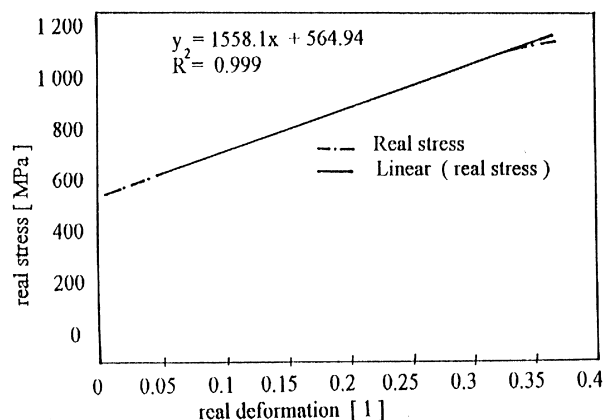


Fig. 3 Determination of deformation strengthening coefficient

4.1.2 Simulation of tensile test

FEM simulation of tensile test was made to evaluate proposed rheological parameters for P900 steel. Similar simplifications as in the previous case were used - Fig. 3. Problem was calculated as a symmetric task and jaws were mentioned to be perfectly rigid.

After calculation, the stress curve deformation relationship was evaluated again and simulated was almost identical with the measured one - Fig. 3.

4.1.3 Computer simulation evaluation

Computer simulation gave informations about loading during specimen deformation, geometry of deformed bodies and stress distribution in cross-section of the component after deformation. The course of loading related to deformation was transferred from Forge 2 into Microsoft Excell and evaluated.

Relationship obtained by simulation were recalculated to the values of real stress and deformation, and such prepared curves compared. Curves obtained after deformation strengthening coefficient "tuning" are in a good agreement with experimentally found values.

Some deviation from the experimental curve is visible in case of pressure test. The deviation may be caused by inaccuracy in determination of friction coefficient. Friction coefficient value determined by ring specimen tests is probably lower than the real value.

Higher value of friction coefficient should result in the growth of deformation stress and simulated curve should approach to the measured one.

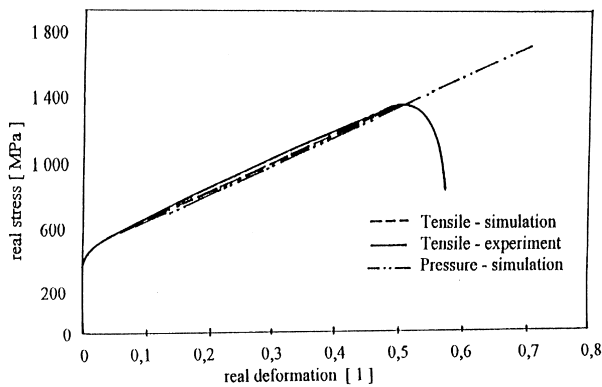


Fig. 4 Comparison of FEM simulation and experimental results

4.2 Simulation of free forging of CrMo steel shafts

The 42CrMo4 steel is used for the manufacture of large crankshafts in inland and abroad.

This CrMo steel possesses relatively good hot formability and, in soft annealed state also good machinability. It is suitable for quenching in oil, reaching comfortable value of notch toughness at high strength. It possesses increased resistance against tempering and is suitable for application at increased temperatures up to 500 °C. Heat treated at strength over 1050 MPa it proves also an increased wear resistance. It is suitable for surface quenching and is not sensitive to the temper brittleness.

Experimental verification of structure, and properties in the whole volume of forging spends time and money and puts high demands on technical realization. One possibility how to solve this problem is modelling of processes passing during the own manufacture. This could substitute a large part of experiments. Forming and heat treatment are simulated by Forge 3D and Sysweld programmes; their combination allows to model hot forming, quenching and tempering. Simulation is aimed at final structure, hardness, strength and notch toughness.

Presented partial study demonstrates the application of Sysweld programme for the estimation individual structural com-

ponents fraction during cooling of 16 343 steel from quenching temperature. Experimental values were obtained by dilatometric measurement and quantitative image analysis.

Procedure to determine parameters for Leblond model is included in Sysweld +. Coefficients necessary for calculations; are determined from ARA diagram, the beginning and end of transformation and final fraction of each phase according to the cooling rate. On the basis of these coefficients, the set representing metallurgical transformations in material is formed. Sysweld + programme includes the tool for drawing of ARA diagram too.

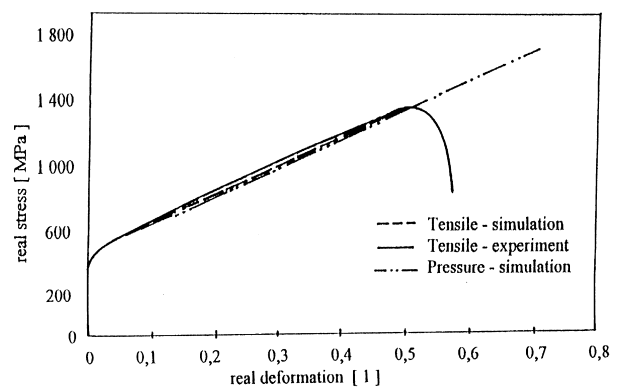


Fig. 5 Comparison of final phase fractions determined from dilatometric curves, by image analysis and numerical calculation

The values obtained by dilatometric measurement and values from quantitative image analysis are well comparable. Dilatometric analysis gives systematically by 4 - 5 % higher amount of bainite than image analysis measurements for all five investigated specimens (fig. 5). The values obtained by calculation in Sysweld programme depend on the accuracy of assigning ARA diagrams into programme. ARA diagram accuracy is given by the correctness of thermophysical material values, measured transformation temperatures and qualitative evaluation of phase fractions. More precise description of individual phase transformation gives more precise results of phase fractions for applied cooling of experimental material.

5. Conclusion

Simulation methods prove important qualitative as well as quantitative contribution to the optimization of technological processes and properties of products.

Reviewed by: I. Hrivnák, O. Bokůvka

Literatúra - References

- [1] FISCHMEISTER, H., EXNER, H.: *Zeitschrift für Metallkunde*, 80, 1989, 12
- [2] MACHOVÁ, A.: *Materials Science and Engineering*, A 149, 1992
- [3] KÁNOCZ, A., ŠPANIEL, M.: *Metoda konečných prvků v mechanice poddajných těles*. 1. vyd., ČVUT Praha, 1995

- [4] LEBLOND, J. B., DEVAUX, J.: *Mathematical modelling of transformation plasticity in steels*. Proceedings of Int. Conference on Residual Stresses, Nancy, 1988
- [5] BERGHEAU, J. M., LEBLOND, J. B.: *Coupling between heat flow, metallurgy and stress-strain computations in steels*. The approach developed in computer code SYSWELD for welding and quenching. Proceedings of Conference on Modelling of Casting, Welding and Advanced Solidification Processes, Davos 1990.
- [6] SPEIDEL, M. O., UGGOWITZER, P. J.: *Stickstofflegierte Stähle*. 1. Auflage, Zürich, 1991
- [7] DEXTER, J. B.: *Residual Stress Analysis of Reactor Pressure Vessel Attachments*. Proceedings of Int. Conference on Residual Stresses, Tokushima, 1991.

Werner Mombrei - Peter Ottlinger *

PRÍSPEVOK K OPTIMALIZÁCIÍ VLASTNOSTÍ OCELE POUŽÍVANEJ PRE ŽELEZNIČNÉ KOLESÁ Z HĽADISKA ICH OPOTREBENIA

A CONTRIBUTION TO THE OPTIMIZATION OF WEAR BEHAVIOUR OF STEEL USED FOR RAILWAY WHEELS

Článok sa zaoberá vplyvom tepelného spracovania na odolnosť voči opotrebovaniu ocele používanej na dvojkolesia v súvislosti s ich predvídzanou životnosťou.

In the next chapter the paper deals with the influences in the state of heat treatment of the wheel steel related both to the wear resistance and to the reason of the runout.

1. Problem

With regard to the wear behaviour of wheels two problems are in the centre of interest:

1. Running time up to the given limit of the flange profile (wear of wheel flange and running in depth) and
2. Development of unwished deviations of roundness before the conditions are reached, which are mentioned under point 1.

The velocity of development of both facts is determined by the wear resistance of the material. The reason for the runout can be found in tribological differences in the state of material distributed in the circumference of the wheel. Such differences can be caused by variable conditions in the wheel circumference during the manufacturing process of the running tread, by special conditions at the beginning of using the wheel caused by vibrations of the wheel or the wheel set, but mainly it is caused by conditions of the heat treatment which differs along the circumference of the wheel.

2. Influences in the state of heat treatment to the wear behaviour

The following results were obtained from laboratory investigations using a block test bed with such test conditions that between the least wear state and the state of the highest wear resistance the whole range of wear mechanism was covered, i.e. from mainly metallic wear up to mainly oxidic wear.

The variation of heat treatment was performed by using specimen made of unalloyed wheel-steel with 0.72 % C; the counterpart of test specimen was made of temper hardened unalloyed (rail-) steel with 0.75 % C and a hardness of 335 HV.

The test results are shown in Fig.1. Following conditions of heat treatment have been recorded:

- temper hardening state above the martensite state with a variable tempering temperature,
- temper hardening state above the martensite state with a variable austenizing temperature,

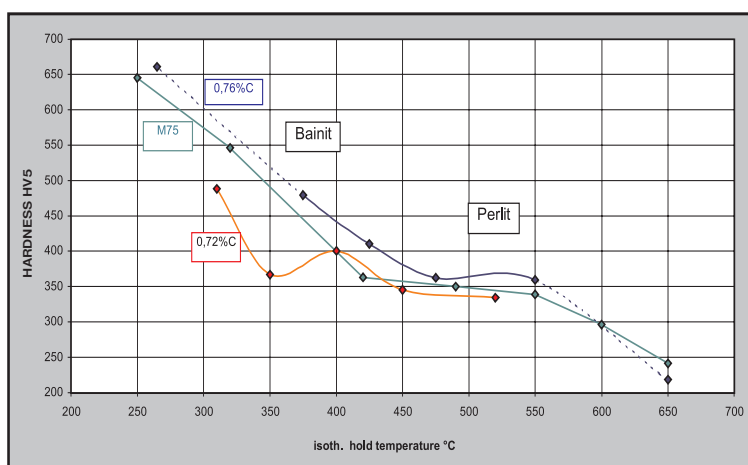


Fig. 1 Wear versus hardness for variable tempering temperatures, resp. austenizing temperatures for temper hardening states and for reduced holding temperature (direction of arrow) with isothermal temper hardening of unalloyed steel with 0.72 % C

* Prof. Dr.-Ing. habil. Werner Mombrei, i. R., Prof. Dr.-Ing. habil. Peter Ottlinger
University of Applied Sciences Dresden (HTW Dresden), Friedrich-List-Platz 1, D-010 69 Dresden

- an overhardened (austenizing temperature 1.200 °C) not tempered state,
- a continuous cooling state using moved air,
- isothermal transformed state with variable holding temperature.

In general, the results reflect that the wear resistance of steel with a determined hardness (and a determined structure) is the higher the less the cooling velocity is at the time of the last austenite formation. In parallel we can see the influence from the shape of cementite formation; the laminar shape of cementite (pearlite) shows the best, coarse globular cementite (high tempered martensite) the worst wear behaviour.

If the tempering state is formed from a bigger share of residual austenite (austnizing temperature 1.200 °C) then this tempering state in the mentioned sense - related to hardness- shows a remarkably better wear behaviour than a tempering state which is obtained directly from the martensite under all other conditions remaining the same.

Bainite obtained by isothermal transformation shows a similar wear level like pearlite formed with continuous cooling. Both show a wear behaviour which is remarkably better than a tempered hardened structure. The pearlite which was formed by isothermal transformation shows the most advantageous wear behaviour. The overhardened state (austenisation at 1.200 °C/water) is an exception in this range of hardness: The especially high wear resistance results obviously from transformation of residual austenite to martensite in the friction area. In case of practical operation in such a state exists the danger, especially at lower surrounding temperatures, that the mentioned transformation of residual austenite appears also in wheel, wear-flange-cross-section with all negative consequences especially through the increase of volume and brittleness.

3. Realization of constant conditions of heat treatment

The necessary constancy of the state of heat treatment for reducing the tendency of runout of wheels relates in the first place to the circumference of a single wheel but also to a pair of wheels within a wheel set.

Therefore, the conditions of the heat treatment should be chosen in a way that unavoidable deviations in the heat treatment process will cause only insignificant differences in structure. Applying continuous cooling this requirement is the better met the slower the cooling velocity is chosen.

At isothermal transformation in the range of a holding temperature within 450 °C and 500 °C a large independence of the hardness towards the height of the holding temperature is shown

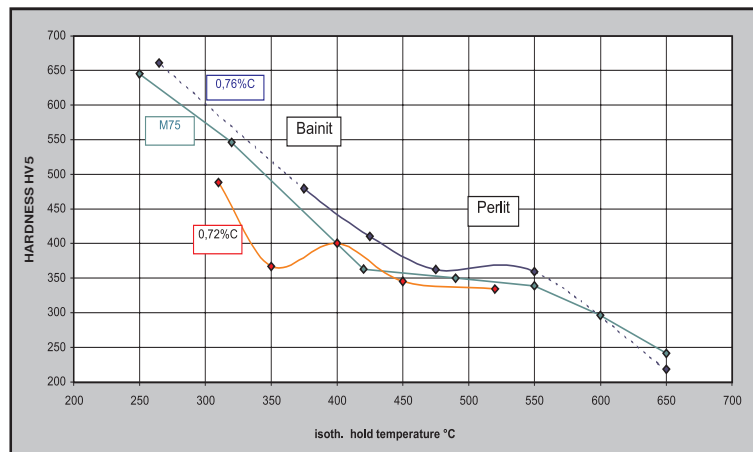


Fig. 2 Hardness versus isothermal holding temperature for different unalloyed steels (by own findings and after HERBST, B., Dissertation A 1978)

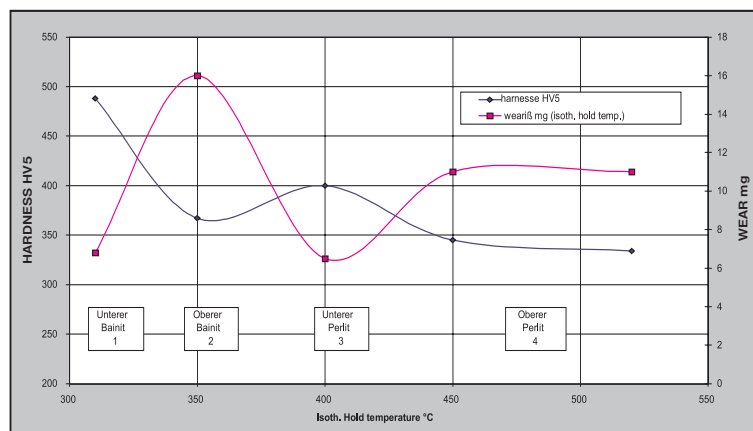


Fig. 3 Hardness and wear versus isothermal holding temperature for an unalloyed steel with 0.72 % C

(Fig. 2). Appropriate investigations of the steel with 0.72 % C, which you can see in the diagram, showed that this constancy is also valid for the wear behaviour (Fig. 3).

4. Summary

From the numerous variants for the realization of the heat treatment states for transformable steels results the possibility, that even for equal hardness very different wear behaviour can be reached.

“Normal” temper hardening provides the most unfavourable wear behaviour, isothermal temper hardening during the pearlite step the most favourable.

The least of the influences from deviations in the conditions of the heat treatment to the structure result from continuous transformation with a slow cooling rate, for isothermal transformation at a holding temperature around 500 °C.

Reviewed by: J. Koutský, L. Várkony

Literatúra - References

- [1] MOMBREI, W.: *Vorgänge in der Lauffläche von Rädern schiebengebremster und ungebremster Radsätze*. Gesamtstaatliche Konferenz "Moderne Schienenfahrzeuge" Zilina Mai 1988
- [2] MOMBREI, W.; OTTLINGER, P.: *Metallkundliche Untersuchungen an schiebengebremsten Vollrädern*. Unveröffentlichter Forschungsbericht HfV Dresden
- [3] MOMBREI, W.; OTTLINGER, P.: *Werkstofftechnische Probleme bei Eisenbahnrädern*. Sektionskolloquium HfV Dresden
- [4] MOMBREI, W.: *Untersuchungen über den Einfluss des Gefügestandes auf das Gleitverschleißverhalten von unlegierten Stählen*. Dissertation A 1967

János Takács - Péter Gál, MSc - Antal Lovas - Joachim Belt *

FLUX POKOVOVANIE ZOSILNENÉ ABSORPCIOU AI POVRCHOV PRI CHARAKTERISTICKEJ VLNOVEJ DĹŽKE CO₂ LASEROVÉHO ŽIARENIA

FLUX COATING ENHANCED ABSORPTION OF AI SURFACES AT THE CHARACTERISTIC WAVELENGTH OF CO₂ LASER IRRADIATION

Hliníkové tvrdé spájkovanie je metóda pre spojenie Al-častí v tesnom dotyku pomocou kvapalnej zliatiny, ktorá sa tavi nad 577 °C. Na základe použitého tepelného zdroja, je možno rozlíšiť konvenčnú metódu (plameň) alebo metódu energetického zväzku lúčov (laser). Laserová metóda umožňuje rýchle lokálne tavenie v okolí povrchov, ktoré majú byť spájané. Napriek vysokej hustote energie (reprezentovanej laserovým žiarením) taveninou Al je tavenie často neúspešné. Príčinou je nízka absorpčná schopnosť Al v blízkosti vlnovej dĺžky charakteristickej pre CO₂ laser. Z dôvodu zvýšenia absorpcie energie sa preto musia použiť povlaky, ktoré majú vysokú absorpčnú schopnosť.

V práci je diskutovaná zmena absorpčnej schopnosti Al povrchov spôsobená povlakmi vytvorenými NOCOLOK[®] Flux technológiou.

Aluminium brazing is a method for joining Al-parts in close proximity by introducing liquid alloys which melt above 577 °C. On the basis of an applied heat source, conventional (flame) and energy-beam brazing (laser) can be distinguished. The laser is capable to result in rapid local melting around the surface to be joined.

In spite of the high energy density (represented by laser irradiation) the melting of Al is often unsuccessful. The reason is the low absorption ability of Al at around the wavelength characteristic to the CO₂ laser. Coatings with a high absorption ability have to be used in order to facilitate the energy absorption.

In the present study the change in absorption ability of Al surfaces due to NOCOLOK[®] Flux coatings will be presented.

Introduction

In principle, all kind of laser can be used for brazing as a heat source. However, their efficiency in the brazing process is very different, and depends highly on the absorption ability of the irradiated material around the characteristic wavelength of the applied laser. For this reason CO₂ laser can not be used for brazing of Al and its alloys [1, 2].

The explanation of this fact can be drawn from Fig. 1. where the room temperature absorption ability as a function of wavelength is plotted for several metals.

While the absorption ability for steels at 10.6 μm is appreciable, (~ 0.1) this value is very low for Al (lower than 0.02).

The absorption ability can be risen by applying appropriate coatings. Graphite is commonly used in laser technology to rise the absorption ability of sample surfaces. Due to the corrosion risk attributed to graphite, its application is undesirable in the case of Al joining. It is plausible that absorption ability can be enhanced by addition of good absorber material to the flux. This condition seems to be fulfilled automatically by applying the

NOCOLOK[®] Sil Flux, as a consequence of Si particles being dispersed in the NOCOLOK[®] Flux.

To verify this supposition the change of absorption ability at 10.6 μm was investigated on different Al surfaces covered by this type of flux. For the successful application of CO₂ laser irradiation to the Al brazing, the mechanism of NOCOLOK[®] procedure will be briefly described [3].

The NOCOLOK[®] aluminium brazing process and the NOCOLOK[®] Flux

The flux dissolves the aluminium oxide before the melting of filler material has started and protects the eutectic join against the oxidation during the whole process. The eutectics composition of filler material ensures lower melting point than that for the parts to be joined. (See Al-Si phase diagram in Fig. 2.) The Flux material (Trade mark: NOCOLOK[®] Flux) is also eutectic system with the composition of KAlF₄ + K₂AlF₅·H₂O with the melting temperature of 562 °C - 577 °C, which is slightly below the melting

* ¹Prof. Dr. János Takács, ¹Péter Gál, MSc., ¹Ass. prof. Antal Lovas, ²Dr. Ing. Joachim Belt

¹Budapest University of Technology and Economics, Dept. of Mechanical Engineering Technology Bertalan L. Street 2., 1111. Budapest, Hungary, Tel.: +36-1-463 1694

²SOLVAY Fluor und Derivate GmbH, Hans-Bickler-Allee 20, 30173. Hannover, Germany, Tel.: 49-511-8570

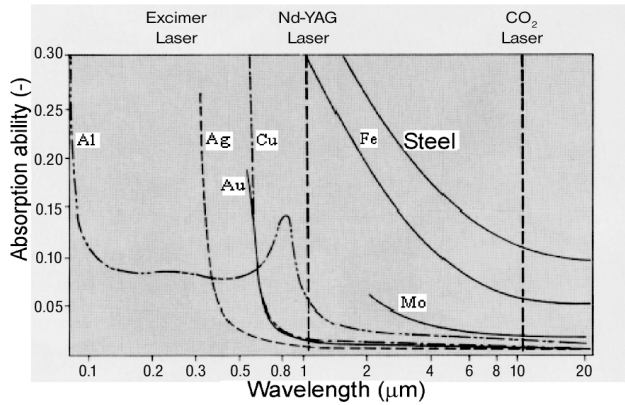
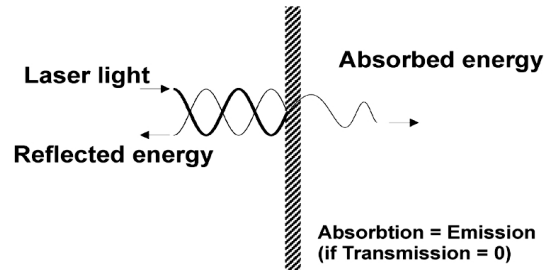


Fig. 1 Absorption ability of several metals at room temperature [6]



point of eutectic Al-Si [4]. The eutectic filler liquid with sufficiently low melting point can also be formed via local dissolution of Si-particles in the neighbouring Al parts. The Si particles are previously mixed into the Flux material. (Trade mark: NOCOLOK Sil. Flux) The oxide dissolving ability is the same for both type of Flux material.

The brazing process is schematically illustrated in Fig. 3. No change can be observed below 562 °C when the material is heated. (Fig. 3a) In the temperature range of 562 °C - 577 °C the Flux has melted and the aluminium oxide layer is dissolved. (see Fig. 3b) When the temperature rises beyond 577 °C, the filler material (Al/Si12wt % alloy) is also melted. In case of using NOCOLOK[®] Sil Flux the silicon particles dissolve in the Al forming an eutectic liquid near the surface (Fig. 3c). The mechanical joint between the parts is formed via the freezing of this liquid layer. After the completion of brazing process the surface is covered by the remainder part of Flux (no need to remove, see Fig. 3d).

$$a_{\lambda,T} = \epsilon_{\lambda,T}$$

where $a_{\lambda,T}$ is equal to the absorption coefficient and $\epsilon_{\lambda,T}$ is equal to the relative emission coefficient of a grey body at a given temperature and wavelength

According to this one can suppose that the determination of temperature dependence of the relative emission coefficient on the wavelength of CO₂ laser (10.6 μm) can supply useful information also about the absorption ability of the same partner materials. So, the intensity of infrared emission spectra was measured using filter on the wavelength of CO₂ lasers (10.6 μm) during continuous heating of a series of samples, covered by the same Flux composition used for the laser brazing. In the next chapter the measuring techniques, and the temperature dependence of the relative emission coefficient on the applied materials will be summarised.

Measurement of the absorption ability

The absorption ability cannot be measured directly. Therefore the emission coefficient was measured for the individual partner materials. According to the Kirchoff law (which is the basis of our measurements) [7]:

Experimental settlement and procedure

The essence of measurements is the continuous monitoring of the surface temperature of a sheet radiator on which the samples are placed. The spectral distribution of the emissivity is compositional dependent. Besides it may also depend on the tribological character of the surface at the observed wavelength. So, the local

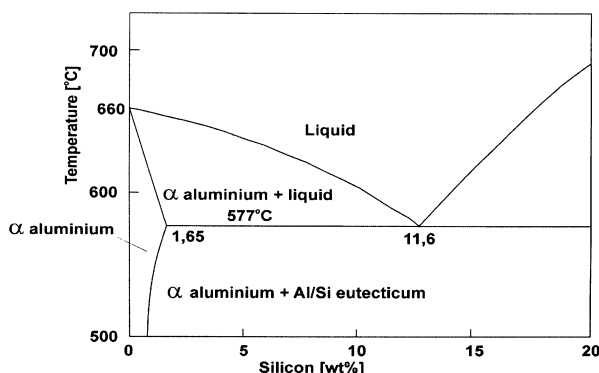


Fig. 2 Al-Si phase diagram [4]

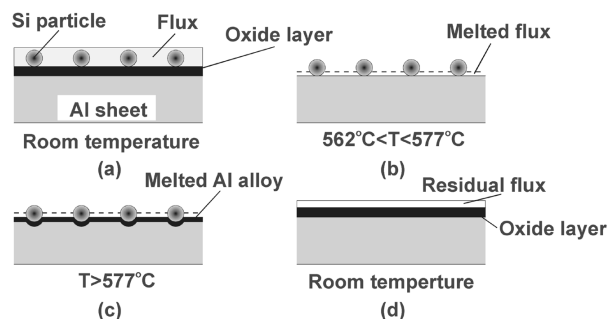


Fig. 3 The NOCOLOK[®] aluminium brazing process [3]

temperature on the surface of a given sample measured by thermovision can significantly differ from the physical temperature measured by a thermocouple at the same point of the surface [10]. Therefore, the first task was to ensure a nearly constant temperature on the surface of the sheet radiator. In order to improve the temperature homogeneity of the heated sheet surface, it was covered with a 5 mm thick Cu plate. In addition, Ni-Cr powder was layered under and on the surface of the Cu plate. The samples were pressed into the Ni-Cr powder in order to ensure perfect heat contact between the samples and the surface-radiator. Ni-CrNi thermocouples are used for the measurement of the physical temperature at several points of the surface embedding them into the powder layer. The experimental arrangement of the system is illustrated in Fig. 4.

The temperature was continuously increased during the experiments from the room temperature up to the melting point of aluminium, then the radiator was cooled down, switching the controllable power supply off. During the whole process the thermal emission was continuously monitored using a THERMOVISION® 880 LWB type infrared camera.

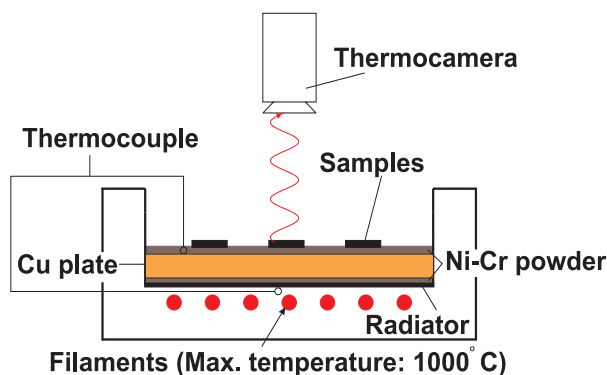


Fig. 4 Experimental arrangement for the thermal emission measurements

Sample preparation

Sample geometry are 20 x 20 mm squares or Ø10 mm circles, being cut or punched either from a simple 1 mm thick Al-plate (without laminated layer) or from a laminated Al-plate.

After mechanical flattening, burring-off, and degreasing in acetone, the samples were clad, using NOCOLOK Flux (water-based dispersion of Flux powder) and NOCOLOK Sil-Flux (Flux, containing Si powder) with three different concentrations in each case (Flux: 5 %, 10 %, 15 %, Sil Flux: 10 %, 15 %, 20 %). From the sets of Flux 15 % and Sil Flux 20 % several samples were dried in a furnace (150 °C, 2 hours heat treatment in a box-furnace) in order to remove the chemically bonded crystal water. Another fraction of samples was dried at the room temperature. The specimens were pressed into the NiCr powder layered on the surface. In this way a perfect heat-contact between the samples and the heated surface is ensured.

Experimental results

The increase in emissivity was often found in the low-temperature range of our heating experiments (Fig. 5 - 10). In principle, the change of emissivity is not expectable if a phase transformation or a compositional change is absent. In fact, the change in $\epsilon(T)$ can be resulted from the sensitivity limitation in the low temperature range. In spite of the possible sensitivity limitation- there is a definite compositional dependence of the observed slope of $\epsilon(T)$ in this temperature range, i. e. the emissivity is lower for lower concentrations. So the upraise can be detected, when the Flux concentration is low (between 5 - 15 %). It was found that slope of $\epsilon(T)$ increases with decreasing concentration of Flux in the covered layer. For the laser brazing the higher concentration of Flux will be good because of its higher absorption coefficient. Therefore, it was highly suspected that the low-temperature increase of $\epsilon(T)$ is connected with a compositional change (water evaporation) during the experiments. This hypothesis was verified by continuous heating-cooling experiments where several samples (including 5, 10, 15 and 20 % Flux content, with and without Si particles) were continuously heated from the room temperature to 700 °C, and then cooled below 100 °C again with the reference samples, monitoring continuously the actual temperatures as was previously described.

The main feature of the heating-cooling curves can be characterised by subtracting the measured ϵ values obtained during the heating and cooling experiments. The difference increases with decreasing Flux content, as it is obvious from Figs. 5 - 10. It is clear that $\epsilon(T)$ increases at the heating side, especially at around 10 - 15 % of Flux content. The measured $\epsilon(T)$ values seems to be higher for the Si-Flux samples.

Another interesting feature of the curves is that $\epsilon(T)$ value at the cooling side is nearly independent from the initial Flux concentration (about 0.42 for all cases), which hints again to the possible compositional change being nearly completed during the heating process. *The main conclusion is that temperature dependence of the relative emission coefficient at around 20 % Flux content is nearly identical both on the heating and cooling side, consequently the effect arising from the possible compositional change is negligible.* The quantity of chemically bonded water may contribute to the observed differences in the lower temperature range. At higher temperature this difference is negligible.

The melting process of the Flux material takes places at around 570 °C dissolving the thin Al_2O_3 layer on the surface of Al. Rising the temperature eutectic Al-Si melt is formed via the diffusion of Si into the Al surface. Comparing the heating and cooling side of the $\epsilon(T)$ curves a definite difference can be seen in the case of samples covered either by Flux or Sil Flux.

The difference arises from the phase transformation (melting) and from the chemical reactions (alloy formation, Al_2O_3 dissolution) started at high temperatures.

The cooling side of the $\epsilon(T)$ curves are practically unaffected by the Si content of the Flux. On the contrary Si addition causes

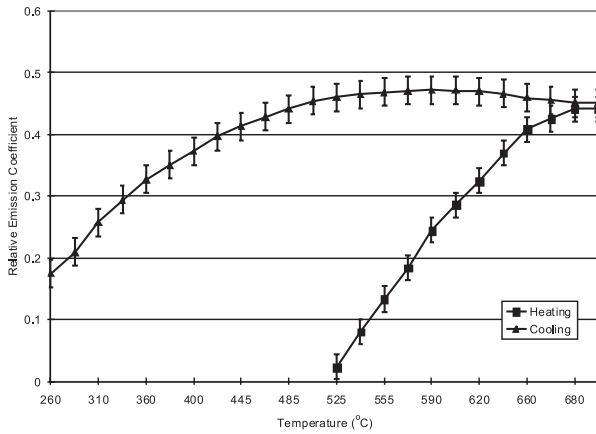


Fig. 5 The temperature dependence of Relative Emission Coefficient (5 % Flux, dried on air)

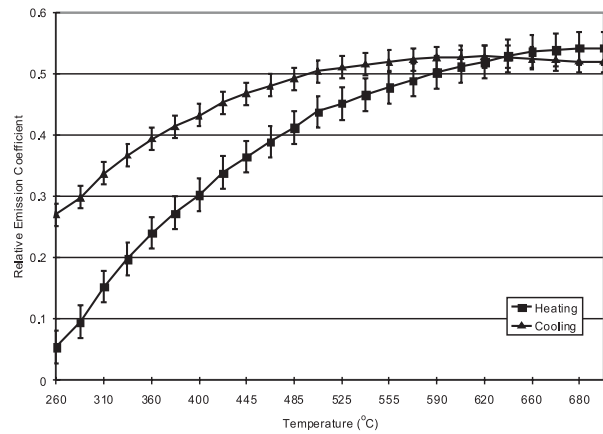


Fig. 6 The temperature dependence of Relative Emission Coefficient (15 % Flux, dried on air)

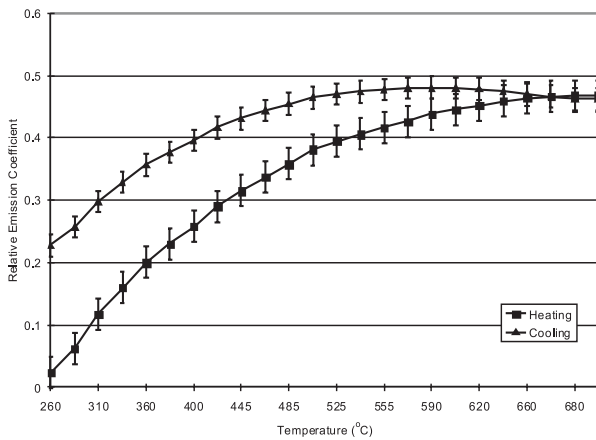


Fig. 7 The temperature dependence of Relative Emission Coefficient for 10 % Sil Flux, cladding, dried in air

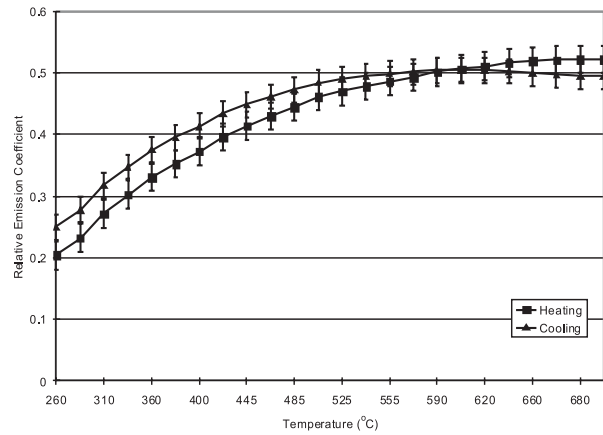


Fig. 8 The temperature dependence of Relative Emission Coefficient for 20 % Sil Flux, dried on air

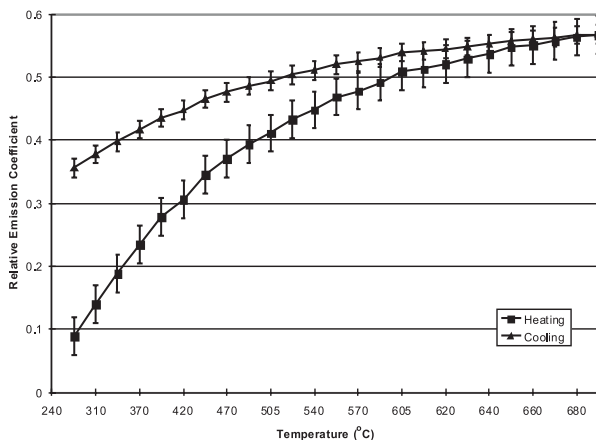


Fig. 9 The temperature dependence of Relative Emission Coefficient for 15 % Flux, dried in furnace

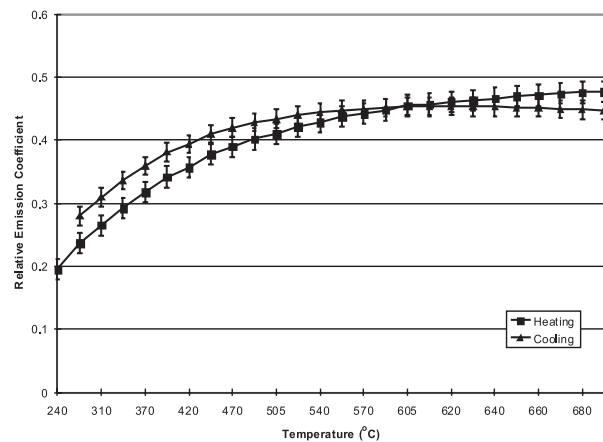


Fig. 10 The temperature dependence of Relative Emission Coefficient for 20 % Sil Flux, dried in furnace

a significant change in $\varepsilon(T)$ on the heating side. Flux with Si addition has a higher emissivity than one without Si powder.

Control experiments with CO₂ laser

Applying the results of thermovision measurements, pure and Flux-covered aluminium sheets were irradiated by laser beam. Except the exposure time, all of the applied irradiation parameters were the same during the experiments. Experimental arrangement can be seen in Fig. 11.

additional agent is not needed for the successful laser-brazing of aluminium parts.

Conclusions

- The CO₂ laser energy absorption in Al surfaces can be significantly enhanced by applying surface coatings with NOCOLOK Flux or NOCOLOK Sil Flux prior to the laser irradiation.
- The emissivity (so the absorption ability) is improved by increasing Flux concentration in the coating.

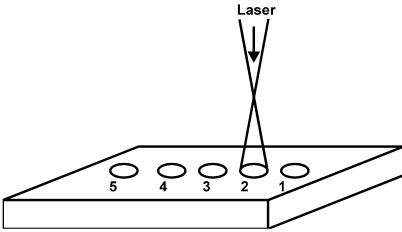
<p>Al without 20 % Sil Flux P: 600 W v : 0 Focal diameter: 2 mm Shielding gas: argon Exposure time: 1: 0.2 s 2: 0.4 s 3: 0.6 s 4: 0.8 s 5: 1 s</p>		<p>Al with 20 % Sil Flux P: 220 W v : 0 Focal diameter: 2 mm Shielding gas: argon Exposure time: 1: 0.2 s 2: 0.4 s 3: 0.6 s 4: 0.8 s 5: 1 s</p>
--	--	---

Fig.11. Experimental arrangement and irradiation parameters for laser brazing

In spite of the highest power density applied, melting of pure aluminium sheet cannot be detected due to the low absorption ability of pure aluminium. On the contrary, the melting has definitely started on the flux-covered sheets using the same power density.

Therefore it can be established that absorption of CO₂ laser energy in aluminium is highly enhanced if surface cladding by NOCOLOK[®] Flux or by Sil Flux is applied. Consequently, further

- The increasing absorption ability (caused by the Flux covering) is also supported by the CO₂ laser irradiation experiments.

Acknowledgement

This work has been supported by SOLVAY Fluor und Derivate GmbH. Germany.

Reviewed by: L. Kunz, T. Domić

Literatúra - References

- [1] PRIMKE, K.: *Az alumínium hegesztése és forrasztása* Műszaki Könyvkiadó, Budapest, 1975. p.: 314
- [2] HANEBUTH, H.: *Laserstrahlhartlöten mit Zweistrahltechnik* Meisenbach Verlag Bamberg, Erlangen, 1996. p.: 157
- [3] TIMSIT, R. S., JANEWAY, B. J.: *A novel brazing technique for aluminium* Welding Journal, June 1994. pp.: 119s-128s
- [4] *The NOCOLOK[®] Flux brazing process* Reklám anyag SOLVAY Fluor und Derivate GmbH.
- [5] VERÁ, J., KÁLDOR, M.: *Fémtan Nemzeti Tankönyvkiadó*, Budapest, 1996. p.: 636
- [6] DAWES, C.: *Laser welding* Abington Cambridge, 1992. p.: 258
- [7] RUDOWSKI, G.: *Az infratelevízió és alkalmazásai* Műszaki Könyvkiadó, Budapest, 1982. p.: 226
- [8] GREENSTEIN, M.: *Optical absorption aspects of laser soldering for high density interconnects* *Applied Optics*, Vol. 28, No. 21, pp.: 4595-4603
- [9] WITHERELL, C. E., RAMOS, T. J.: *Laser Brazing* Welding Journal, October 1980. pp.: 267s-277s
- [10] KISS, Gy., SKLÁNITZ, A., SZILÁGYI, A., TAKÁCS, J.: *Surface Treatment and Modification by Laser Beam* *Bewertung, Behandlung und anwendung von Konstruktionswerkstoffen in Fahrzeugbauteilen VII. Kolloquium*, Dresden, 1990. pp.: 1-15.

Stefania Greszczyk - Grzegorz Lipowski *

REOLOGICKÉ VLASTNOSTI CEMENTOVÝCH ZMESÍ OBSAHUJÍCICH POPOLČEK S RÔZNOU VEĽKOSŤOU ZŔN

THE RHEOLOGICAL PROPERTIES OF CEMENT PASTES CONTAINING FLY ASH WITH DIFFERENT PARTICLE SIZE DISTRIBUTION

Príspevok analyzuje vplyv cementových zmesí, ktoré obsahujú popolček s rôznou veľkosťou zŕn. Žiada sa zdôrazniť, že reologické vlastnosti cementových zmesí, ktoré obsahujú popolček z bitúmenového uhlia, závisia od obsahu popolčeka v cemente, od množstva podielu popolčeka a tvaru častíc.

The paper presents the analysis of fly ash influence on rheological properties of cement pastes with content different type of fly ash concerning particle size distribution. It was pointed that rheological properties of cement pastes containing fly ash from bituminous coal (hard coal) depend mostly on content fly ash in cement and on the quantity of fine fraction in fly ash as well as on the shape of fly ash particle.

1. Introduction

Fly ash presence in cement result in modification of the rheological properties of cement pastes, which means the influence on the rheological properties of the fresh concrete mixes and mortars [1-4].

Analysis of studies of many authors concerning the influence of the fly ash on the rheological properties of cement paste shows, that the addition of fly ashes to cement can have the result in improvement or deterioration of rheological properties [5-9]. Different rheological reactions have been observed of cement pastes from cement with additions of fly ash and are the summary of influence of many factors superposition [10-11]. They are mainly such factors as type and quantity of fly ash in cement, particle size, shape and porosity of grains of ash and also contents of unburned coal in ash.

In this study the researches were carried out aiming at the defining the role of factors which have influence on rheological properties of pastes from cement including fly ash.

2. Experimental

2.1. Materials

Low-calcium fly ashes (A, B) from the bituminous coal combustion were used. The chemical composition of the materials used is given in table 1.

The phase composition of fly ashes was characterized by XRD. The following crystalline phases have been detected: quartz, mullite, hematite.

Chemical composition of fly ashes A and B

Table 1

Component	fly ash A	fly ash B
	% by wt.	
Loss on ignition	1.0	3.1
SiO ₂	50.4	51.9
Fe ₂ O ₃	8.6	8.0
Al ₂ O ₃	26.8	26.1
CaO	4.3	3.1
MgO	2.6	1.9
SO ₃	1.2	0.3
Na ₂ O	1.6	0.8
K ₂ O	1.4	3.2
CaO free	0.2	0.0

Specific surface area of fly ashes (Blaine)

Table 2

Fly ashes	Specific surface area of fly ashes (Blaine) [m ² /kg]
A	288
B	271
B-1	379
B-2	425

Fly ash - cement blends designed for rheological studies were obtained by homogenizing the components. The ashes A and B were applied in the raw state (A, B) and the B fly ash was ground in a laboratory mill to obtain a larger Blain's specific surface area (B1, B2). The fly ash content in cement was 20, 40,

* Prof. dr. hab. Stefania Greszczyk, Dr. inż. Grzegorz Lipowski
Technical University of Opole 45-233 Opole, ul. St. Mikołajczyka 5, Poland

60 and 80 percent wt. The Blain's specific area of the fly ash used are given in table 2.

2.2. Methods

The rheological measurements were carried out using the rotative viscosimeter type Rheotest RV - 2.1, with the modified surfaces of both cylinders. All the cement - fly ash samples were prepared and measured following the same procedure and in the same conditions. The tests were performed at a constant temperature 21 °C and at a constant water to solid ratio 0.4. Measurements started 10 minutes after mixing with water. The rheological properties of pastes with fly ashes were determined from the flow curves at growing and reduced rates of shearing in the range from 0 to 146 s⁻¹. The yield value and plastic viscosity were determined from the descending part of flow curve, according to the Bingham's model.

The particle size analysis of fly ash was made by the laser analyser type LAU -10.32 fractions were determined in range 0,5 - 200 μm. On the base of size analysis of fly ash the following parame-

where: ϕ_{min} - diameter of finest fraction,
 ϕ_{max} - diameter of coarsest fraction,
 $d\phi$ - elementary fraction,
 $q(\phi)$ - fly ash particles distribution,
 ρ - density of grains of fly ash,
 pow_{wt} - specific surface area of fly ash.

Conventional diameters D of particles were defined basis on the function of cumulative fly ash grains distribution. They characterise the conventional diameters of fly ash grains equal to the value of cumulative curve distribution 0.25; 0.50; 0.75 and are defined D25, D50, D75 respectively [12].

3. Results of analyses

In table 3 the values of yield value (τ_o) and plastic viscosity (η_{pl}) of analysed pastes are presented. Figures 6 - 10 show the partial size distribution in percent wt. of particular fractions of fly ash in range 0 - 200 μm and cumulative curve fly ash A and B raw and grinded B-1 and B-2. Table 4 presents calculated parameters characterising particles of the fly ashes.

Yield value τ_o [Pa] and plastic viscosity η_{pl} [Pa · s] of cement pastes containing fly ashes A, B, B-1, B-2.

Table 3

No	Composition of cement - fly ash mixtures	A		B		B-1		B-2	
		τ_o	η_{pl}	τ_o	η_{pl}	τ_o	η_{pl}	τ_o	η_{pl}
0	100 % C	69.1	0.83	69.1	0.83	69.1	0.83	69.1	0.83
1	80 % C + 20 % FA	30.0	0.45	57.6	0.89	33.2	0.60	32.1	0.51
2	60 % C + 40 % FA	25.1	0.43	32.4	0.92	29.4	0.61	21.3	0.49
3	40 % C + 60 % FA	16.3	0.39	23.6	0.82	21.5	0.58	17.2	0.43
4	20 % C + 80 % FA	13.1	0.39	15.6	0.58	15.6	0.57	14.9	0.46

ters characterised the file of particles of fly ash were determined [12]: average diameter of particle \bar{d} , conventional diameters (D25, D50, D75), spherical shape coefficient Ψ and contents of grains less then 24 μm in % wt.

They were calculated by equations:

$$\bar{d} = \frac{\int_{\phi_{min}}^{\phi_{max}} \phi \cdot q(\phi) d\phi}{\int_{\phi_{min}}^{\phi_{max}} q(\phi) d\phi} \quad (1)$$

$$\int_{\phi_{min}}^{\phi_{max}} q(\phi) d\phi = 1 \quad (2)$$

$$\bar{d} = \int_{\phi_{min}}^{\phi_{max}} \phi \cdot q(\phi) d\phi \quad (3)$$

$$\Psi = 6 \frac{\int_{\phi_{min}}^{\phi_{max}} \phi^2 q(\phi) d\phi}{pow_{wt} \cdot \rho \int_{\phi_{min}}^{\phi_{max}} \phi^3 q(\phi) d\phi} \quad (4)$$

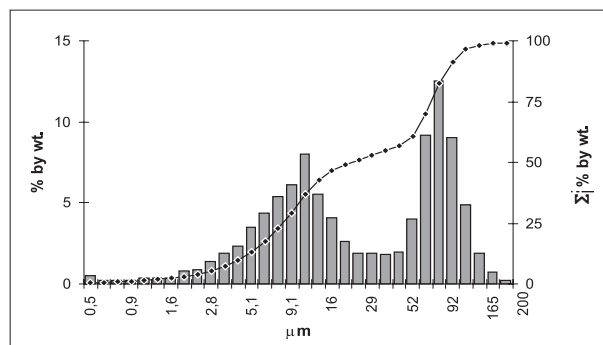


Fig. 1 Partial size distribution and cumulative curve of fly ash A

Analysis of the results shows, that content of fly ash from bituminous coal in cement causes the decreasing of the yield value and plastic viscosity of pastes. Moreover, it was stated that the cement pastes including low-calcium fly ash A and B with the similar chemical contents and specific surface display significant differences of rheological properties (tab. 3). In aim to explain those differences the size analysis was made of fly ash by the laser diffraction method.

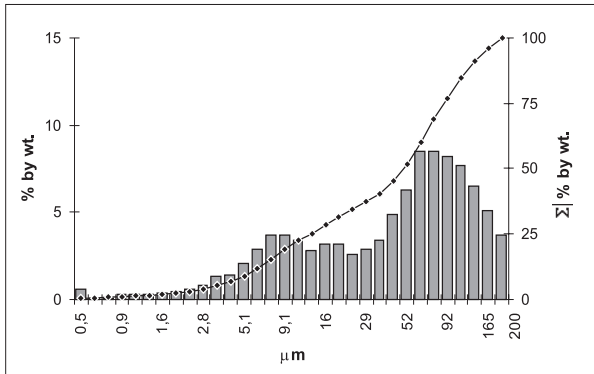


Fig. 2. Partical size distribution and cumulative curve of fly ash B

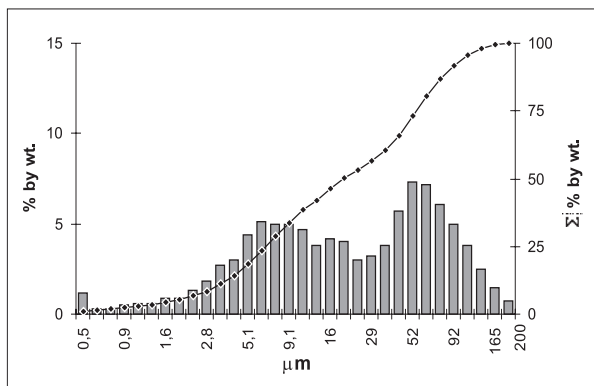


Fig. 3. Partical size distribution and cumulative curve of fly ash B-1

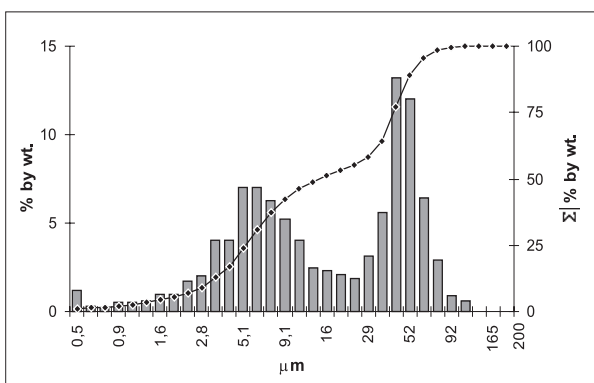


Fig. 4. Partical size distribution and cumulative curve of fly ash B-2

On the base of the calculated parameters of size analysis it can be stated, that the average size of fly ash particles A is 77.2 μm , 25 percent of grains in fly ash has he diameter less than 7.7 μm , 50 percent of grains has the diameter less than 18.2 μm and 75 percent has less than 66.1 μm . The average size of particles B is 109 μm , 25 percent of grains in fly ash B have the diameter less than 12.8 μm , 50 percent of them - less than 49.4 μm and 75 percent has the diameter less than 88.1 μm . Participation of grains less 24 μm is 34.3 percent in case of B ash, while in A ash it is 53.1 percent. The conclusion is, that the fly ash A are cha-

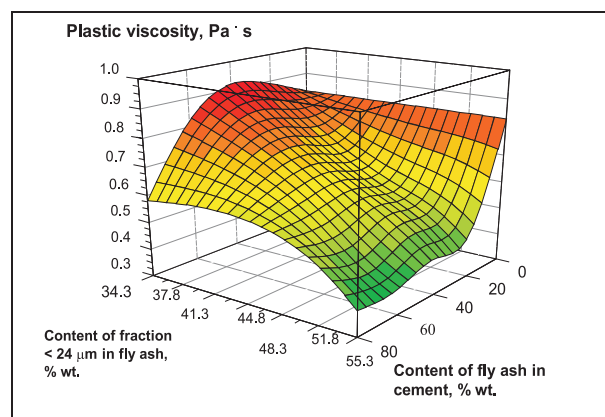


Fig. 5 Effect of contents fine fraction < 24 μm in fly ash and contents of fly ash in cement on the plastic viscosity of cement pastes

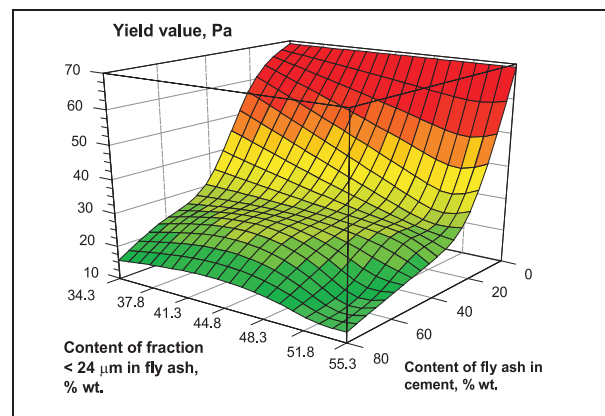


Fig. 6. Effect of contents fine fraction < 24 μm in fly ash and contents of fly ash in cement on the yield value of cement pastes

Calculated parameters of particles of fly ashes

Table 4

Fly ash	average diameter of particle [μm]	D25 [μm]	D50 [μm]	D75 [μm]	spherical shape coefficient Ψ	contents of grains less than 24 μm [% wt.]
A	77.2	7.7	18.2	66.1	0.245	53.1
B	109.0	12.8	49.4	88.1	0.170	34.3
B-1	80.8	6.6	19.7	54.6	0.194	53.3
B-2	47.9	5.3	14.3	41.7	0.237	55.3

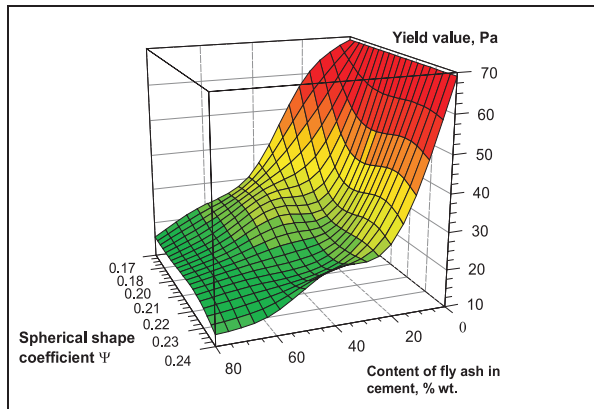


Fig. 7. Effect of spherical shape coefficient of fly ash particles and contents of fly ash in cement on the yield value of cement pastes

racteristic for the greater participation of fine fraction comparing with B fly ash. Figures 5 - 6 present quantity and influence of fine fractions participation $< 24 \mu\text{m}$ in fly ash and content of fly ash in cement on plastic viscosity and yield value of cement paste.

The spherical shape coefficient calculation relating to the grains of fly ash A and B (tab. 4) moreover showed, that the shape of fly ash grains A is closer to the spherical shape comparing with B grains. That was confirmed by the microscope analysis SEM.

The above explains, why the pastes containing fly ash with the similar chemical composition and specific surface show differences in rheological properties of cement pastes.

Figure 7 presents the influence of spherical shape coefficient Ψ of fly ash grains and their quantities in cement on yield value of paste. Grinding of ashes results in the growth of participation of fine fractions and increase of spherical shape coefficient of fly ash grains (tab. 4), this explains the improvement of rheological properties of pastes with these ashes (tab. 3).

4. Conclusions

- Content of fly ash from bituminous coal in cement has the result in decrease of yield value and plastic viscosity of pastes - the more significant, the greater is contents of fly ashes in cement.
- Rheological properties of pastes including fly ash from bituminous coal depend mainly on the participation of fine fractions in ashes and on shape of particles of fly ashes. The level of fluidity of cement-ash pastes is more visible at the greater number of fine fractions $< 24 \mu\text{m}$ in ashes and the more spherical shape of fly ash particles.

Reviewed by: T. Ďurica, K. Šlopková

5. Literatúra - References

- [1] ALONSO, J. L., WESCHE, K.: *Characterization of Fly Ash*, w *Fly Ash in Concrete*, Ed.: K. Wesche, E & FN SPON, London, 1991, pp. 3-23.
- [2] REHSI, S. S.: *Portland Fly Ash Cement*, w *Mineral Admixtures in Cement and Concrete*, Ed.: S. N. Ghosh, ABI Books Pvt. Ltd., New Delhi, 1995, pp. 158-173.
- [3] BANFILL, P.F.G.: *An experimental study of the effect of PFA on the rheology of fresh concrete and cement paste*. International Symposium. The use of PFA in Concrete, Leeds 1982, pp. 161 - 171.
- [4] ROY, D. M., SKALNY, J., DIAMOND, S.: *Effects of Blending Materials on the Rheology of Cement Pastes and Concretes*. Proceedings Annual Meeting of Material Research Society, M4.4, Boston 1982, Concrete Rheology, pp. 152-173.
- [5] COSTA, U., MASSAZZA, F.: *Rheological properties of fly ash cement pastes*. Il Cemento, nr 4, 1986, pp. 397-414.
- [6] GRZESZCZYK, S., LIPOWSKI, G.: *Effects of Low-Calcium Fly Ash on The Rheology of Fresh Cement Pastes*. Applied Mechanics and Engineering, vol. 3, nr 4, 1998, pp. 589-600.
- [7] GRZESZCZYK, S., LIPOWSKI, G.: *Effect of Content and Particle Size Distribution of High-Calcium Fly Ash on the Rheological Properties of Cement Pastes*. Cement Concrete Research, vol. 27, nr 6, 1997, pp. 907-916.
- [8] HOBBS, D. W.: *The effect of pulverized-fuel ash upon the workability of cement paste and concrete*. Magazine of Concrete Research, vol. 32, nr 113, 1980, pp. 219 - 226.
- [9] MASSIDDA, L., SANNA, U.: *Rheological behaviour of portland cement pastes containing fly ash*. Il cemento, nr 4, 1982, pp. 317-322.
- [10] JIANG, W., ROY, D. M.: *Rheology in hydration and setting*. Proceedings of the RILEM Workshop on Hydration and Setting of Cement. Ed. A Nonat, F. N. Spon, London 1992, pp. 333-340.
- [11] UCHIKAWA, H.: *Effect of blending componenet on hydration and structure formation*. Journal of Research of the Onoda Cement Company, 1986, vol. XXXVIII, nr 115, pp. 1-77.
- [12] KOCH, R., NOWORYTA, A.: *Procesy mechaniczne w inżynierii chemicznej*. Wydawnictwo Naukowo Techniczne, Warszawa, 1992.

Andrzej Surowiecki - Zenon Zamiar *

MODEL ZEMNÉHO ZÁKLADU S VYSTUŽENÍM V HLBOKOM VÝKOPE

MODEL OF EARTHEN FOUNDATION WITH REINFORCEMENT IN A DEEP EXCAVATION

V tomto článku sú uvedené výsledky modelu skúmania silových charakteristík pre prípad vodorovne vystuženej sypkej zeminy. Charakteristické veličiny sú teda využité pre vytvorenie modelu s vertikálnou výstužou. Vertikálne vystuženie bolo navrhnuté pre model zemného základu v hlbokom výkope, v ktorej zemina dna je určená na výmenu.

In this paper, the results of model investigation of strength characteristics are discussed for the case of horizontally reinforced loose soil medium. The characteristics are then employed to create a model with vertical reinforcement. The vertical reinforcement has been proposed for the model of earthen foundation in a deep excavation whose bottom is subjected to displacement.

1. Introduction

The paper presents the adaptation of a classical reinforced soil-testing stand for the model with vertical reinforcement.

Investigation results for the model with vertical reinforcement will be applied in the strengthening of a deep excavation bottom subjected to the horizontal pressure exerted by surrounding soil medium. Schema of problem is presented in Fig. 1.

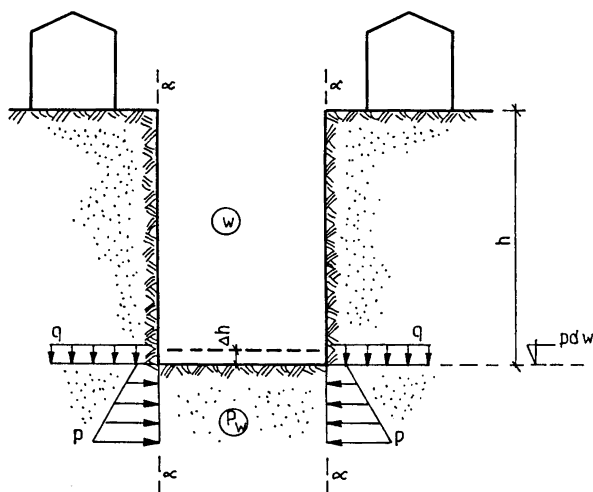


Fig. 1 Schema of problem: w - excavation, pdw - bottom level of excavation, h - excavation depth, Δh - measure of soil displacement from under the excavation bottom, q - pressure in bottom level of excavation from soil overlay, p - horizontal pressure of soil medium in intersections $\alpha - \alpha$, which enclose the excavation, p_w - subsoil of excavation

2. Model description

The subject of testing is a non-cohesive soil sample of cubic or rectangular shape, reinforced horizontally by means of inserts laid in layers with the spacing e_z . The particular layers are made of parallel strips placed with even horizontal spaces e_x . The reinforcement layer planes are perpendicular to the direction of static load. The model investigated is presented in Fig. 2. The reinforced soil is treated as a composite material.

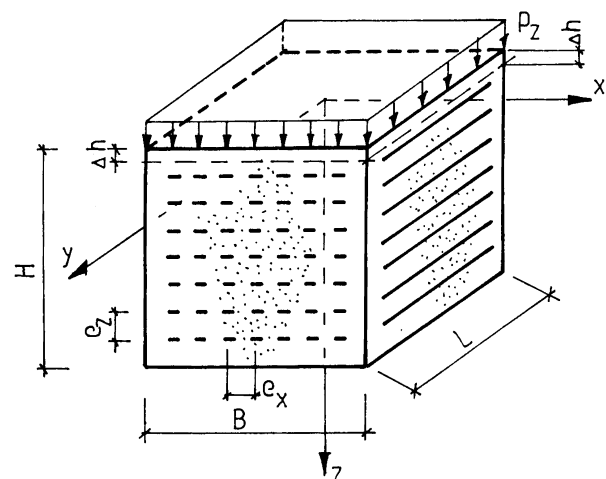


Fig. 2. Model diagram: unitary load p_z

The studies are aimed at determining the macroscopic mechanical features of a composite material, especially the effect

* ¹Dr.hab. inž. Andrzej Surowiecki, ²Doc. inž. Zenon Zamiar

¹Institute of Civil Engineering, Wrocław University of Technology, Wyb. Wyspiańskiego 27, 50-370 Wrocław, Department of Military Engineering, T. Kosciuszko Military University, Obornicka 108, 51-100 Wrocław, Poland

²Department of Military Engineering, T. Kosciuszko Military University, Obornicka 108, 51-100 Wrocław, Poland

of reinforcement on soil cohesion and internal friction angle as well as the deformation module.

The analysis of reinforced soil is carried out on the basis of the results of tests performed on a large-size lab model by means of a comparative analysis - the "reference" is made up of a non-reinforcement medium model.

The lab test data, referring to the model, necessary to calculate the strength parameters of the reinforced medium include:

- p_z - minimum unitary load necessary to create the limiting condition of the sample's active pressure (the so-called calculation load) [MPa];
- $p_{z,e}$ - unitary load exerted on the sample in the range of elastic deformations [MPa];
- p_y - horizontal pressure created by the load p_z [MPa];
- Δh - vertical deformation of the soil sample measured by the mean vertical displacement of a special plate loading the soil sample [m].

3. Lateral pressure coefficient

The pressure coefficient K_a in the equation of the limiting condition of the sample was calculated from the following dependence:

$$K_a = p_y (p_z)^{-1} \text{ for non-reinforced soil} \quad (1)$$

and

$$K_a^* = p_y^* (p_z)^{-1} \text{ for reinforced soil sample.} \quad (2)$$

The pressure coefficient K_a allows us to estimate the increase in a load capacity of soil due to the reinforcement and to calculate the shear strength of reinforced soil. The value of this coefficient depends on the quantity and distribution of the reinforcement. The model tests imply that in reinforced soil the value of K_a^* is smaller compared to a sample of soil with no reinforcement.

4. Effect of load capacity increase

The possibility of increasing the load p_z at steady lateral pressure p_y is treated as a measure of the increase in the load capacity of reinforced soil compared to non-reinforced soil.

The experimental coefficient of the lateral pressure K for a non-reinforced sand sample (reference sample) is as follows:

$$K = p_{y,mean} (p_z)^{-1} \quad (3)$$

where $p_{y,mean}$ is mean lateral pressure exerted on the surface of a wall of the width B obtained empirically.

The experimental coefficient of pressure K^* for a reinforced soil sample was calculated from the following formula:

$$K^* = p_{y,mean}^* (p_z)^{-1} \quad (4)$$

where: $p_{y,mean}^*$ - mean lateral pressure obtained empirically,
 p_z - external load (treated as vertical stress in the sample).

By adopting the horizontal stress p_y , mean in non-reinforced soil as the basis, it is possible to determine the dependence between the load p_z exerted on non-reinforced soil and the load p_z^* exerted on reinforced soil with the proportionality coefficient $1/K^*$:

$$p_z^* = p_y^* (K^*)^{-1} > p_z, \quad p_z^* = p_y^* p_z (p_{y,mean}^*)^{-1} \quad (5)$$

where: $p_y^* = p_{y,mean}^*$ - basic vertical stress,
 p_z^* - maximum external load, which can be exerted on a reinforced soil sample unless the horizontal pressure p_y^* is exceeded.

The effect of the increase in the load capacity of a sample due to the reinforcement is expressed by the difference between the maximum load p_z^* exerted on reinforced soil sample and the maximum load p_z exerted on the reference sample:

$$\Delta p_z = p_z^* - p_z > 0 \quad (6)$$

or, in other way, by the quotient of the same maximum loads:

$$\delta p_z = p_z^* (p_z)^{-1} > 1.0 \quad (7)$$

The model tests imply that, depending on the change of reinforcement position, one can control the load capacity of a soil sample. The appropriate position is of critical economic importance: a smaller number of reasonably placed inserts brings about a higher increase in soil load capacity than a greater number of such inserts placed accidentally.

5. Shear strength of a reinforced soil sample

5.1. General remarks

The model of loose reinforced soil is analysed according to two cases:

Case I: Loose soil is treated as soil with no cohesion. In such a type of soil, the value of the internal friction angle increases due to the reinforcement. Hence, the following dependences are valid:

$$c = 0; \Delta\varphi > 0. \quad (8)$$

Case II: In a pressure-limiting condition, loose reinforced soil behaves like an anisotropic cohesive medium of the internal friction angle as in non-reinforced soil, but displaying features implying cohesion proportional to the values of the tensile forces transferred through the reinforcement. Then, the model is described by the dependence:

$$c > 0; \Delta\varphi = 0. \quad (9)$$

5.2. The effect of internal friction increase in reinforced soil (case I)

The assumption that the sample remains in the limiting condition of active pressure is valid.

Hence, the values p_z , p_y and the pressure coefficient K were treated as extreme and the notation K_a was accepted. Having inserted the values p_z and p_y into the classical limiting condition equation, it is possible to determine the effect of increasing the angle in the soil due to the reinforcement. Such a procedure was recognised permissible in order to compare quantitatively the mechanical features of physical models of non-reinforced and reinforced soils subject to identical test conditions.

The limiting condition requirement for non-reinforced soil with no cohesion has the following form:

$$p_y (p_z)^{-1} = \operatorname{tg}^2 (45^\circ - 0.50\varphi) = K_a \quad (10)$$

and, analogically, for reinforced soil:

$$p_y^* (p_z)^{-1} = \operatorname{tg}^2 (45^\circ - 0.50\varphi) = K_a^* \quad (11)$$

Formulas (10) and (11) allow us to calculate the internal friction angle:

- in non-reinforced soil sample

$$\varphi = 90^\circ - 2 \operatorname{arctg} (K_a)^{0.5}, \quad (12)$$

- in reinforced soil sample

$$\varphi^* = 90^\circ - 2 \operatorname{arctg} (K_a^*)^{0.5} \quad (13)$$

There also exists a dependence:

$$\varphi^* > \varphi, \quad \Delta\varphi = \varphi^* - \varphi \quad (14)$$

where φ means the effect of internal friction angle increase.

Having determined the values of φ and φ^* from formulas (12) and (13), we calculated the shear strength of soil from the Coulomb formula [3] for loose soils:

- in non-reinforced soil sample

$$\tau_f = p_z \operatorname{tg} \varphi, \quad (15)$$

- in reinforced soil sample

$$\tau_f^* = p_z \operatorname{tg} \varphi^* \quad (16)$$

5.3. The effect of cohesion in loose reinforced soil (case II)

According to [2], in the considered case of the reinforced soil sample, the destruction curve (Fig. 3) is, in the system of vertical (p_z) and horizontal (p_y) stresses, determined by the equation:

$$p_z = p_y \operatorname{tg}^2 (45^\circ + 0.50\varphi) + p_0 \quad (17)$$

where:

$$p_0 = 2c \operatorname{tg} (45^\circ + 0.50\varphi) \quad (18)$$

is the "initial" stress (when $p_y = 0$), proving that reinforced soil behaves as if it exhibited cohesion.

The maximum cohesion effect was calculated from formula (18):

$$c = p_0 [2 \operatorname{tg} (45^\circ + 0.50\varphi)]^{-1} \quad (19)$$

where:

$$p_0 = p_y^* p_z (p_y^*)^{-1} - p_z = p_z [p_y^* (p_y^*)^{-1} - 1] \quad (20)$$

where: $p_0 = p_z^* - p_z = P$ - the effect of the increase of load capacity due to the reinforcement, according to formula (6),

φ - internal friction angle of non-reinforced soil.

Shear strength of reinforced soil was calculated from the Coulomb [3] formula for soil with cohesion:

$$\tau_f = p_z \operatorname{tg} \varphi + c. \quad (21)$$

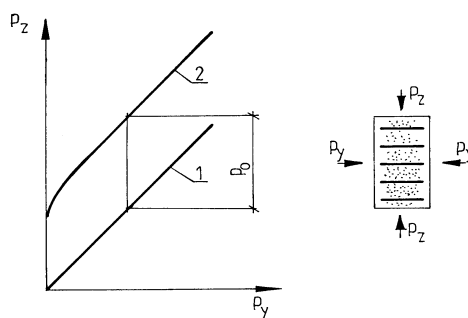


Fig. 3 Destruction curves representing a reinforced sand soil in the plane of main stresses: 1 - non-reinforced sand, 2 - reinforced sand

In this formula, the first component refers to non-reinforced soil, and the second is an addition due to the reinforcement.

6. Deformation module of soil sample

Deformation module E_d was calculated following [3] from the formula:

$$E_d = p_{z,e} h (\Delta h)^{-1} \quad (22)$$

where: $p_{z,e}$ - unitary load exerted on the sample in the range of elastic deformation,

Δh - soil sample deformation as mean vertical displacement of the special plate loading the soil sample,

h - initial height of soil sample.

7. The rationale for selecting the test stand parameters for the model with vertical reinforcement

7.1. Calculation of the length b_1 of the zone of limiting load condition

Fig. 4 shows schematically the vertical profile of the physical model in the form of a cut with its bottom exposed to the displacement Δh suggested for testing. The size proportions of the model's particular elements were chosen so that the essential part with a vertical reinforcement in the zone 1 be subject to the limiting condition created by the load q_f .

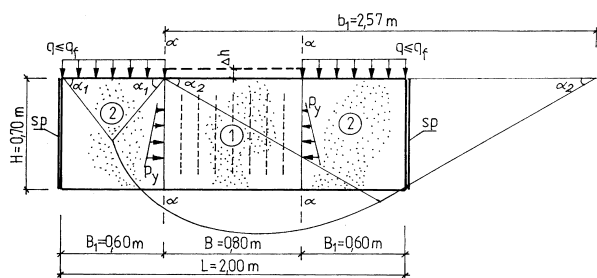


Fig. 4 Model diagram (vertical profile): 1 - model of subsoil with vertical reinforcement; 2 - zones of active pressure of the model 1; 3 - measuring wall of the lateral pressure p_y

The length of the zone b_1 in the limiting condition created was calculated according to [1]:

$$b_1 = B_1 \operatorname{tg} (0.25 \pi + 0.5 \varphi) e^{0.5 \pi \operatorname{tg} \varphi} \quad (23)$$

where: $B_1 = 0.60$ m - width of the surface on which the load q is transferred,
 $\varphi = 30^\circ$ - initially assumed internal friction angles of sand.
 After inserting this data, formula (23) yielded
 $b_1 = 2.57$ m.

7.2. Calculation of the limiting load in the zones 2

The value of the limiting load q_f of the soil medium in the zones 2 (Fig. 4) surrounding the essential part of the model was calculated from the Terzaghi-Schulze formula according to [3]:

$$q_f = [1 + 0.3 B_1 (L')^{-1}] c N_c + \gamma_D D N_q + [1 - 0.2 B_1 (L')^{-1}] \gamma_B B_1 N_y \quad (24)$$

where: $c = 0$ - cohesion of soil medium,

γ_D, γ_B - soil volumetric weight (for the erratic subsoil it should be precised: γ_D till depth D and γ_B below the bottom of foundation on the depth from D to $D + B$);
 $\gamma_D = \gamma_B = \gamma = 19.0$ kN/m³ - initially accepted soil volumetric weight,

$B_1 = 0.60$ m - loading surface width,

$L' = 1.20$ m - loading surface length - measured perpendicular to the $L = (B + 2B_1)$ dimension,

$D = 0.0$ m - founding depth,

$N_c = 37.0$; $N_q = 23$; $N_y = 10.0$ - load capacity coefficients according to Terzaghi, adopted from table 9-2 [3] for $\varphi = 30^\circ$.

Having inserted the above data into formula (24), we obtained $q_f = 0.103$ MPa. We assume that the size of the loading surface is 0.60 m x 1.20 m = 0.72 m² and then the vertical force P , necessary to exert the load $q_f = 0.103$ MPa, equals 74.16 kN.

8. Summary

In order to calculate the strength parameters of a reinforced soil medium, the following data obtained from model studies are indispensable:

$q \leq q_f$ - vertical loads in the range up to the limiting condition (Fig. 3),

p_y - horizontal pressure due to the action of the load q ,

Δh - vertical displacement (measure of soil displacement) of the model's zone 1 due to a bilateral horizontal thrust of the zone 2.

The suggested physical model allows a measurement of these values for both non-reinforced and reinforced media with not only horizontal, but also vertical inserts. Following the test so performed, it will be possible to determine the increase in the resistance of a reinforced medium to horizontal pressure and the decrease in soil vertical displacement h , which is a consequence of horizontal loads.

Reviewed by: E. Krličková, F. Schlosser

Literatúra - References

- [1] DMITRUK, S., SUCHNICKA, H.; *Geotechnology protection of output*. Lecture of Wrocław University of Technology, Wrocław 1976 (in Polish)
- [2] LONG, N.T., SCHLOSSER, F.; *Principle of operation and behaviour of reinforced soil*. Selected problems of geotechnology, Ossolineum, PAN-IBW, Wrocław, 1978, pp. 157-184 (in Polish)
- [3] WIĘUN, Z.; *Epitomes of geotechnology*. WKiŁ, Warszawa 1989.

Sylwester Kobielał - Grzegorz Troszczyński *

ZIŠŤOVANIE POZDĹŽNYCH SÍL NA OHÝBANOM NOSNÍKU

INDEPENDENT FORMATION OF LONGITUDINAL FORCES IN BENT BEAMS

Príspevok sa zaoberá obmedzením deformácií v horizontálnom smere na ohýbaných trámoch. Nastáva pri pootočení koncových prierezov trámu obmedzovaných uložením v podperách. Výsledkom sú prídavné tlakové namáhania. Výsledné vzťahy sú odvodené pre dva zaťažovacie stavy: rovnomerné zaťaženie a osamelé bremená v strede rozpätia trámu. Umožňujú určiť namáhanie a stanoviť účinky na deformácie, ako aj únosnosť pomocou lineárnej, aj nelineárnej teórie. Numerické riešenie ukazuje priaznivý dopad popisovaného fenoménu na pôsobenie trámu. Ukazuje sa, že pri vzraсте horizontálnej tuhosti podpíer deformácie významne klesajú a napätia vzrastajú. Mimoriadny nárast únosnosti sa konštatuje pri materiáloch s nízkou ťahovou pevnosťou a vysokou tlakovou únosnosťou.

This paper deals with the phenomenon of horizontal constraints being strutted by bent beams. This phenomenon takes place when rotating ends of beam sections encounter the resistance of horizontal constraints. Consequently, reactions occur between the constraints and the beam horizontal which induce a longitudinal compression force. Equations for two load cases: a uniformly distributed and concentrated force applied to the span centre, allowing to determine the value of this force and its influence on deflection and load capacity on the on the basis of the linear and non-linear theory were derived. The analysis carried out on this base showed an advantageous effect of the discussed phenomenon on the beam behaviour. It was proved that as horizontal supports stiffness increases the deflection decreases considerably and its strength increases. An especially significant increase in the load capacity was observed in the case of materials with low tensile strength and high compression strength.

Introduction

In order to carry out static calculations indispensable for the designing of engineering structures designers use theoretical construction models. Every model, especially one of an engineering structure, should reflect the real object as faithfully as possible. Only when the theoretical solution obtained from an analysis of the model conforms to the real object the designer will have the proper basis for designing a structure capable of carrying the loads acting on it and be able to assess its safety.

The models of structure calculations most often contain several simplifications. Although the use of such imperfect models makes calculations easier, the results thus obtained include anticipated errors. They may be, for instance, a lowering of the value of internal forces occurring in the structure (e.g., the first order theory based on the stiffening principle which takes no account of the displacement effect on the value of internal forces or disregards advantageous phenomena occurring in the structure). Generally speaking, the use of a simplified model might result in a condition where the structural safety is endangered or the structure has an excessive (superfluous) capacity reserve (it is uneconomically designed). Neither of these two situations is acceptable.

The correct (tallying with reality) picture of the distribution of internal forces in the structure, a picture issuing from a static analysis is indispensable for a correct designing of an engineering structure. This should be warranted by employed methods of con-

struction analyses. As the bent elements is regarding, solutions conforming to structural mechanics sometimes fail to meet this condition. It was proved [1], [2] that in certain conditions of fixing - due to the strutting of supports - in structure elements such as beams or slabs occurs an intrinsic longitudinal compressing force inconsistent with solutions deduced from structural mechanics which did not allow for such forces. This kind of an incomplete set of internal forces occurring in the structure, though involving an error, has been used most frequently in dimensioning beams and slabs. This need not involve dangerous situations because - as will be shown - the longitudinal compression force exerts an advantageous effect on the work of the bent beam or slab causing an increase in capacity and a decrease in deflections. An analytical solution of this problem is necessary if we are to consider the effect of support strutting in static-endurance calculations.

This paper presents a solution based on certain simplified assumptions concerning only two load schemes: one, uniformly distributed and another, concentrated in the centre of the beam span.

Strutting of supports

The mechanism of the longitudinal force occurring in a free-supported bent beam is explained in Fig. 1. Affected by a transverse load the extreme cross-section of the beam tends to turn.

* Sylwester Kobielał, Prof. Dr.hab. inż., Grzegorz Troszczyński, PhD., Student
Inst. of Bldg. Engrg., Wrocław Univ. of Technol. 27, Wybrzeże Wyspiańskiego, 50-370 Wrocław, Poland

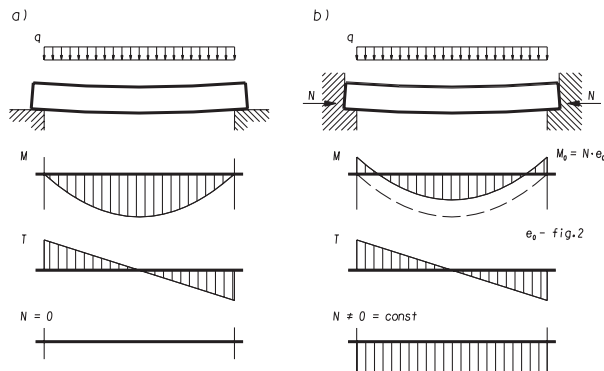


Fig. 1 Differences in internal forces distribution in beam with flexible and stiff support

Due to this rotation the lower edges of these sections shift horizontally (outwards). Depending on their design, beam supports may give way to such displacements or counteract them. The method of support, shown in Fig. 1, does not limit the rotation of the support section. Thus, the “traditional” solution of the beam, compatible with structural mechanics, renders a correct image of the distribution of internal force within the element - bending moments and transverse forces appear there. However, if the supports exhibit a non-zero rigidity in the horizontal direction and are designed so that they are pressured by the lower edges of the rotating support section, there will - as a result of the beam and its supports - occur horizontal forces compressing the beam (Fig. 1b). Besides the bending moments and transverse forces a longitudinal compression force will appear in the beam acting as a self-compression. Moreover, the distribution of the bending moments in a horizontally supported beam tends to change. This takes place because the horizontal force is applied to the beam on an eccentricity e_o (Fig. 2) and thus exerts the moment $M_o = N e_o$ on the

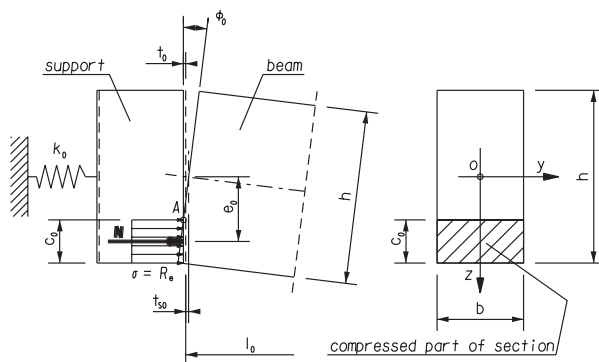


Fig. 2 Contact of beam with support

support generating, in consequence, a reduction of the bending moments in the span. This is illustrated in Fig. 1. The general scheme of support formation shown in Fig. 1b is an indispensable condition for the emergence of the longitudinal force in the beam.

Let us assume that the supports (designed as shown in Fig. 1b) are non-deformed, i. e., their edges remain straight (vertical), yet

affected by the strutting force can move elastically in the horizontal direction. Let us also assume that the beam is made of an ideally elastic-plastic material (Fig. 3), which is characterised by an elasticity modulus E and by the plastic boundary R_e . Due to the rotation of the support section caused by an external load

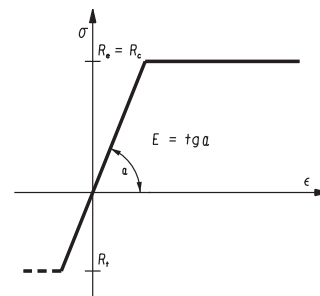


Fig. 3 Material model accepted to analysis

a zone contact appears between the beam and the support (below point A, Fig. 2) where compression stresses occur and a break-off zone (above point A, Fig. 2) without stresses. Thus, according to the accepted assumption, the support edge remains straight and the condition of agreement between beam end displacements (in the compressed zone) and the support must be fulfilled in the entire compression zone. Accordingly:

$$\int_0^l \epsilon_x dx = \Sigma t = const. \quad \text{for } z \geq \frac{h}{2} - c_0.$$

This condition is not fulfilled if we have a free supported working beam in the elastic range of deformations:

$$\int_0^l \epsilon_x dx = \frac{z}{E \cdot J_y} \cdot \int M(x) dx \neq const. \quad \text{for } -\frac{h}{2} \leq z \leq \frac{h}{2}.$$

According to the theory of flat sections the horizontal strains in the extreme section plane vary linearly along the entire height h . Accordingly, the condition of strain agreement, forced by assumptions, will be fulfilled only when plastic deformations appear along the entire height of the compressed zone c_0 , in the support-adjacent section. These deformations are accompanied by stresses: $\sigma = R_e$ (Fig. 2). Assuming such uniform stresses, distribution in the support section the longitudinal force will have the value:

$$N = R_e \cdot b \cdot c_0 \quad (1)$$

The unknown value of the range of the compressed zone for section c_0 can be determined on the basis of the geometric dependencies occurring at the beam-support contact (Fig. 2).

This yields:

$$c_0 = \frac{h}{2} - \frac{t_0 + t_{s0}}{\varphi_0} \quad (2)$$

Geometrical values analogous to those in Fig. 2 but relating to the right support of the beam are denoted with index l instead of index 0 .

If the support is linearly-elastically deformed and dispays a stiffness characteristic of k_0 , its horizontal displacement will be:

$$t_0 = \frac{N}{k_0} = \frac{R_e \cdot b \cdot c_0}{k_0} \quad (3)$$

The total longitudinal deformation of the beam will be:

$$\Delta l = \frac{N \cdot l}{E \cdot A} = \frac{R_e \cdot c_0 \cdot l}{E \cdot h} \quad (4)$$

and equals the sum of the longitudinal displacement of the gravity centres of the two support sections:

$$\Delta l = t_{s0} + t_{sl} \quad (5)$$

The forces equilibrium condition for the forces acting on element ($\Sigma X = 0$) indicates that: $c_0 = c_l$ (for a beam with a constant cross-section). Hence, (2):

$$\frac{t_0 + t_{s0}}{\varphi_0} = \frac{t_l + t_{sl}}{\varphi_l}$$

By substituting: $t_{sl} = \Delta l - t_{s0}$ from (5), we obtain:

$$t_{s0} \cdot \left(1 + \frac{\varphi_0}{\varphi_l} \right) = \frac{\varphi_0}{\varphi_l} \cdot (\Delta l + t_l) - t_0 \quad (6)$$

If the load acting on the beam is symmetrical, then: $\frac{\varphi_0}{\varphi_l} = 1$ and:

$$t_{s0} = \frac{1}{2} \cdot (\Delta l + t_l - t_0) \quad (6a)$$

Should, apart from this, the stiffness of the two supports be identical ($k_0 = k_l$) then: $t_0 = t_l$ and the displacement t_{s0} is:

$$t_{s0} = \frac{\Delta l}{2} = \frac{R_e \cdot c_0 \cdot l}{2 \cdot E \cdot h} \quad (6b)$$

After substituting (3) and (6b) into equation (2) and after the transformations, we get:

$$c_0 = \frac{h}{2 + \frac{R_e}{\varphi_0} \cdot \left(\frac{2 \cdot b}{k_0} + \frac{l}{E \cdot h} \right)} \quad (7)$$

On the other hand, after substituting dependencies (3) and (6a) into equation (2), we get a more general form of the above quotation, also including the case in which the two beam supports are of different stiffness ($k_0 \neq k_l$):

$$c_0 = \frac{h}{2 + \frac{R_e}{\varphi_0} \cdot \left[b \cdot \left(\frac{1}{k_0} + \frac{1}{k_l} \right) + \frac{l}{E \cdot h} \right]} \quad (7a)$$

Denoting: $\frac{1}{k'} = \frac{1}{k_0} + \frac{1}{k_l}$, we get:

$$c_0 = \frac{h}{2 + \frac{R_e}{\varphi_0} \cdot \left[\frac{b}{k'} + \frac{l}{E \cdot h} \right]} \quad (7b)$$

It is evident that the value denoted by k' is the substitute stiffness of the system of the two horizontal support constraints, which are connected in a row. When calculating the range of the compressed zone in support section of the beam, it is more convenient to use the stiffness of the entire frame system, i. e., formula (7b), considered to be more universal.

Expressions (7, 7a, 7b) show that in order to determine the range of the compressed zone in the support section, it is necessary to calculate the compression force value (1). In addition, we must have the value of the rotation angle of this section. Apart from the section stiffness and span, its value is also affected by the value and method of beam loading. We may say that φ_0 is a specific feature of a given load regime.

Subsequent considerations will be confined to two specific load cases: uniformly distributed along the entire beam length and concentrated at the span centre. These load regimes were chosen due to their generality. What is more, they are symmetrical and previously introduced equations (7) and (7b) may, therefore, be used. The solution of such (simple) methods of beam-loading will adequately show the advantages of a beam-end horizontal support.

Uniform load

Figure 4 illustrates a static diagram and loads acting on the beam in question. Apart from the transverse load q , we have an axial force N acting on the beam, resulting from the strutting of support and supports moments: $M_0 = N \cdot e_0$, resulting from the eccentric action of the compression force N . Let us assume that

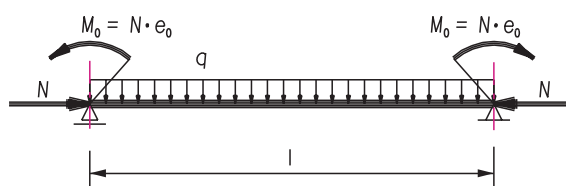


Fig. 4 Internal forces acted on beam

the beam is elastically deformed and the local plasticization of the material in the support-adjacent zones has little effect on the deformation of the element. If we apply the linear theory, the solution is trivial: the rotation of the support section is a superposition of the rotations produced by the transverse load q and the support moment M_0 :

$$\varphi_0 = \frac{1}{E \cdot J_y} \cdot \left(\frac{1}{24} \cdot q l^3 - \frac{1}{2} \cdot N \cdot e_0 \cdot l \right) \quad (8)$$

After substituting dependence (1) into the above quotation, and then substituting it to formula (7b), for a rectangular beam $b \cdot h$ in size, we get the following third degree equation:

$$c_0^3 - \frac{3}{2} \cdot h \cdot c_0^2 + \left(\frac{1}{6} \cdot \frac{q \cdot l^2}{R_e \cdot b} + \frac{2}{3} \cdot h^2 + \frac{1}{6} \cdot \frac{E \cdot b \cdot h^3}{l \cdot k'} \right) \cdot c_0 - \frac{q \cdot h \cdot l^2}{12 \cdot R_e \cdot b} = 0 \quad (9)$$

Testing its discriminant, we can say that it has always two complex roots and one real root which is the sought value of the compressed zone range for section c_0 at the support. It is also possible to derive an algebraic expression to determine the real root of this equation. However, its form is complex and difficult to analyse. This is why it is much easier to solve the above equation using a computer.

Equation (9) was derived in accordance with the linear theory, based on the stiffening principle. Hence, it fails to take into account the effect of deflection on the distribution of bending moments in the beam and, thereby, on the value of the rotation angle of the support section. This is not without importance in a situation where the element is affected by a compression force. The non-linear theory will assist in obtaining the accurate solution.

According to the 2nd order theory, the bending moments in the beam under discussion assume the following distribution:

$$M(x) = M_q(x) - N \cdot [e_0 - w(x)] = M_q(x) - N \cdot e_0 + N \cdot w(x) \quad (10)$$

The total beam deflection $w(x)$ is the sum of the deflection due to the transverse load $w_q(x)$ and the deflection due to the longitudinal force $w_N(x)$ (at a concurrent appearance of load q):

$$w(x) = w_q(x) + w_N(x) \quad (11)$$

By substituting (10) into the equation, we get:

$$M(x) = M_q(x) + N \cdot w_q(x) + N \cdot w_N(x) - N \cdot e_0. \quad (12)$$

The unknown function $w_N(x)$ expressing a deflection increase due to the longitudinal force N , will be determined by means of the differential equation:

$$M_N(x) = -EJ_y \cdot w_N''(x) = -N \cdot [e_0 - w_q(x) - w_N(x)] \quad (13)$$

After the transformation, we get:

$$EJ_y \cdot w_N''(x) + N \cdot w_N(x) = -N \cdot w_q(x) + N \cdot e_0 \quad (14)$$

As mentioned above, the deflection $w_q(x)$ results from the transverse load acting on the beam (it is the axis equation of a deflected beam under this load only). As we know, this equation has - for a uniformly loaded beam - the following form:

$$w_q(x) = \frac{q}{24EJ_y} \cdot x^4 - \frac{q \cdot l}{12EJ_y} \cdot x^3 + \frac{ql^3}{24EJ_y} \cdot x \quad (15)$$

whereas the bending moments equation:

$$M_q(x) = -\frac{q}{2} \cdot x^2 + \frac{q \cdot l}{2} \cdot x \quad (16)$$

After substituting dependence (15) into the differential equation (14) and solving it, we get an equation for the deflection at any point of the beam, the deflection due to the longitudinal force N , at the concurrent uniform load q :

$$w_N(x) = -\frac{q}{24EJ_y} x^4 + \frac{q \cdot l}{12EJ_y} x^3 + \frac{q}{2N} x^2 - \left(\frac{q \cdot l^3}{24EJ_y} + \frac{q \cdot l}{2N} \right) x + e_0 - \frac{q \cdot EJ_y}{N^2} + \left(\frac{q \cdot EJ_y}{N^2} - e_0 \right) \cdot \cos(\beta \cdot x) + \left[\frac{q \cdot EJ_y}{N^2} \cdot \left(\frac{1 - \cos(\beta \cdot l)}{\sin(\beta \cdot l)} \right) + e_0 \cdot \left(\frac{\cos(\beta \cdot l) - 1}{\sin(\beta \cdot l)} \right) \right] \cdot \sin(\beta \cdot x) \quad (17)$$

The dependence thus obtained can be substituted into formula (12) together with the equations (15) and (16). After its transformation, we get the equation of moments in a beam bent by the uniform load q and compressed eccentrically by force N :

$$M(x) = \frac{q \cdot EJ_y}{N} \left[\cos(\beta \cdot x) - 1 + \left(\frac{1 - \cos(\beta \cdot l)}{\sin(\beta \cdot l)} \right) \cdot \sin(\beta \cdot x) \right] + N \cdot e_0 \cdot \left[\left(\frac{\cos(\beta \cdot l) - 1}{\sin(\beta \cdot l)} \right) \cdot \sin(\beta \cdot x) - \cos(\beta \cdot x) \right] \quad (18)$$

Starting from the differential equation of the deflected beam axis, we can show that, for such a distribution of bending moments in the beam, the rotation angle of the support section would be:

$$\varphi_0 = \frac{1}{\beta} \cdot \left(\frac{N \cdot e_0}{EJ_y} - \frac{q}{N} \right) \cdot \left(\frac{\cos(\beta \cdot l) - 1}{\sin(\beta \cdot l)} \right) - \frac{q \cdot l}{2N} \quad (19)$$

After substituting dependencies (19) and (1) into equation (7b), we shall get (for a rectangular section) the equation:

In this equation, the sought value of the compressed zone range for support section c_0 occurs in an implicit form. It is, therefore, impossible to solve it with general numbers. Equation (20) can be solved only numerically. Knowing the range of c_0 equation (1) will yield the axial compression force, whereas equation (18) - the bending moment at any section of the beam.

On the other hand, the axis equation of the deformed beam may be expressed:

$$(2 \cdot c_0 - h) \cdot \left\{ \frac{E \cdot h^3}{12 \cdot R_e \cdot c_0} \cdot \left[\frac{6 \cdot R_e \cdot c_0}{E \cdot h^3} \cdot (h - c_0) - \frac{q}{R_e \cdot b \cdot c_0} \right] \cdot \left[\frac{\cos\left(\sqrt{\frac{12 \cdot R_e \cdot c_0}{E \cdot h^3}} \cdot l\right) - 1}{\sin\left(\sqrt{\frac{12 \cdot R_e \cdot c_0}{E \cdot h^3}} \cdot l\right)} \right] - \left(\frac{q \cdot l}{2 \cdot R_e \cdot b \cdot c_0} \right) \right\} + R_e \cdot c_0 \cdot \left(\frac{b}{k'} + \frac{l}{E \cdot h} \right) = 0 \quad \text{for } k' \neq 0 \quad (20)$$

$$w(x) = \frac{q \cdot E \cdot J_y}{N^2} \left[\cos(\beta \cdot x) + \frac{N}{2 \cdot E \cdot J_y} \cdot x^2 + \left(\frac{1 - \cos(\beta \cdot l)}{\sin(\beta \cdot l)} \right) \cdot \sin(\beta \cdot x) - 1 \right] + \frac{1}{2} \cdot (h - c_0) \cdot \left[\left(\frac{\cos(\beta \cdot l) - 1}{\sin(\beta \cdot l)} \right) \cdot \sin(\beta \cdot x) - \cos(\beta \cdot x) + 1 \right] - \frac{q \cdot l}{2 \cdot N} \cdot x \quad \text{for } N \neq 0 \quad (21)$$

Concentrated force load

For a beam loaded at its span centre with a concentrated force P we can derive the equation for bending moments, the deflection line and the equation to determine the range of the compressed zone in the support section in a manner analogous to a uniformly loaded beam. For this reason, we confine ourselves to the solution only.

According to the linear theory, it will be:

$$\varphi_0 = \frac{1}{EJ_y} \left(\frac{1}{16} \cdot P \cdot l^2 - \frac{1}{2} \cdot N \cdot e_0 \cdot l \right) \quad (8a)$$

$$c_0^3 - \frac{3}{2} \cdot h \cdot c_0^2 + \left(\frac{P \cdot l}{4 \cdot R_e \cdot b} + \frac{2}{3} \cdot h^2 + \frac{P \cdot l \cdot h}{6 \cdot k' \cdot l} \right) \cdot c_0 - \frac{P \cdot l \cdot h}{16 \cdot R_e \cdot b} = 0 \quad (9a)$$

According to the 2nd order theory:

$$(2 \cdot c_0 - h) \cdot \left\{ \frac{P}{2 \cdot R_e \cdot b \cdot c_0} \cdot \left[\frac{1}{\cos\left(\sqrt{\frac{3 \cdot R_e \cdot c_0}{E \cdot h^3}} \cdot l\right)} - 1 \right] - (h - c_0) \cdot \sqrt{\frac{3 \cdot R_e \cdot c_0}{E \cdot h^3}} \cdot \operatorname{tg}\left(\frac{3 \cdot R_e \cdot c_0}{E \cdot h^3} \cdot l\right) \right\} + R_e \cdot c_0 \cdot \left(\frac{b}{k'} + \frac{l}{E \cdot h} \right) = 0 \quad \text{for } k' \neq 0 \quad (20a)$$

$$w(x) = \left(\frac{P}{2 \cdot \beta \cdot l} \cdot \frac{1}{\cos\left(\frac{\beta \cdot l}{2}\right)} - \frac{1}{2} \cdot (h - c_0) \cdot \operatorname{tg}\left(\frac{\beta \cdot l}{2}\right) \right) \cdot \sin(\beta \cdot x) - \frac{1}{2} \cdot (h - c_0) \cdot \cos(\beta \cdot x) - \frac{P}{2 \cdot N} \cdot x + \frac{1}{2} \cdot (h - c_0) \quad \text{for } x \leq \frac{l}{2} \quad (21a)$$

$$m(x) = \frac{P}{2 \cdot \beta} \cdot \frac{1}{\cos\left(\frac{\beta \cdot l}{2}\right)} \cdot \sin(\beta \cdot x) - N \cdot e_0 \cdot \left(\operatorname{tg}\left(\frac{\beta \cdot l}{2}\right) \cdot \sin(\beta \cdot x) + \cos(\beta \cdot x) \right) \quad (18a)$$

for $x \leq \frac{l}{2}$

$$\varphi_0 = \frac{P}{2 \cdot N} \left(\frac{1}{\cos\left(\frac{\beta \cdot l}{2}\right)} - 1 \right) - \beta \cdot e_0 \cdot \operatorname{tg}\left(\frac{\beta \cdot l}{2}\right) \quad (19a)$$

Equations (8a), (9a), (18a), (19a), (20a) and (21a) correspond to the analogous formulas derived for a uniformly loaded beam (8), (9), (18), (19), (20) and (21) respectively.

Using the equations derived for either of the two load cases we can determine the distribution of the internal forces in the beam. The range of the compressed zone on the support is determined for a given beam geometry (l, b, h) support stiffness (k'), material characteristics (E, R_c) and load (q or P). For the linear theory we use formulas (9) or (9a) and (20) or (20a) - for the non-linear theory, respectively. Knowing the compressed zone range, we can calculate from formula (1) the value of the longitudinal compression force and then determine the distribution of the bending moments (for the non-linear theory, according to formula (18) or (18a). The transverse force distribution is the same as for a beam bent only. Equation (21) or (21a) may yield a deflection at any point of the beam.

Analysis of results

The derived equations show how many factors affect, in a general manner, the behaviour of a beam supported at its ends by horizontal constraints. It is essential on the basis of which theory, linear or non-linear, these calculations are carried out. Of all factors included in our considerations the most important role is that of the support stiffness k' . It is also interesting to know the way it affects the distribution of the internal forces, deflection and, above all, the load capacity of the beam.

Answers to these questions for the two cases here discussed are given by the following graphs - made for an exemplary beam:

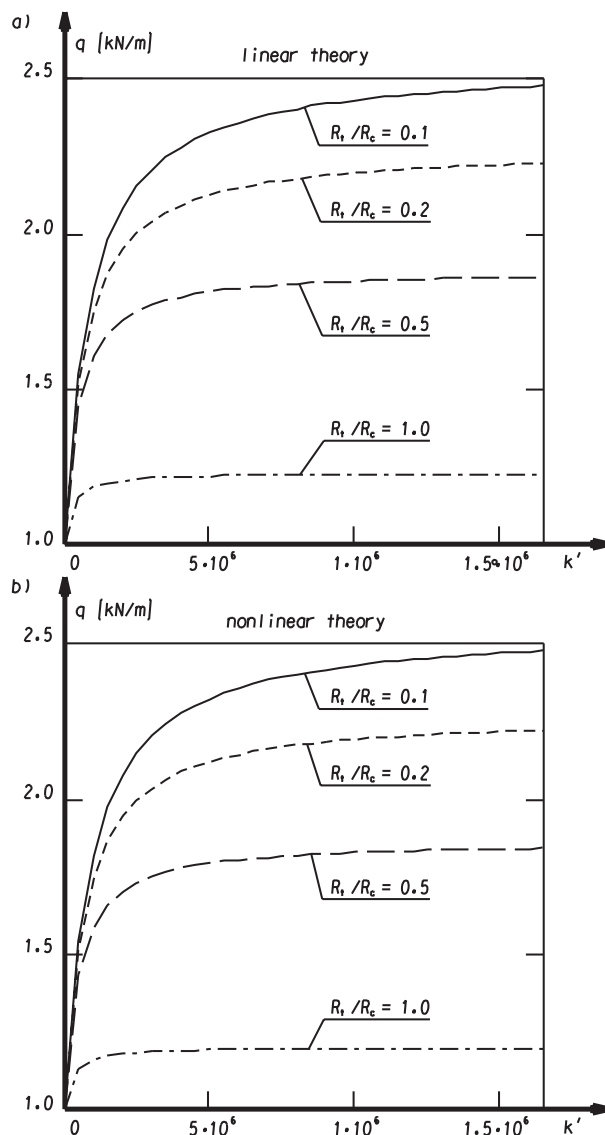


Fig. 5 Strenght increase caused by horizontal support constraints by uniform loading

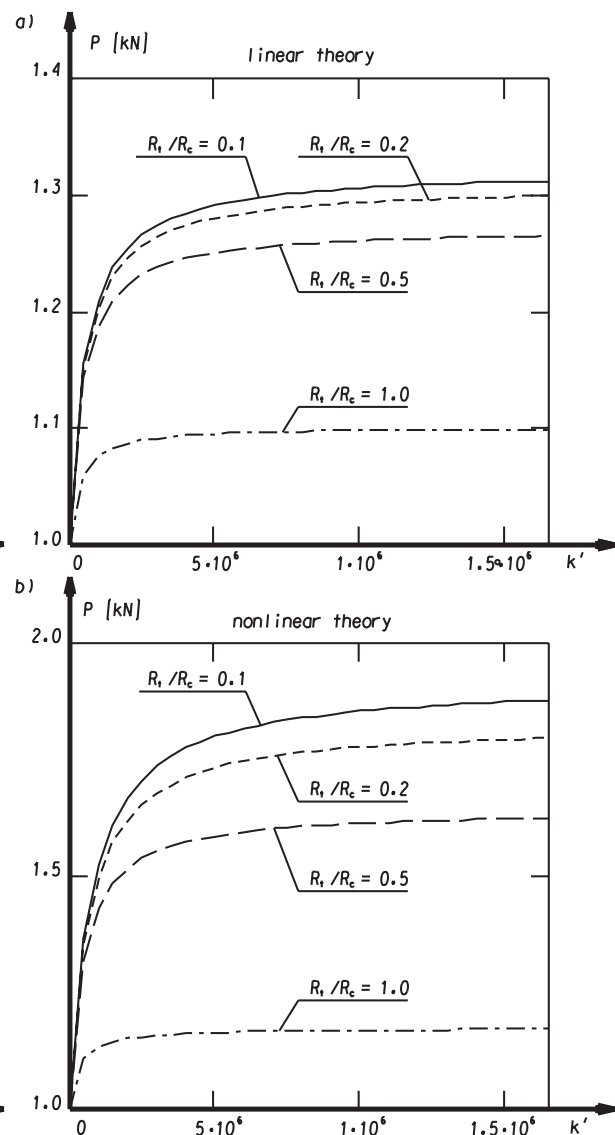


Fig. 6 Strenght increase caused by horizontal support constraints by concentrated loading

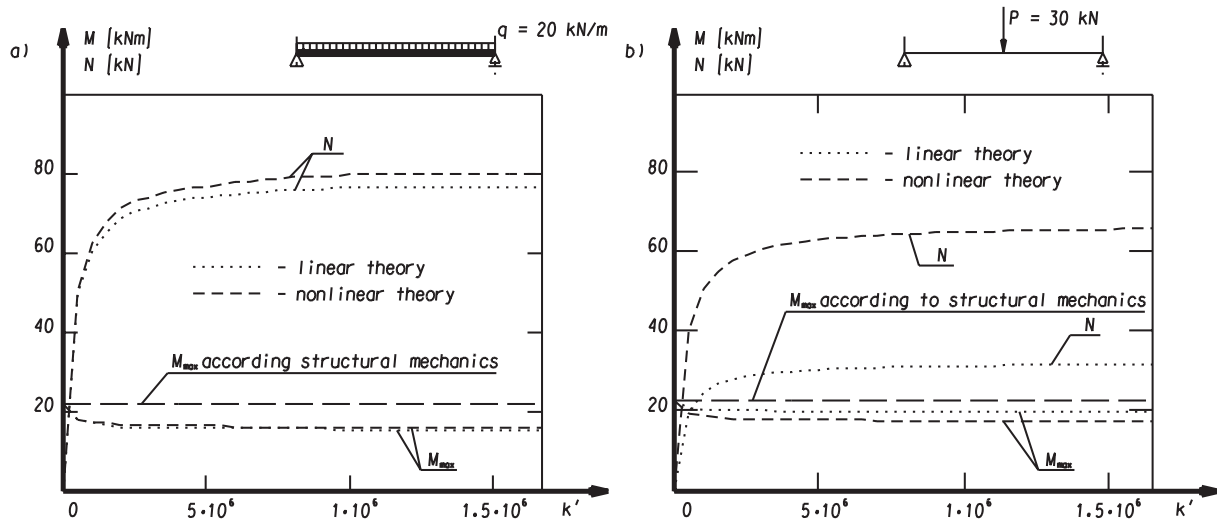


Fig. 7 Relationship diagrams between longitudinal force and maximum bending in beam and support rigidity

$l = 3$ m, $h = 0.2$ m, $b = 0.1$ m in size, assuming the following material characteristics: $E = 25000$ MPa and $R_c = 25$ MPa.

Figures 5 and 6 show the dependence between support stiffness and the relative load capacity of the beam (i.e., referring to the capacity of a beam where no longitudinal force emerges; at $k' = 0$). The graphs were made for different proportions of R_t / R_c . The calculations were performed according to the linear (Figs. 5a, 6a) and non-linear (Figs. 5b, 6b) theories using the previously obtained equations. The strength of compression (R_c) or tension (R_t) the material attained in the extreme fibres of the beam, in the most strained sections, has been accepted as the criterion of capacity exhaustion. At the same time it was assumed that $R_c = R_c$.

Figure 7 presents a graph of the dependence between the longitudinal compression force N emerging in the beam, the value of the bending moment in the middle section of beam, M_{max} and the stiffness of the supports k' (at a fixed load on the beam: $q = 20$ kN/m or $P = 30$ kN).

On the other hand, Figure 8 illustrates the differences in the distribution of the bending moments in the beam, resulting from the application of different theories, assuming an infinite stiffness of the supports ($k' = \infty$). Similar differences, yet referring to deflections, are presented by graphs in Fig. 9.

Figure 10 shows the effect of the horizontal constraint stiffness k' on value of the beam deflection rise.

Conclusions

As it may be inferred from the graphs (Figs. 5 and 6) a horizontal support of the beam's ends produced obvious advantages. Working under the conditions causing a longitudinal compression force the beam shows a higher load-bearing capacity and lower

deflections (Figs. 9, 10) than a beam working under "normal" conditions. Here, the key issue is the stiffness of the system of horizontal constraints k' . The appearance of the longitudinal compression force results from these constraints. When the support stiffness is close to zero, we obtain the solution (capacity) convergent with the solution relating to a merely bent beam. When the support stiffness increases, the load capacity of the beam grows as well.

Analysing the graphs in Fig. 5 (for a uniformly loaded beam) and Fig. 6 (for a beam loaded with a concentrated force), we see that, regardless of the R_t / R_c ratio, there initially exists a range in which, as stiffness k' grows, is an intense (and almost linear) increase in capacity. Then, not with standing a further increase in support stiffness, the capacity increases much more slowly, asymptotically tending toward a certain value. Hence, after having reached a certain support stiffness value its further increase is ineffective. Therefore, a very high stiffness of the horizontal support constraints is not necessary in order to obtain a significant reinforcing effect. It suffices for these constraints to have a certain small (and finite) stiffness and the benefit issuing from the capacity increase is already considerable. Especially for the beam in question, uniformly loaded and made of a material with a $R_t / R_c = 0.1$ ratio, at stiffness k' approximately equal to half of

its compression strength ($k' = \frac{E \cdot A}{2 \cdot l}$), the capacity is already

about twice as high, whereas in the case of infinitely stiff supports ($k' = \infty$) it is about 2.6 times as high as at bending without the longitudinal force effect (Fig. 5).

The capacity due to horizontal constraints is particularly visible when the material the beam is made of has a low tensile strength (e. g., concrete!). In this case, a high relative growth of beam capacity stems from the fact that the longitudinal force mark-

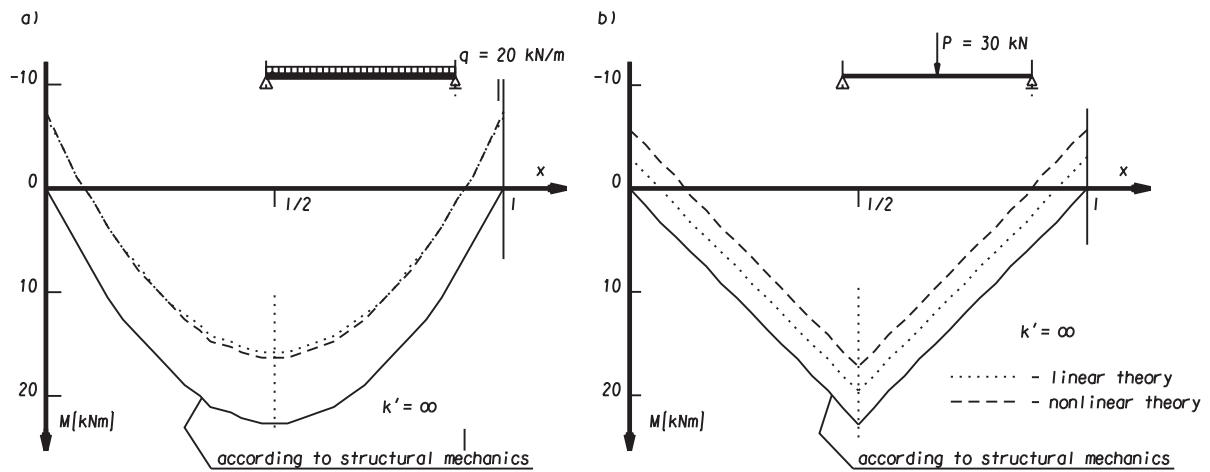


Fig. 8 Changes of bending moment distribution caused by horizontal support constraints

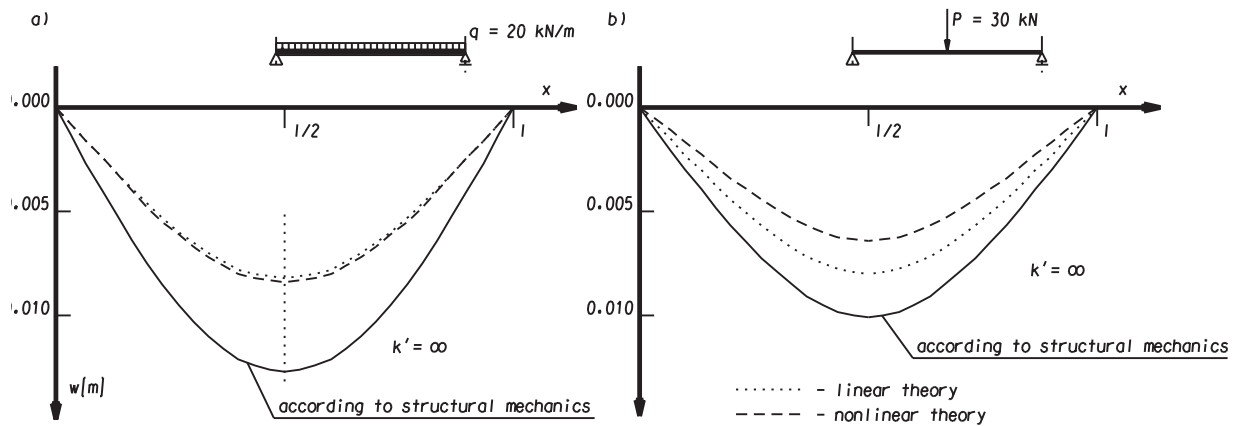


Fig. 9 Changes of beam deflection line caused by horizontal support constraints with infinite stiffness

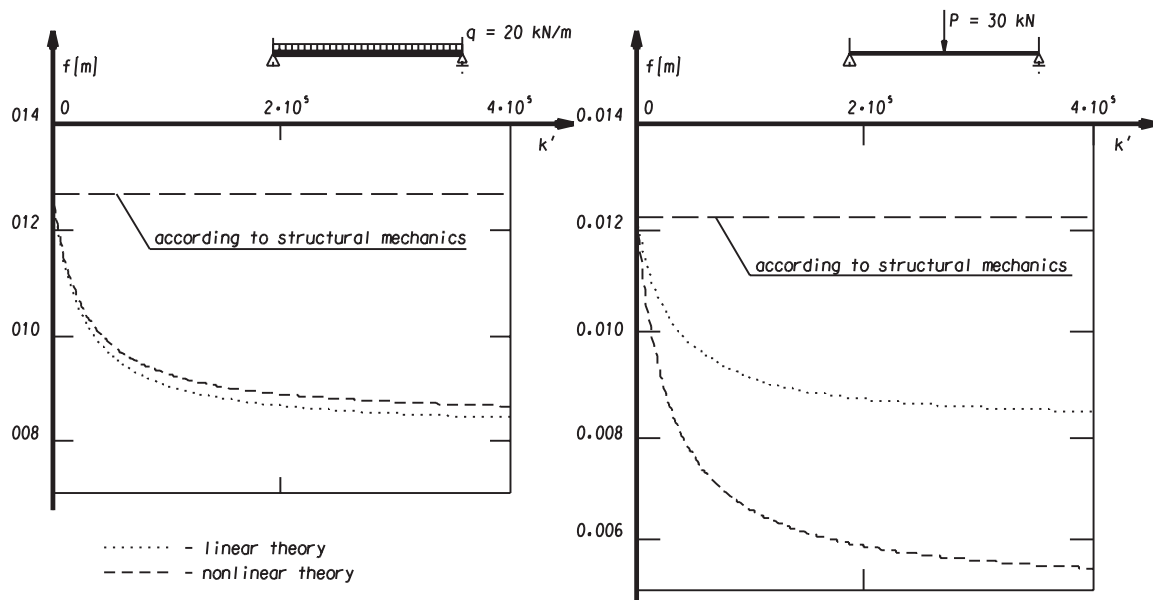


Fig. 10 Changes of maximum beam deflection caused by horizontal support constraints

edly reduces tensile stresses which, when the tensile strength of the material is low, are decisive in attaining the critical capacity of the beam (according to the capacity exhaustion criterion previously defined). On the other hand, if we deal with material whose tensile strength is equal or close to its compression strength, the capacity exhaustion occurs when the stresses on the compressed part of the section attain the value of compression strength. Despite being a compression force, the longitudinal force also decreases the compression stresses, though to a much smaller extent. This happens because force N , acting on eccentricity e_0 in relation to the gravity centre of the section, reduces the bending moments in the beam span (Fig. 8). The decrease of stress due to the reduction of bending moments is bigger than the stresses caused by compression. In consequence, the resultant compression stresses (caused by force N and the bending moment M) in the particular sections are lower than in the beam in which the longitudinal force does not occur. This allows the beam, whose ends are supported by horizontal frames, to transfer a higher load. When $R_t \approx R_c$, the capacity increase is generally not so high; it does not exceed 25 percent at uniform loads and 20 percent at concentrated loads (for $k' = \infty$).

In addition, it is worth noticing that in reality the reserves are even bigger in a beam supported at its ends with horizontal constraints and made of a low tensile strength material. We assumed, in the presented examples, the moment of capacity exhaustion to be equal to the stresses attaining compression or tensile strength in the extreme fibres of the most strained section; tensile stresses are decisive in $R_t \ll R_c$. Such a criterion is justified for a beam supported in a way not causing the emergence of the longitudinal force in it (for $k' = 0$, Fig. 1a) and when the material, if stretched, shows brittle properties - this is when a crack in the span is tantamount to damage. On the contrary, if the beam is supported as shown in Fig. 1b, a crack in the span, due to the stresses exceeding tensile strength, will not damage the element. Following the cracking (in the most strained section) a quasi-joint will form and the structure will transform itself into a three-joint system. Its geometric invariability will be ensured by the horizontal support constraints. For this reason, the beam supported in such a way may efficiently transfer loads acting on it. Disregarding the capacity of the supports, and thus their ability to transfer the strutting forces acting on them, the destruction of such a system may occur in two-fold: by compression strength exhaustion (plasticization) of the material in the middle joint or due to the structure transforming itself into a mechanism. The transformation of a three-joint system into a kinematics chain will occur at big vertical displacements of the middle joint. This might be caused either by a low stiffness of the horizontal support constraints, k' , or low material stiffness coefficient E . Under such circumstances, the reserve of an extraelastic load capacity is practically insignificant. Otherwise, of the two above mentioned conditions occur much later than the exhaustion of the material's tensile strength in the phase of the elastic work of the beam. Nonetheless, the equations for the two load regimes, presented in this paper, do not allow us to estimate the real (limiting) capacity of the beam as they were derived in accordance with the theory of elasticity based on the assumption of material continuum.

There will be a negligible inaccuracy if the capacity of a uniformly loaded beam is calculated according to the 1st order theory. The difference between the capacity calculated according to the linear and non-linear theories is about 3 percent. The difference is significant however, in the case of a beam loaded with a concentrated force. It becomes bigger with a decrease in the R_t / R_c ratio. The consequence of applying the linear theory leads to a remarkable underestimation of the beam capacity (in certain cases as big as 40 percent).

The way of supporting the beam for the purpose of hindering the rotation of the support section also leads to a considerable limitation of beam deflections (Figs. 9, 10). Initially as the support stiffness grows, they are remarkably reduced, even by more than 30 %. A further increase of this stiffness becomes, as in the case of load capacity, ineffective (Fig. 10).

Summary

To reiterate: the condition necessary to produce a longitudinal force in an element being bent comprises stiff horizontal supports capable of counteracting the pressure of beam ends or slab edges. Such conditions occur fairly often in real engineering structures, chiefly in those made of reinforced concrete. Primarily, they occur in uni-or bidirectionally bent slabs of slab-rib systems (Fig. 11), and also other floor systems such as slab or column-slab structures. In such systems, the role of the horizontal constraints counteracting outward slab expansion is assumed by the ribs surrounding the slab, spandrel beams and the neighbouring panels of the floor slab. The phenomenon of reinforced concrete slabs displaying compression forces is known in literature as the compressing membrane effect [1], [2] and has been investigated in world research centres. The beam with its ends protected from displacements can be exemplified by a lintel beam supported on the wall.

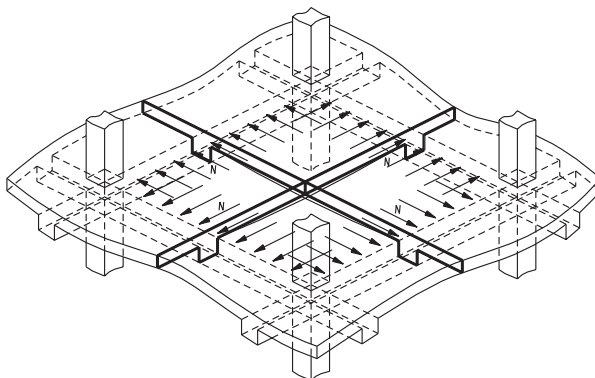


Fig. 11 Example of support strutting by plate in real structure

It is obvious that the equations here derived cannot be applied to estimate reinforced concrete beams (or slabs). This is because they omit to include the rheological phenomena in concrete, the

concrete-specific $\sigma - \varepsilon$ dependence or other composite-specific features of reinforced concrete (e. g., cracking). Contraction and creeping undoubtedly reduce the strengthening effect. The increase in the load capacity of the elastic beam (Figs. 5 and 6) caused by the horizontal support of its ends, encourages us to continue theoretical and practical studies on reinforced concrete beams and slabs. Especially inciting to use this effect in concrete structures is the fact that such materials as concrete (i.e., of low tensile strength) offer the most noticeable advantages.

A detailed investigation of this problem will make it possible to precisely calculate the load capacity of these elements and, by the same token, exploit the inherent reserves. It will open the way to a better determination of the (especially horizontal) effects of a slab or beam on other structural elements surrounding it and the consequences of the effects upon these elements, in the form of additional internal forces.

Notation

Symbols used in this paper:

- b - width of beam cross-section;
 c_0 - range of compressed zone in the support section (Fig. 2);
 $e_0 = \frac{1}{2}(h - c_0)$ - longitudinal force eccentricity;

- E - elasticity modulus;
 h - height of the beam cross-section;
 J_y - section inertia moment in relation to y-axis (Fig. 2);
 k_0 - stiffness characteristic of support;
 M_0 - support moment;
 $M_q(x)$ - bending moment induced by transverse load q ;
 $M_N(x)$ - bending moment induced by longitudinal force N applied on eccentricity e_0 in relation to section gravity centre;
 N - longitudinal force;
 P - force concentrated at the span centre,
 R_c - compressive strength;
 R_e - yield stress;
 R_t - tensile strength;
 t_0 - horizontal displacement of the support;
 t_{s0} - horizontal displacement of beam support section gravity centre due to longitudinal deformations of the beam;
 $\sum t$ - sum of support horizontal displacements;
 $w(x)$ - beam deflection;
 z - distance between beam fibre and section gravity centre;
 ε_x - longitudinal unit strain in the beam;
 φ_0 - rotation angle of the support section of the beam;
 $\beta = \sqrt{\frac{N}{EJ_y}}$.

Reviewed by: J. Vičan, J. Bujňák

Literatúra - References

- [1] PARK, R.: "Ultimate Strength of Rectangular Concrete Slabs Under Short Term Uniform Loading with Edges Restrained Against Lateral Movement", Proceedings, Institution of Civil Engineers (London), V.28, June 1964, pp. 125-150.
[2] PARK, R.: "The Ultimate Strength and Long Term Behaviour of Uniformly Loaded Two-Way Concrete Slabs with Partial Lateral Restraint at all Edges", Magazine of Concrete Research (London), V.16, No. 48, Sept. 1964, pp. 139-152.

**POKYNY PRE AUTOROV PRÍSPEVKOV DO ČASOPISU
KOMUNIKÁCIE - vedecké listy Žilinskej univerzity**

1. Redakcia prijíma iba príspevky doteraz nepublikované alebo inde nezaslané na uverejnenie.
2. Rukopis musí byť v jazyku slovenskom a anglickom (týka sa autorov zo Slovenska). K článku dodá autor resumé v rozsahu maximálne 10 riadkov v slovenskom a anglickom jazyku).
3. Príspevok prosíme poslať: e-mailom na adresu **holesa@nic.utc.sk** alebo **polednak@fsi.utc.sk** alebo **vrablova@nic.utc.sk** alebo doručiť **na diskete 3,5"** v programe Microsoft WORD, 1 kópia článku na adresu: ŽU - rektorát, Ing. Vrablová, odd. vedy a výskumu, Moyzesova 20, 010 26 Žilina.
4. Skratky, ktoré nie sú bežné, je nutné pri ich prvom použití rozpisovať v plnom znení.
5. Obrázky, grafy a schémy, pokiaľ nie sú spracované v Microsoft WORD, je potrebné priložiť na diskete (ako .GIF, .TIF, .CDR, .BMP, .WMF, .PCX, .JPG súbory), prípadne nakresliť kontrastne na bielom papieri a predložiť v jednom exemplári. Pri požiadavke na uverejnenie fotografie priložiť ako podklad kontrastnú fotografiu alebo diapozitív. Pre obidve mutácie spracovať jeden obrázok s popisom v slovenskom a anglickom, resp. len v anglickom jazyku.
6. Odvolania na literatúru sa označujú v texte alebo v poznámkach pod čiarou príslušným poradovým číslom v hranatej zátvorke. Zoznam použitej literatúry je uvedený za príspevkom. Citovanie literatúry musí byť podľa záväznej STN 01 0197 „Bibliografické citácie“ (ISO 690).
7. K rukopisu treba pripojiť presnú adresu autora, tituly, plné meno a priezvisko, dátum narodenia, rodné číslo, adresu inštitúcie v ktorej pracuje, e-mail adresu, funkciu, ktorú zastáva, číslo telefónu alebo faxu.
8. Príspevok posúdi redakčná rada na svojom najbližšom zasadnutí a v prípade jeho zaradenia do niektorého z budúcich čísel podrobí rukopis recenzii a jazykovej korektúre. O výsledku bude redakcia informovať autora ústne alebo písomne. Po korektúrach a zabudovaní pripomienok recenzentov bude posledný obťah príspevku (pred tlačou) poslaný autorovi na definitívnu kontrolu a odsúhlasenie.
9. Termín na dodanie článkov jednotlivých čísiel je 30. 11., 28. 2., 31. 5. a 31. 8.
10. V číslach 4/2000 až 2/2001 budú tieto nosné témy jednotlivých čísiel: Dopravná infraštruktúra, Dopravný prostriedok a jeho časti a Elektrická trakcia v doprave.

**COMMUNICATIONS - Scientific Letters of the University of Žilina
Writer's Guidelines**

1. Submissions for publication must be unpublished and not be a multiple submission.
2. Manuscripts written in English language must include abstract also written in English. The abstract should not exceed 10 lines.
3. Submissions should be sent: by e-mail to one of the following addresses: **holesa@nic.utc.sk** or **polednak@fsi.utc.sk** or **vrablova@nic.utc.sk** or on a 3,5" **diskette** in Microsoft WORD, a hard copy to the following address: University of Žilina, OVAV, Moyzesova 20, SK-010 26 Žilina, Slovakia.
4. Abbreviations which are not common must be used in full when mentioned for the first time.
5. Figures, graphs and diagrams, if not processed by Microsoft WORD, must be sent on a diskette (as .GIF, .TIF, .CDR, .JPG, .PCX, .VMF, .BMP files) or drawn in contrast on white paper, one copy enclosed. Photographs for publication must be either contrastive or on a slide.
6. References are to be marked either in the text or as footnotes numbered respectively. Numbers must be in square brackets. The list of references should follow the paper (ISO 690).
7. The authors exact mailing address, titles, full names, e-mail address (telephone or fax number), the address of the organisation where he works and contact information must be enclosed.
8. The submission will be assessed by the editorial board in its forthcoming session. In the case that the article will be the accepted for future volumes, the board submits the manuscript to the editors for review and language correction. After reviewing and incorporating the editors' remarks, the final draft (before printing) will be sent to authors for final review and adjustment.
9. The deadlines for submissions are as follows: November 30, February 28, May 31 and August 31.
10. In the numbers 4/2000 till 2/2000 the basic topics of the separate editions will be: Transport infrastructure, A vehicle and its parts and Electric traction in transport.



VEDECKÉ LISTY ŽILINSKEJ UNIVERZITY
SCIENTIFIC LETTERS OF THE UNIVERSITY OF ŽILINA

Šéfredaktor:

Editor-in-chief:

Prof. Ing. Pavel Poledňák, PhD.

Redakčná rada:

Editorial board:

Prof. Ing. Ján Bujňák, CSc. - SK
Prof. Ing. Karol Blunár, DrSc. - SK
Prof. Ing. Otakar Bokúvka, CSc. - SK
Prof. RNDr. Jan Černý, DrSc. - CZ
Prof. Ing. Ján Corej, CSc. - SK
Prof. Eduard I. Danilenko, DrSc. - UKR
Prof. Ing. Branislav Dobrucký, CSc. - SK
Prof. Dr. Stephen Dodds - UK
Dr. Robert E. Caves - UK
PhDr. Anna Hlavňová, CSc. - SK
Prof. RNDr. Jaroslav Janáček, CSc. - SK
Doc. Ing. Ján Jasovský, CSc. - SK
Dr. Ing. Helmut König, Dr.h.c. - CH
Doc. Dr. Ing. Ivan Kuric - SK
Ing. Vladimír Mošat, CSc. - SK
Prof. Ing. G. Nicoletto - I
Prof. Ing. Ludovít Parilák, CSc. - SK
Ing. Miroslav Pfliegel, CSc. - SK
Prof. Ing. Pavel Poledňák, PhD. - SK
Akad. Alexander P. Pochechuev - RF
Prof. Bruno Salgues - I
Prof. Dr.hab.ing. Lucjan Siewczynski - PL
Prof. Ing. Miroslav Steiner, DrSc. - CZ
Prof. Ing. Pavel Surovec, CSc. - SK
Prof. Ing. Hynek Šertler, DrSc. - CZ

Technický pracovník:

Technical operator:

Pavol Holeša

Adresa redakcie:

Address of the editorial office:

Žilinská univerzita
Oddelenie pre vedu a výskum
Office for Science and Research
Moyzesova 20, Slovakia
SK 010 26 Žilina
Tel.: +421/89/5620 392
Fax: +421/89/7247 702
E-mail: polednak@fsi.utc.sk, holesa@nic.utc.sk

Vydáva Žilinská univerzita
v EDIS - vydavateľstve ŽU
J. M. Hurbana 15, 010 26 Žilina
pod registračným číslom 1989/98
ISSN 1335-4205

It is published by the University of Žilina in
EDIS - Publishing Institution of Žilina University
Registered No: 1989/98
ISSN 1335-4205

Objednávky na predplatné prijíma redakcia
Výchádza štvrťročne
Ročné predplatné na rok 2001 je 500,- Sk

Order forms should be returned to the editorial office
Published quarterly
The subscription rate for year 2001 is 500 SKK.

<http://www.utc.sk/komunikacie>